Structures Research Report 2003/883

University of Florida
Civil and Coastal Engineering

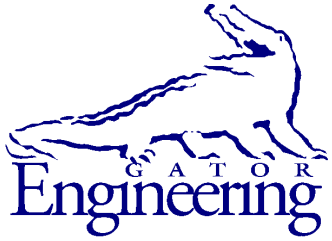

University of Florida
Civil and Coastal Engineering

Final Report **April 2003**

Barge Impact Testing of the St. George Island Causeway Bridge

Phase II : Design of Instrumentation Systems

Principal investigators:
Gary R. Consolazio, Ph.D.
Ronald A. Cook, Ph.D., P.E.

Graduate research assistants:
Alexander E. Biggs
David R. Cowan

Department of Civil and Coastal Engineering
University of Florida
P.O. Box 116580
Gainesville, Florida 32611

Sponsor:
Florida Department of Transportation (FDOT)
Henry T. Bollmann, P.E. – Project manager

Contract:
UF Project No. 4504-883-12
FDOT Contract No. BC-354 RPWO 56

Technical Report Documentation Page

1. Report No.	2. Government Accession No.	3. Recipient's Catalog No.
BC354 RPWO #56		

4. Title and Subtitle

Barge Impact Testing of the St. George Island Causeway Bridge
Phase II : Design of Instrumentation Systems

5. Report Date: April 2003

6. Performing Organization Code:

8. Performing Organization Report No.: 4910 45 04 883

7. Author(s)

G. R. Consolazio, R. A. Cook, A. E. Biggs, D. R. Cowan

9. Performing Organization Name and Address

University of Florida
Department of Civil & Coastal Engineering
P.O. Box 116580
Gainesville, FL 32611-6580

10. Work Unit No. (TRAIS):

11. Contract or Grant No.: BC354 RPWO #56

13. Type of Report and Period Covered: Final Report

12. Sponsoring Agency Name and Address

Florida Department of Transportation
Research Management Center
605 Suwannee Street, MS 30
Tallahassee, FL 32301-8064

14. Sponsoring Agency Code:

15. Supplementary Notes

16. Abstract

The purpose of this research project was to develop instrumentation packages, to create a tentative schedule of events, and to refine the existing analytical models used to plan the impact testing of the SR 300 / Saint George Island Causeway bridge near Apalachicola, Florida. The development of the instrumentation packages included the selection of the sensors, the data acquisition system, and data storage method. The selection of the sensors was based on parameters obtained from a range of finite element simulations conducted using LS-DYNA. The tentative schedule of events for the impact testing was developed based upon coordination of events with the contractor's construction/demolition schedule.

The major aspects of the finite element model refinements are updated soil-pile interaction modeling (both the nonlinear soil curves and the group soil-pile interaction), updated steel material in the nonlinear region of the barge, a refined element integration scheme, and adjusted pile lengths. In addition, a preliminary model for the superstructure was created.

17. Key Words	18. Distribution Statement
Vessel impact load, barge impact, bride pier, finite element modeling, soil-structure interaction	No restrictions. This document is available to the public through the National Technical Information Service, Springfield, VA, 22161

19. Security Classif. (of this report)	20. Security Classif. (of this page)	21. No. of Pages	22. Price
Unclassified	Unclassified	100	

Form DOT F 1700.7 (8-72)

Reproduction of completed page authorized

Barge Impact Testing of the St. George Island Causeway Bridge

Phase II : Feasibility Study

Contract No. BC-354 RPWO#56
UF Project No. 4910-4504-883-12

Principal Investigators :	Gary R. Consolazio, Ph.D. Ronald A. Cook, Ph.D., P.E.
Graduate Research Assistant:	Alexander E. Biggs David R. Cowan
FDOT Technical Coordinator:	Henry T. Bollmann, P.E.

Engineering and Industrial Experiment Station
Department of Civil & Coastal Engineering
University of Florida
Gainesville, Florida

Table of Contents

Table of Contents i

Chapter 1: Introduction 1

Chapter 2: Development of Instrumentation Packages 3

2.1 Introduction 3
2.2 Overview of Instrumentation Network 3
2.3 Load Cell Array 5
2.4 Sensor Position Identification Scheme 8
2.5 Instrumentation Setup for Pier-1 11
2.6 Instrumentation Setup for Pier-3 Test with Superstructure 12
2.7 Instrumentation Setup for Pier-3 Test without Superstructure 14
2.8 Barge Instrumentation 14
2.9 Tracking Motion 15
2.10 Rationale for Sensor Selection 16
2.10.1 Accelerometers 16
2.10.2 Strain Gages 33

Chapter 3: Logistical Planning 34

3.1 Sequence of Tests 34
3.2 Event Scheduling 36
3.3 St. George Bridge Pier Inspection 50
3.3.1 Piers 1S and 2S 50
3.3.2 Piers 3S and 4S 52

Chapter 4: Finite Element Model Updates 54

4.1 Barge Material Model 54
4.2 Integration Comparison 58
4.3 Pile Lengths 60

Chapter 5: Soil-Pile Interaction Modeling 61

5.1 Introduction 61
5.2 Refinement of the Soil Spring Curves 61
5.2.1 Lateral Soil Spring Curves 62
5.2.2 Axial Soil Spring Curves 64
5.3 Soil Spring Alignment 66
5.4 Reversible Group Effect p-y Curve Multipliers 69
5.5 Static Pushover Validation Modeling 71

Chapter 6: Nonlinear Barge Crush Behavior 75

6.1 Introduction 75
6.2 AASHTO Methodology for Prediction of Barge Impact Loads 77
6.3 Finite Element Analysis Procedures and Models 80
6.4 Discussion of Crush Simulation Results 81

Chapter 7: Preliminary Study of Multiple Pier Systems 88
7.1. Overview of the Multiple Pier System 88
7.2. Superstructure Model 89
7.3. Preliminary Results 90
Chapter 8: Conclusions 93
References 94

Chapter 1

Introduction

Replacement of the SR 300–Saint George Island Causeway bridge near Apalachicola, Florida, with a new bridge now under construction has provided an opportunity to directly measure, through experimental means, the impact forces and related structural response parameters that are produced during barge collision events. After the new St. George Island causeway bridge opens to traffic in the Fall of 2003, full-scale barge impact tests will conducted on the existing structure before it is demolished.

Due to the scope and complexity of this research study, the overall effort is being conducted in separate phases of effort:

- Phase I : Feasibility Study
- Phase II : Design of Instrumentation Systems
- Phase III : Preparation, Testing, and Analysis of Results

Phase I consisted of a feasibility study that examined the effect of the proposed barge impact testing on the bridge replacement project. Phase I also included a thorough review of previously conducted testing and preliminary numeric simulation of the proposed barge impact conditions. Detailed information regarding the tasks undertaken and results produced during the Phase I study are presented in the Phase I final report [1].

Phase II has focused primarily of designing instrumentation systems and resolving logistical issues (scheduling, coordination with the construction contractor, permitting, barge acquisition, etc.). In addition, the numerical impact simulation activities initiated during Phase I have also been continued. During Phase II, finite element impact simulations have been used to: design the impact load-cell array that will be used during the physical testing; choose data collection sensors (e.g. load-cells and accelerometers);

adjust the planned sequence of impact-tests (in response to changes that have occurred in the contractor's construction and demolition schedules); and further examine the relationship between dynamic barge impact loads and the equivalent static loads specified in the AASHTO provisions.

Phase III of the barge impact project is currently underway and includes fabrication of physical test devices, full-scale impact testing of the St. George Island Causeway bridge, processing and reduction of test data, and interpretation of the test data.

The remainder of this report documents the key activities that have been carried out during the Phase II project in preparation for the full-scale experimental tests. In addition, selected numerical simulations that provide insight into possible future revisions to code-based impact load determination are also presented.

Chapter 2

Development of Instrumentation Packages

2.1 Introduction

In a normal laboratory event, many obstacles are faced when attempting to record large amounts of data at a high sampling rate. These obstacles become increasingly difficult in the situation of a large-scale collision, such as a jumbo hopper barge impacting a bridge pier. First, the proper instrumentation required to capture the various data from the event must be identified, provided with their necessary power requirements, and then placed in the proper locations throughout the system. Output from these sensors must be recorded while minimizing the amount of random voltage (noise) introduced into the data channels. Data stored in one portion of the system must also be time synchronized with data stored in all other portions for post-processing purposes. All of these components of the system must withstand not only a variety of environmental conditions, but also the stresses introduced from the impact event.

2.2 Overview of instrumentation network

The general setup of the instrumentation network will include various sensors that measure the response of the system to the impact. These sensors will then be connected to the data acquisition (DAQ) system, which will perform signal conditioning and analog to digital (A/D) conversion of the signal. In addition, the DAQ system will be connected to a data storage device to store the conditioned digital signal along with proper time stamps. The general setup for each network is summarized in Figure 2.1.

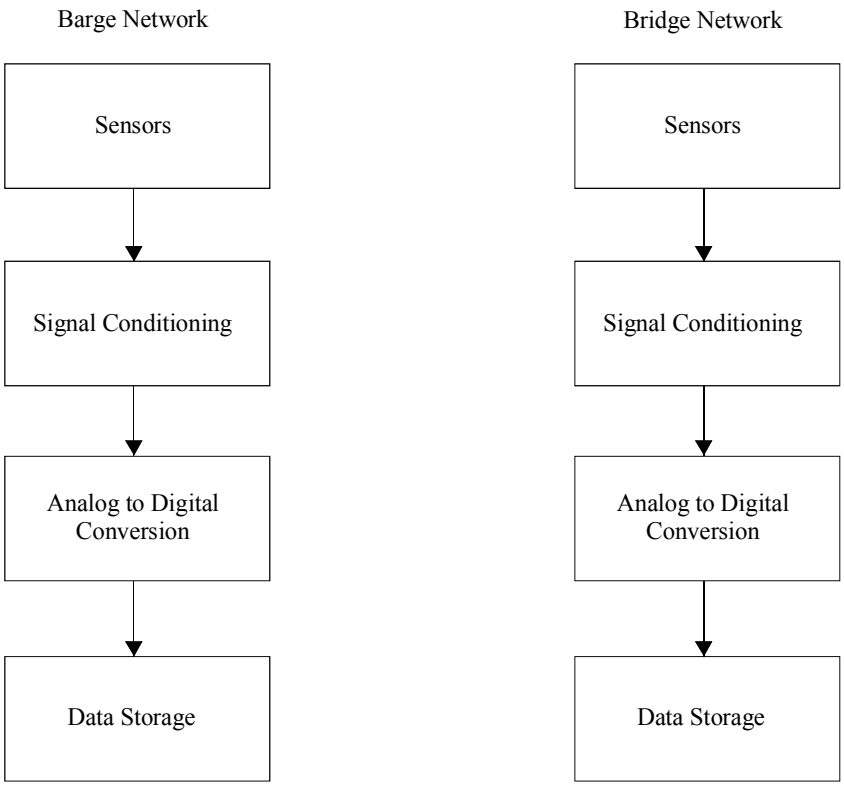

Figure 2.1 - General setup for instrumentation networks

Sensors used in the system will include accelerometers, strain gages, and load cells. Accelerometers will be placed at various locations on the bridge and on the barge to record the acceleration time histories at those positions. A displacement history can then be recovered for each acceleration history by integrating the signal twice with respect to time. Strain gages will be mounted to the piles below Pier-3 in order to measure the pile deformations during impact. Load cells will be placed at the point of impact to measure the force between the barge and the pier.

The data acquisition system in both networks includes a signal conditioner and an analog to digital signal converter. The signal conditioner provides a low-pass filter that filters out noise introduced by the leads that connect each sensor to the signal conditioner. Each signal conditioning card that will be used allows 8 to 32 differential inputs. Analog

signals from the sensors are converted to digital data by the DAQ system, and subsequently stored in the data storage device.

A laptop computer will be used not only to store data for post processing, but also to do real time polling of the various components of the system. Two laptop computers will be required for the experiment: one for the pier network and one for the barge network. The time histories in each network will be related either in real time through a wireless network communication link, or through post-processing by matching the initial sensor readings to their respective time stamps on each system.

2.3 Load cell array

A load cell array will be used to measure the dynamic impact load between the barge and the bridge pier. The load cell array will be positioned at the impact faces of pier-1 (Figure 2.2) and pier-3 (Figure 2.3). Two separate load cell arrays will be created—one for Pier-1 (Figure 2.4) and another for Pier-3 (Figure 2.5). The anticipated loads imparted to Pier-1 and Pier-3 are composed of a lateral force—predicted to be less than 1500 kips and 600 kips respectively, and a vertical force due to the friction between the barge and pier, predicted to be less than 600 kips and 200 kips for Pier-1 and Pier-3 respectively.

An 8" thick concrete impact face will mimic the friction between the barge and pier, and also distribute the load to the individual clevis pin load cells. The biaxial clevis pin load cells will measure both components of impact force. The load cell array will also be rigid enough to not alter the dynamic interaction between the barge and the pier during impact.

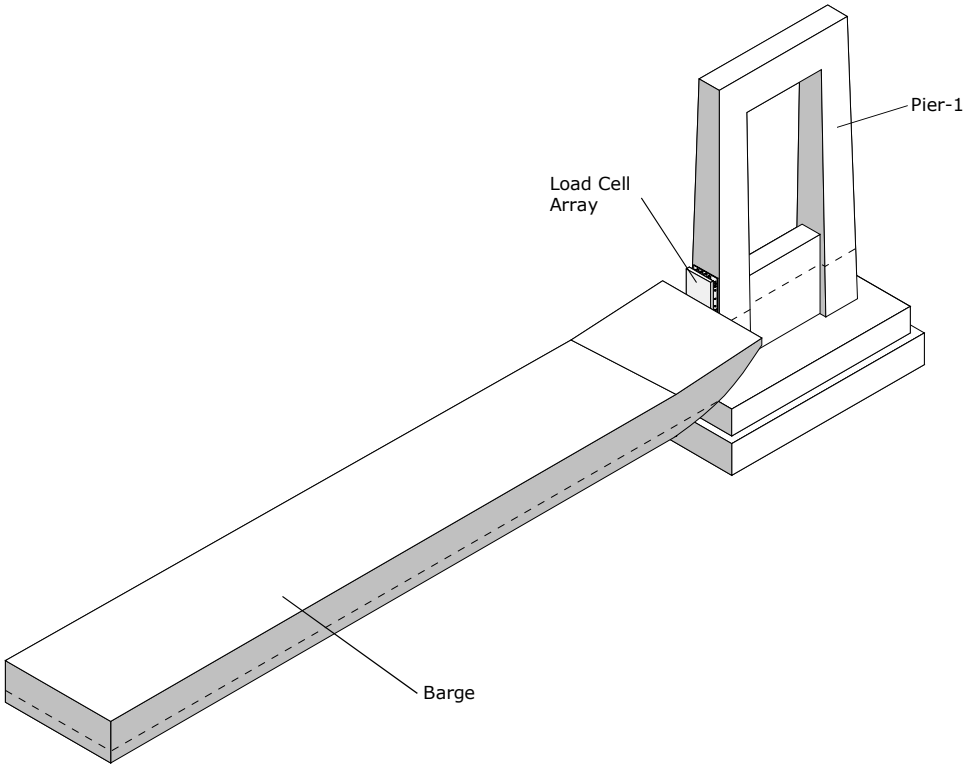

Figure 2.2 - Pier-1, Barge and Load Cell Array for Pier-1

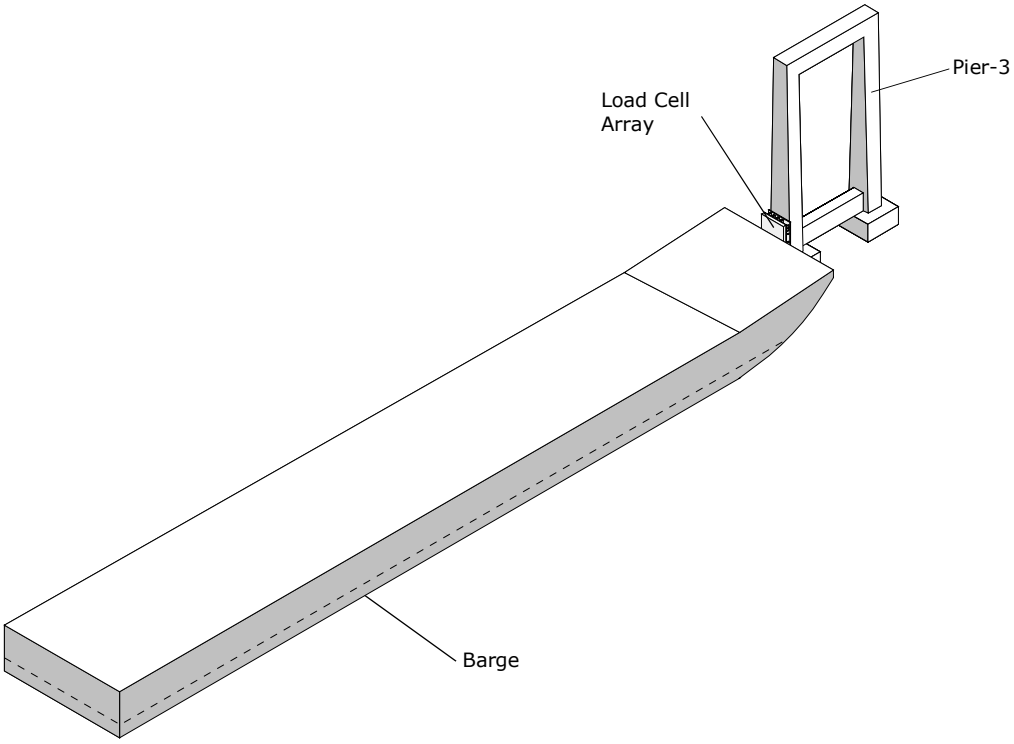

Figure 2.3 - Pier-3, Barge and Load Cell Array for Pier-3

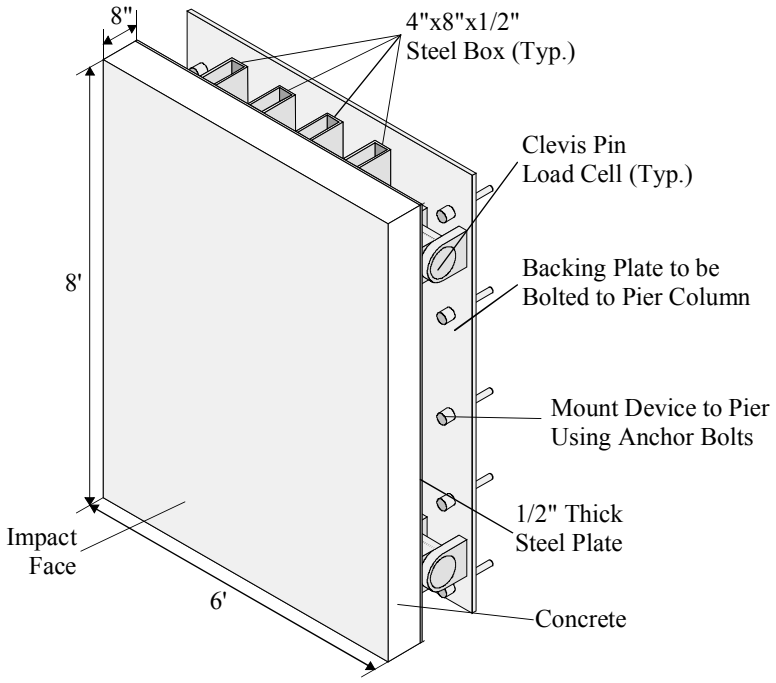

Figure 2.4 - Load Cell Array for Pier-1

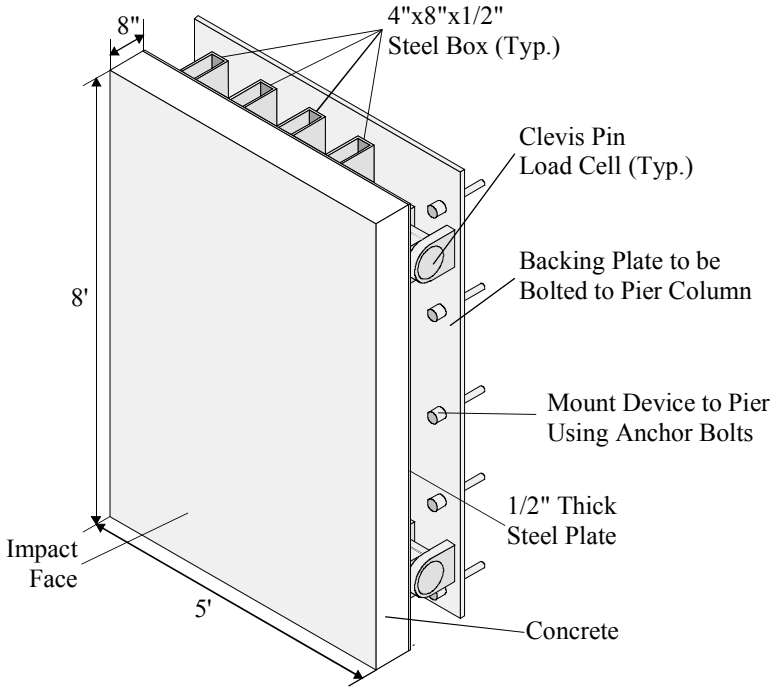

Figure 2.5 - Load Cell Array for Pier-3

2.4 Sensor Position Identification Scheme

Sensor positions on the barge, piers, and superstructure are shown in Figures 2.6 through 2.9. These positions are identified using the following notation: *I-JK*, where *I* is the pier number (1,3), barge (B), or superstructure (S); *J* is the sensor location; and *K* is the direction of the axis of measurement. For example, an accelerometer placed on pier-1 at position 3 (Figure 2.6), and measuring acceleration in the X direction would be designated as "Position 1-3X". This identification scheme is used throughout the remainder of this report.

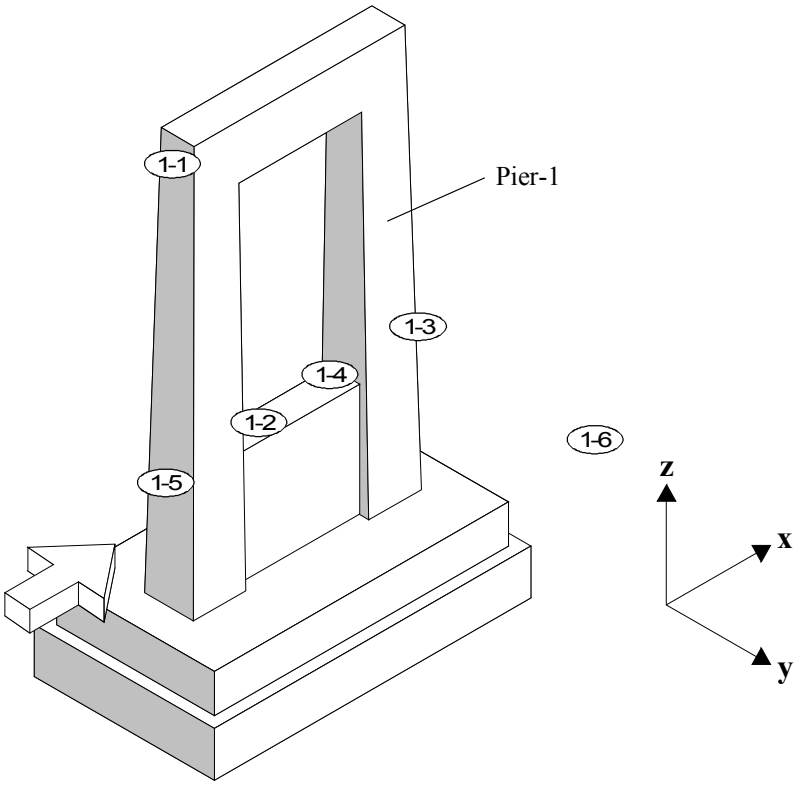

Figure 2.6 – Pier-1 Sensor Locations

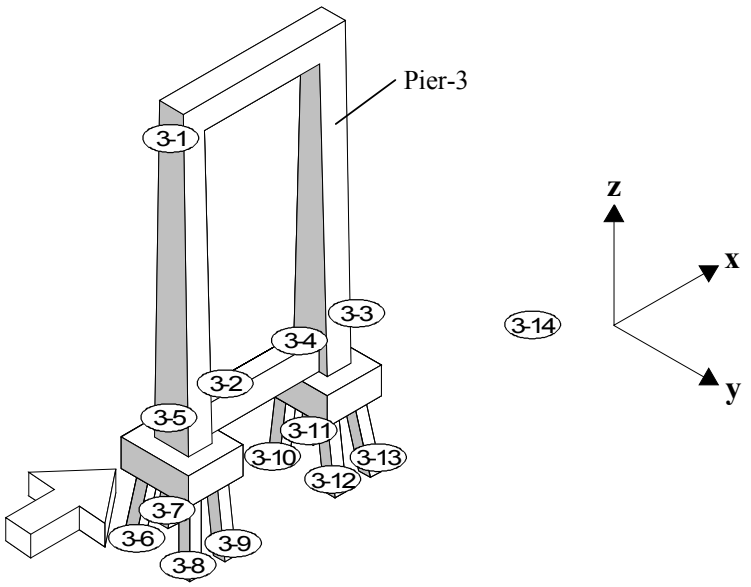

Figure 2.7 – Pier-3 Sensor Locations

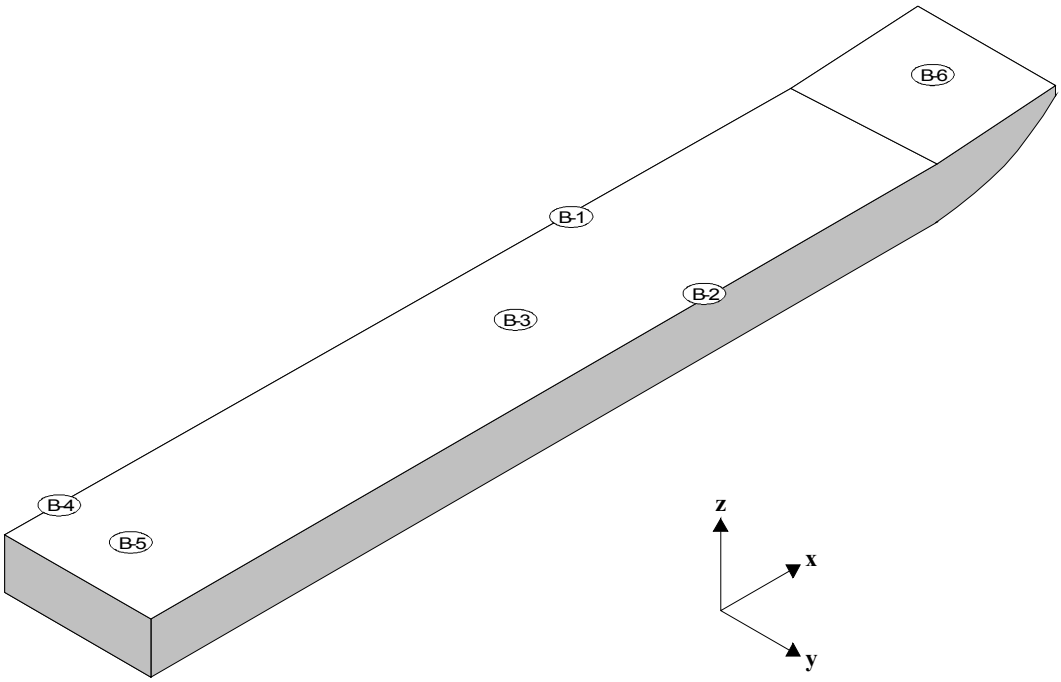

Figure 2.8 – Barge Sensor Locations

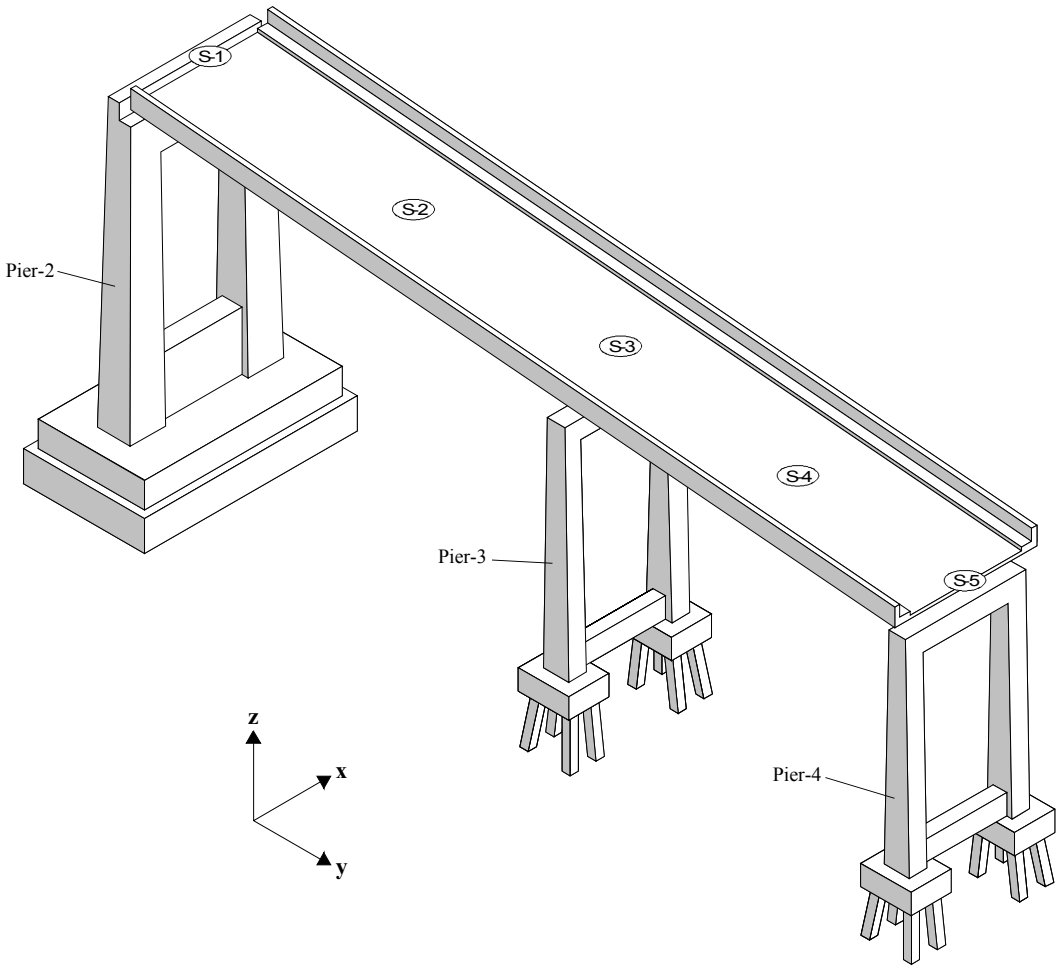

Figure 2.9 – Superstructure Sensor Locations

2.5 Instrumentation setup for Pier-1

The instrumentation setup for Pier-1 will consist of accelerometers, load cells, and the necessary power requirements for each sensor. The DC power supply for the entire system will be provided by a series of car batteries with a voltage regulator located on impact pier. This setup will also include a data acquisition system with a signal conditioner to filter the incoming signals from the sensors, a data acquisition card to perform the digital to analog conversion, and a laptop to store the filtered data with its proper time stamp. Figure 2.10 shows the instrumentation setup for Pier-1.

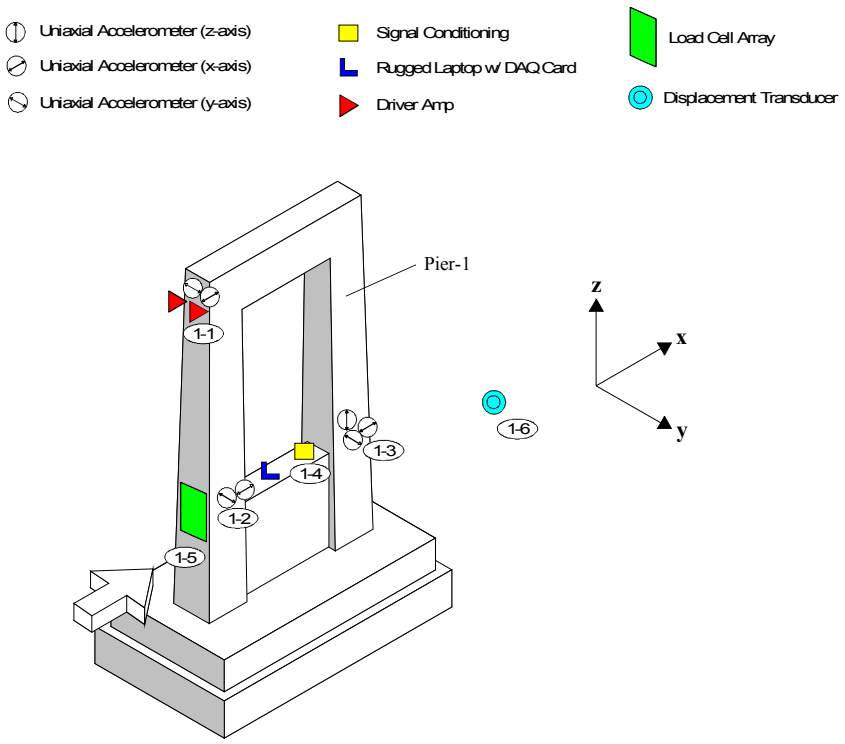

Figure 2.10 - Pier-1 instrumentation setup

The uniaxial accelerometers are positioned to best recover the overall motion of the pier in all three directions, as well as its rotation about each of these axes. Accelerometers that are more that 10 ft from the signal conditioner will need a driver amp to allow the voltage to travel the long lead lengths

A series of signal conditioning cards will take in each sensor lead and filter the data. Each signal conditioning card will provide low-pass filters for a maximum of 32 differential channels of data. The signal conditioning chassis is shock resistant and will survive the impact event, but must be housed in an enclosure to ensure that the terminal block connections are not exposed to the elements.

The data acquisition card will receive the data from each of the signal conditioning cards and perform the A/D conversions for each channel. The DAQ card will be placed in one of the external slots of the rugged laptop computer where the data

will finally be stored. Rugged laptops function the same as regular laptops but are manufactured to pass military specifications for shock and vibration. Furthermore, the laptop will not be damaged by exposure to the elements, and has its own battery power supply, which will also provide power to the DAQ card.

2.6 Instrumentation Setup for Pier-3 Test with Superstructure

The general setup for the impact on Pier-3 with the superstructure attached will be similar to the setup for Pier-1 but will include additional sensors. Underwater strain gages will be placed on the concrete piles below the pier and additional accelerometers will be located on the superstructure and adjacent Piers 2 & 4, as shown in Figure 2.11.

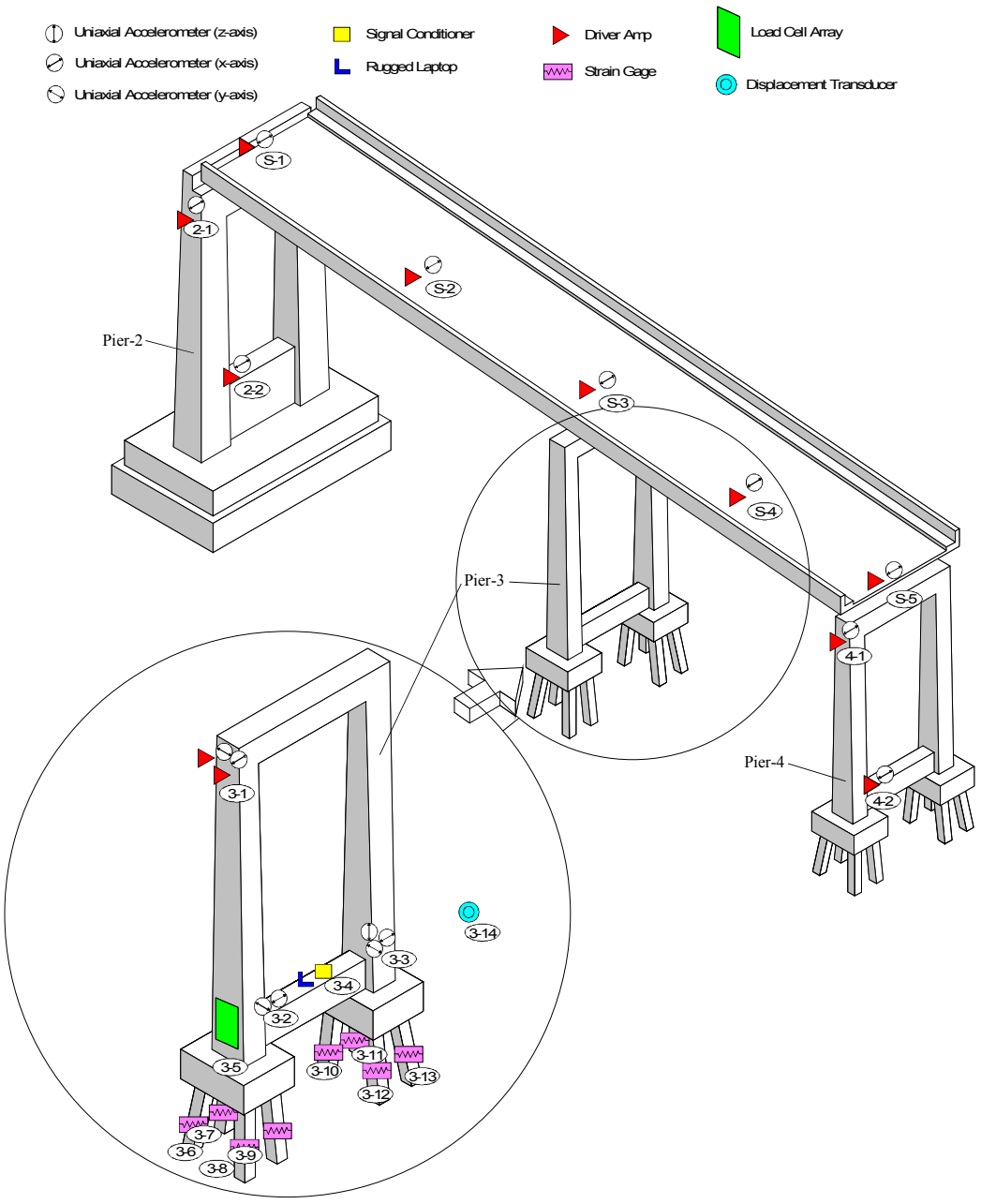

Figure 2.11 - Pier-3 with Superstructure Instrumentation Setup

Data acquisition will be identical to the system on Pier-1; including the signal conditioning, the A/D conversion, and the data storage (which will take place directly on the impact pier).

2.7 Instrumentation Setup for Pier-3 Test without Superstructure

The instrumentation setup for the pier-3 test without the superstructure will be similar to the prior setup with strain gages on the concrete piles, load cells on the impact face, but with accelerometers attached only to the pier. As shown in Figure 2.12, the sensors, power supply, and data acquisition placement will be the same as in the two previous setups.

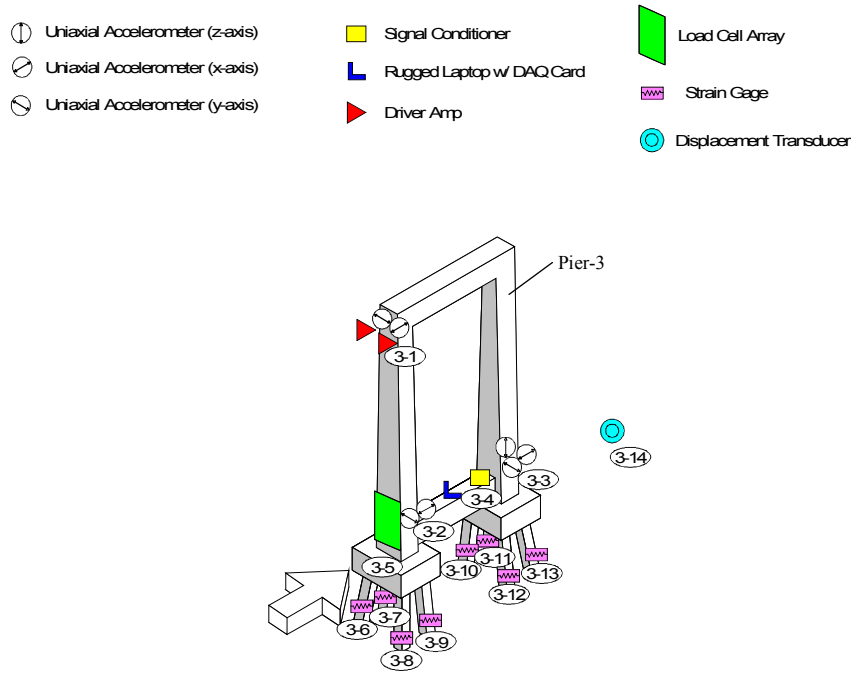

Figure 2.12 - Pier-3 without Superstructure Instrumentation Setup

2.8 Barge instrumentation

Sensors on the barge (Figure 2.13) will include accelerometers to track the motion of the vessel during impact and a device for measuring the crush deformation of the barge hull.

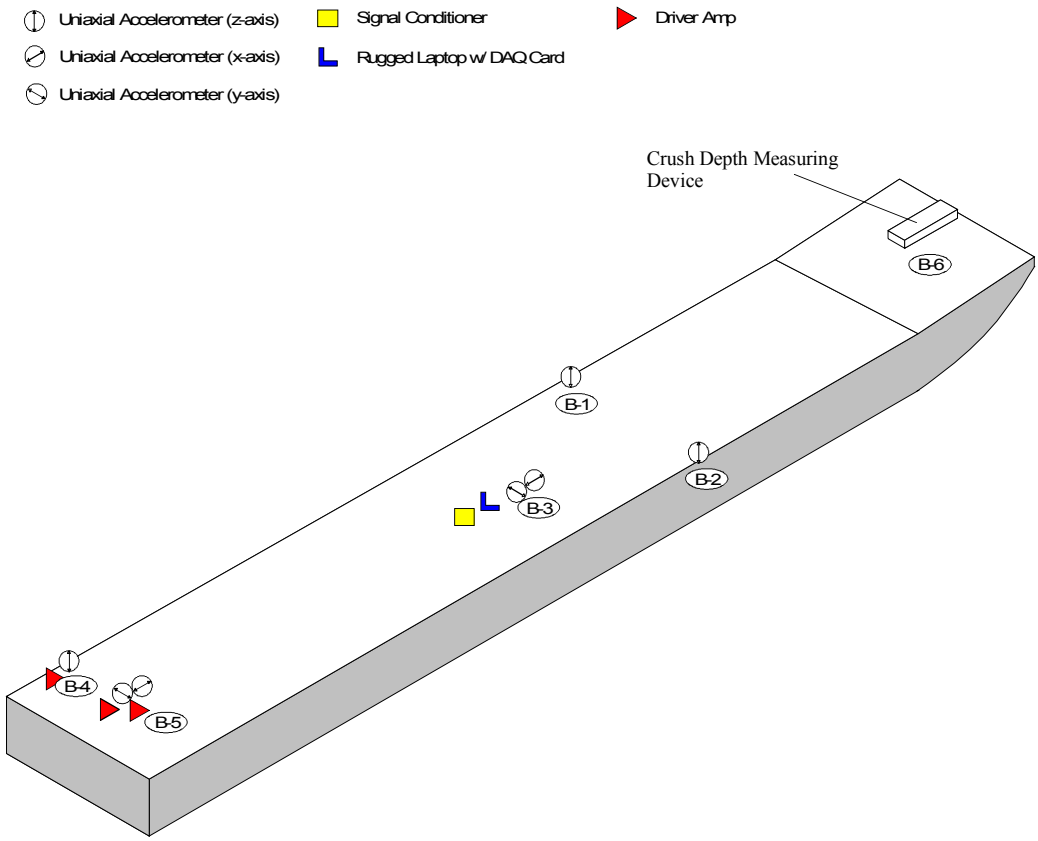

Figure 2.13 - Barge Instrumentation setup

The data acquisition setup will be similar to the pier instrumentation setups, with the sensor output conditioned by signal conditioning cards, the A/D conversion performed by the DAQ card, and data storage in a laptop computer. A series of car batteries with a voltage regulator will provide a DC voltage supply to the components of the system on the barge.

2.9 Tracking motion

Motion of the barge will be monitored by accelerometers placed on the vessel, as shown in Figure 2.13. Acceleration data measured during the impact event will later be used to determine the motion of the barge in all three directions, as well as the rotation about each of its axes.

2.10 Rationale for sensor selection

The selection of each sensor was based on cost and ability to measure expected magnitudes of acceleration, force, strain, etc. taken from finite element simulations of the impact conditions. Detailed information for the selection of accelerometers and strain gages are given in the following sections.

2.10.1 Accelerometers

According to the simulations, the accelerometers must be able to accurately record accelerations below 10 g's. They must also have a low pass filter capable of filtering out high frequency noise, while capturing all of the frequency content critical to recovering displacement histories.

Many accelerometers on the market are very good at measuring high frequency motions, but cannot measure relatively low frequency motion such as the movement of a bridge pier during impact. For example, piezoelectric accelerometers, while commonly used because of their low price and high g ranges, cannot record low frequencies accurately due to the manner in which these sensors measure acceleration. Piezoelectric accelerometers contain piezo-crystals, usually quartz, that produce a voltage when subjected to stress. However, when this type of accelerometer is subjected to low or constant accelerations, the piezo-crystals are not stressed sufficiently to produce a measurable voltage.

Piezoresistive accelerometers, on the other hand, use resistors in a half or full bridge setup with a voltage passed across them and are typically much more expensive than piezoelectric accelerometers. When a force is applied to the sensor, the resistance increases and the voltage output of the sensor decreases as a function of the force applied. The problem with the piezoresistive accelerometer is that they are typically used for

higher accelerations (>100g), and thus would not be very sensitive to the low accelerations (<10g) generated during the barge impacts being conducted in this project.

Capacitive accelerometers cost approximately the same as piezoresistive accelerometers. They consist of a small mass connected to the outer housing by many small arms. The change in strain of these arms is a function of the applied accelerations. Capacitive accelerometers are very accurate at low levels of acceleration (<100g) and have a high enough limit on the low pass filter to capture the full frequency content of the displacement history (~400Hz). For these reasons, the capacitive accelerometer will best fit the requirements of this project.

Modeled Accelerations

The range of each accelerometer was chosen based on maximum accelerations obtained from LS-DYNA simulations. Originally, the selection of the accelerometer ranges was based directly on acceleration histories taken from simulation results. However, these acceleration histories contained large spikes, well above 5 g's. Performing Fast Fourier Transforms on these histories showed that the spikes were at very high frequencies, which were not critical in recovering displacement histories. Therefore, the desired acceleration histories were found by double differentiating the displacement histories at the various accelerometer positions in the system (Figure 2.14 to Figure 2.41).

The acceleration ranges were taken from impact scenarios resulting in maximum acceleration histories. Since low accelerations are expected in the Y-direction in scenarios where the impact is intended to be purely in the X-direction (Figures 2.15, 2.19, 2.31 and 2.37). Y-direction acceleration histories were also taken from a case where the barge impacted pier-1 five-degrees from the X-direction (Figures 2.40 and 2.41). These

accidental, off-center impacts will provide ranges for Y-direction accelerometers, which would ideally record 0 g's on an impact purely in the X-direction.

One-knot, Half-loaded Barge Impact on Pier-3

In the following pages, acceleration histories are shown for LS-DYNA impact simulations conducted on pier-3 with a half-loaded barge, traveling at a speed of one-knot (see Figure 2.14 through Figure 2.28). This data was then used to select accelerometers with appropriate ranges.

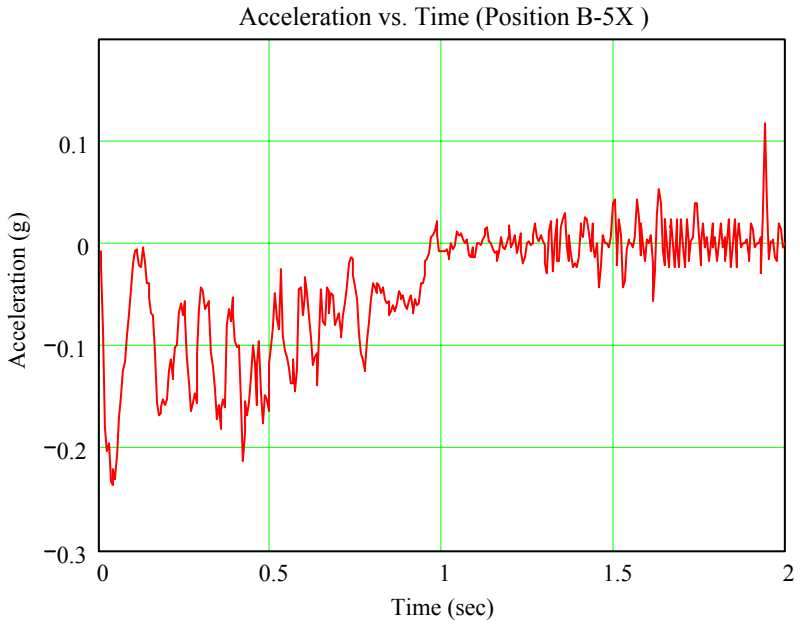

Figure 2.14 – Acceleration history at B-5 in the X direction

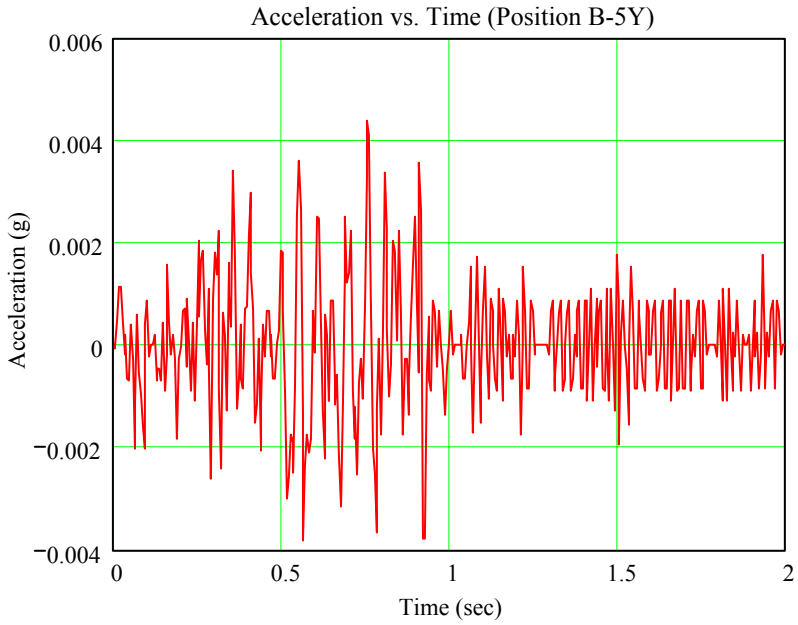

Figure 2.15 – Acceleration history at B-5 in the Y direction

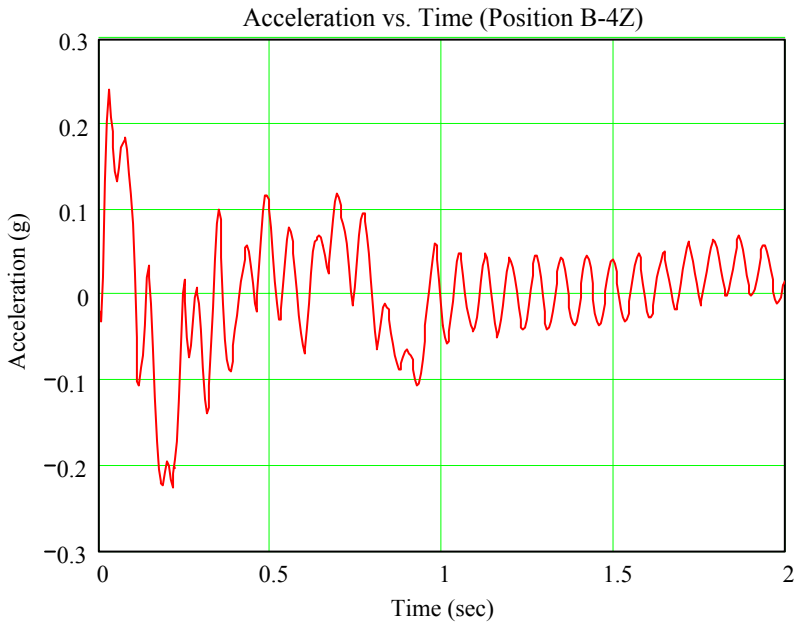

Figure 2.16 – Acceleration history at B-4 in the Z direction

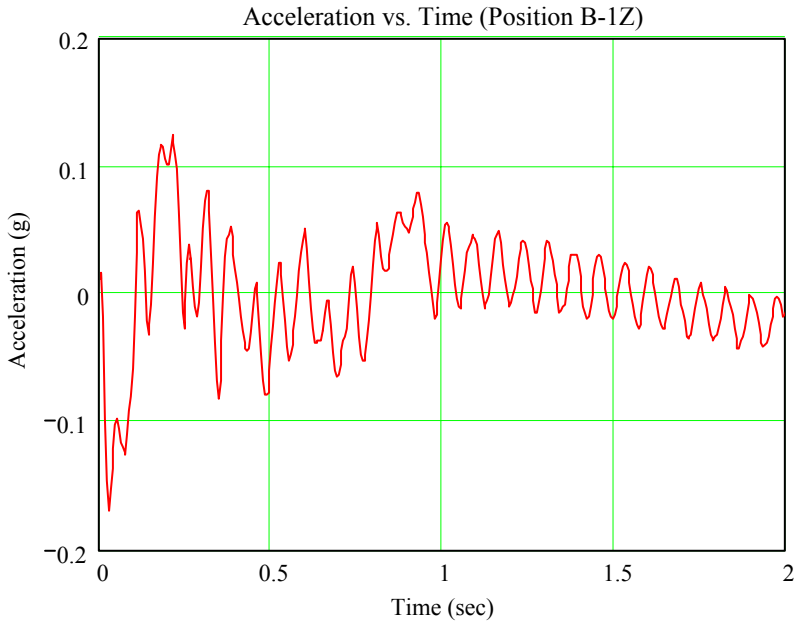

Figure 2.17 – Acceleration history at B-1 in the Z direction

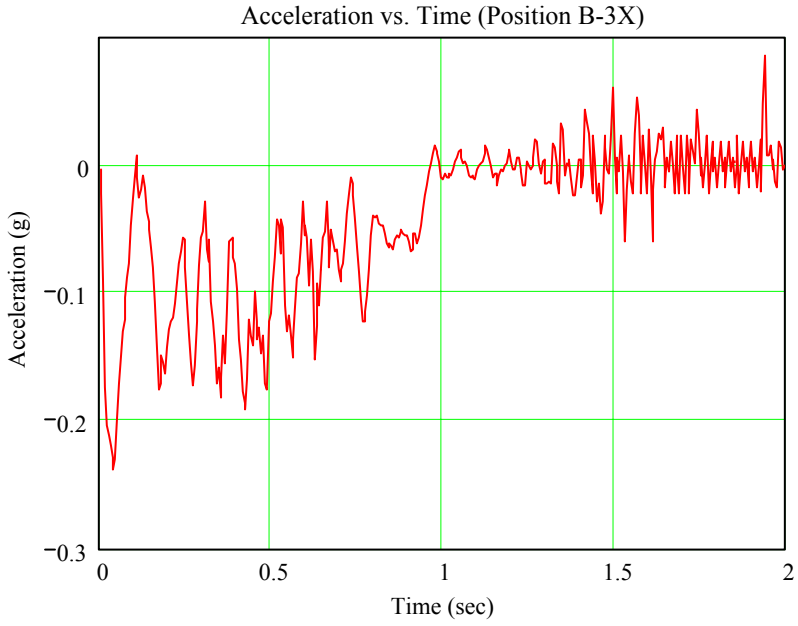

Figure 2.18 – Acceleration history at B-3 in the X direction

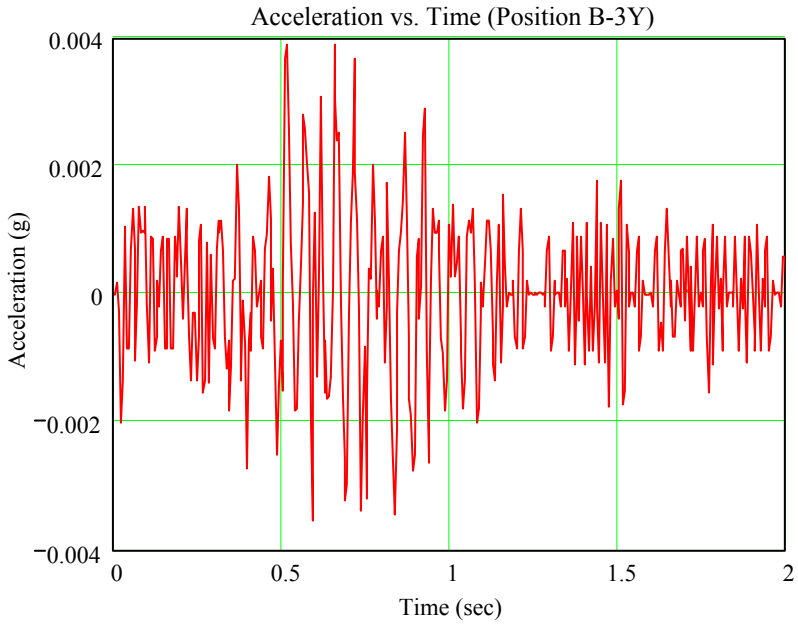

Figure 2.19 – Acceleration history at B-3 in the Y direction

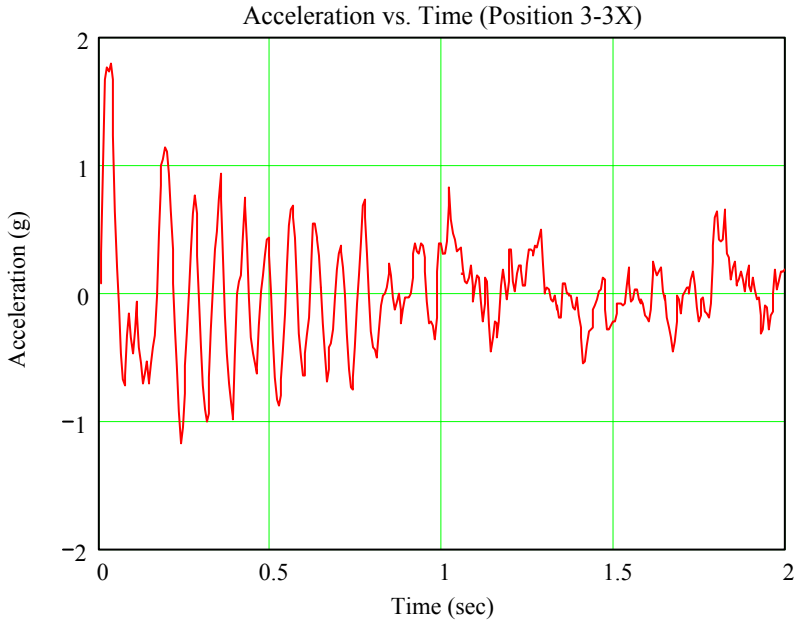

Figure 2.20 – Acceleration history at 3-3 in the X direction

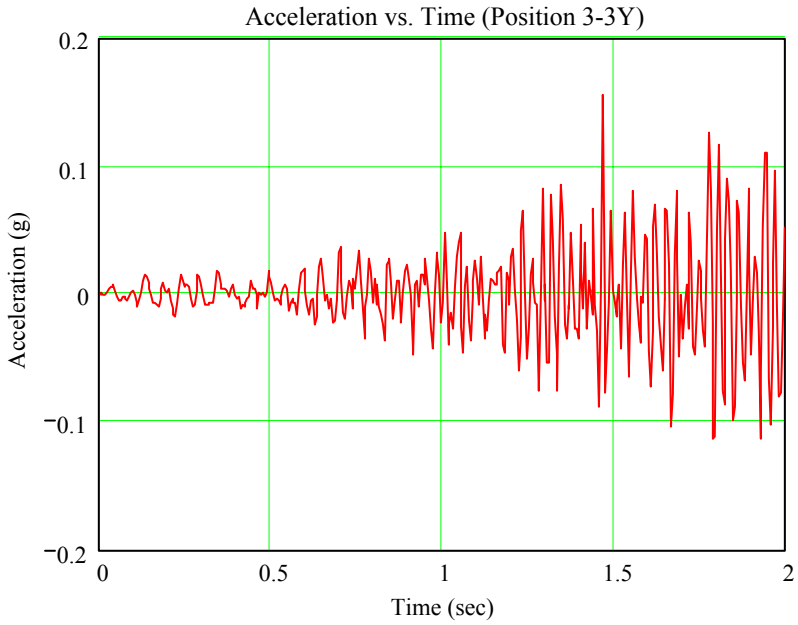

Figure 2.21 – Acceleration history at 3-3 in the Y direction

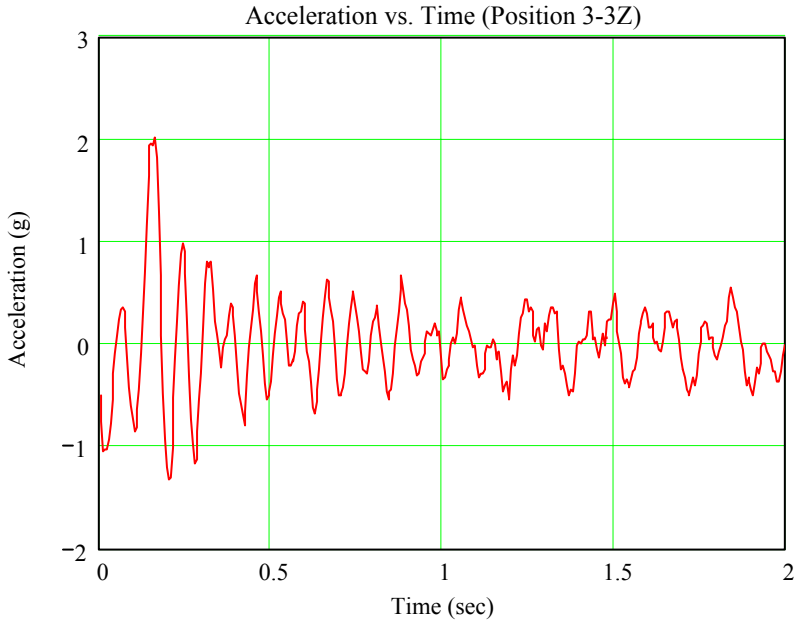

Figure 2.22 – Acceleration history at 3-3 in the Z direction

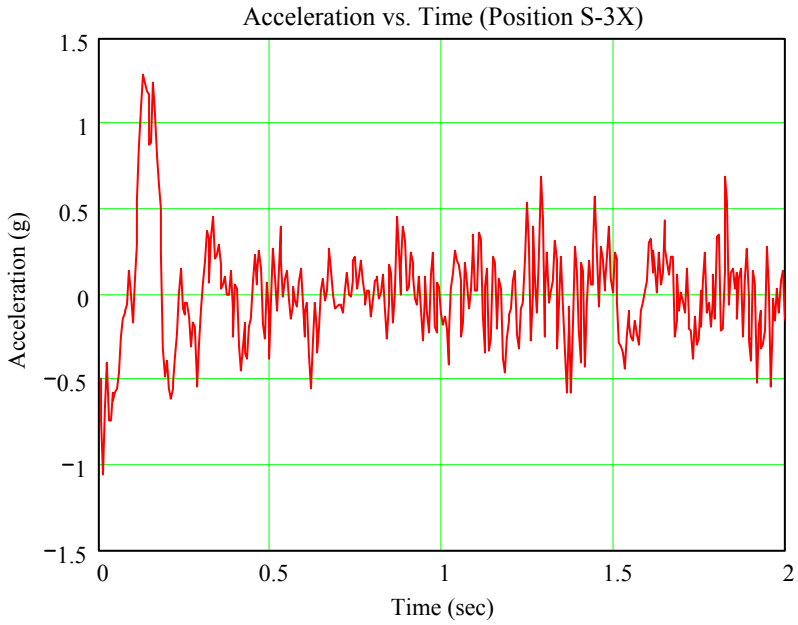

Figure 2.23 – Acceleration history at S-3 in the X direction

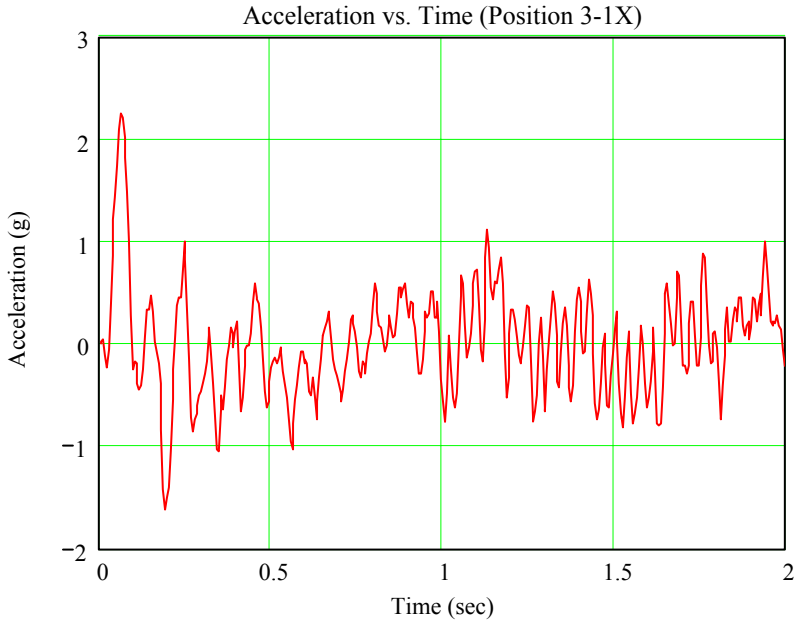

Figure 2.24 – Acceleration history at 3-1 in the X direction

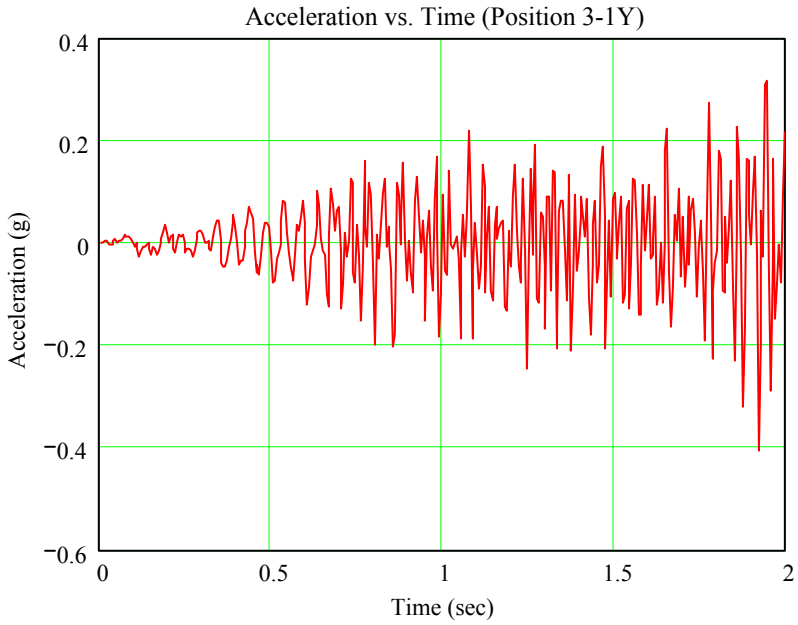

Figure 2.25 – Acceleration history at 3-1 in the Y direction

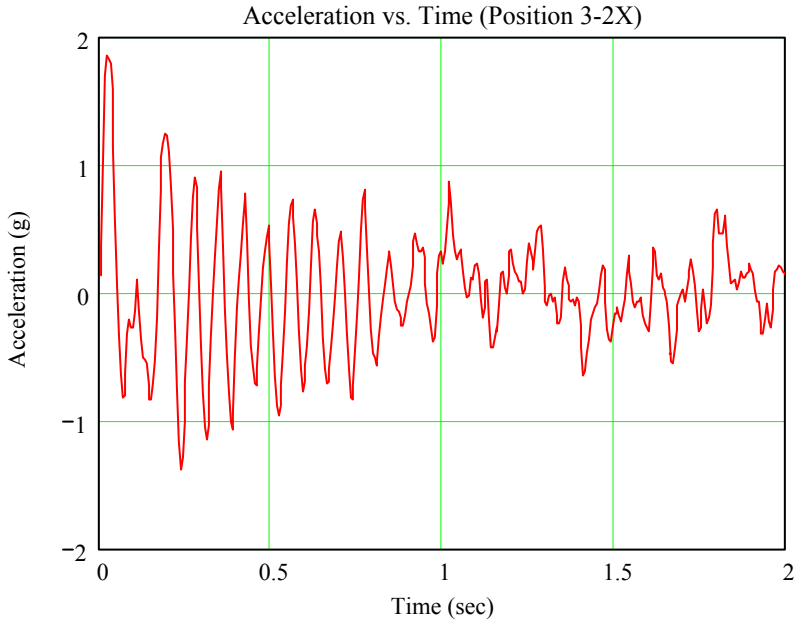

Figure 2.26 – Acceleration history at 3-2 in the X direction

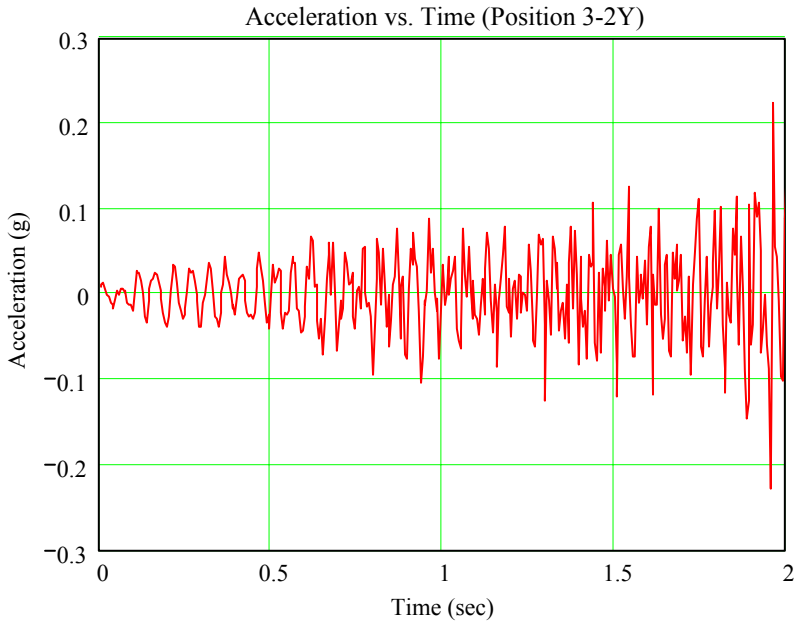

Figure 2.27 – Acceleration history at 3-2 in the Y direction

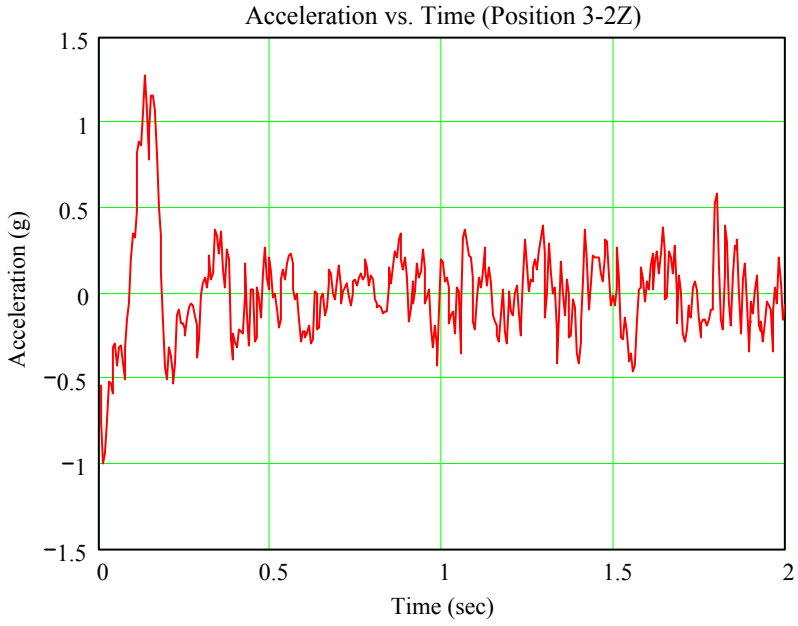

Figure 2.28 – Acceleration history at 3-2 in the Z direction

Six knots, Half-loaded Barge Impact on Pier-1

The following acceleration histories were obtained from simulations conducted on Pier-1 with a half-loaded barge traveling at six-knots (see Figure 2.29 through Figure 2.39).

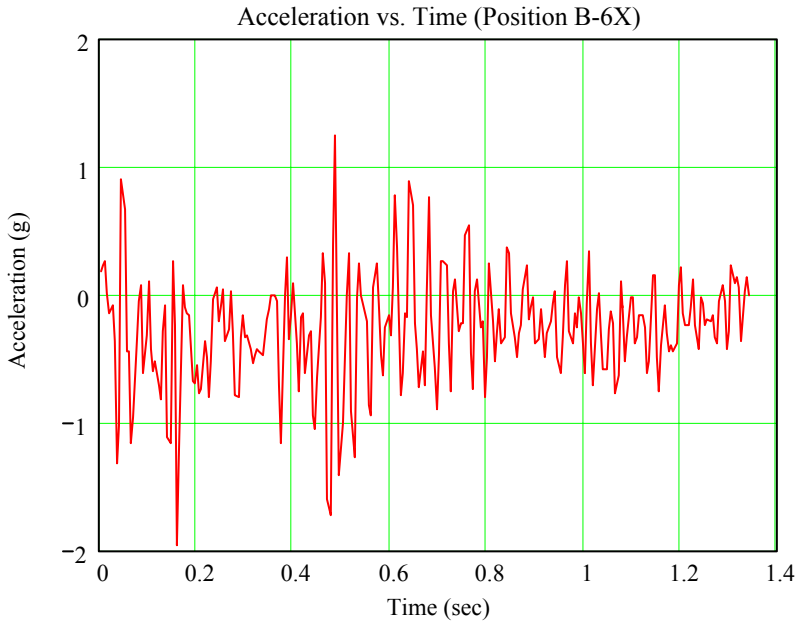

Figure 2.29 – Acceleration history at B-6 in the X direction

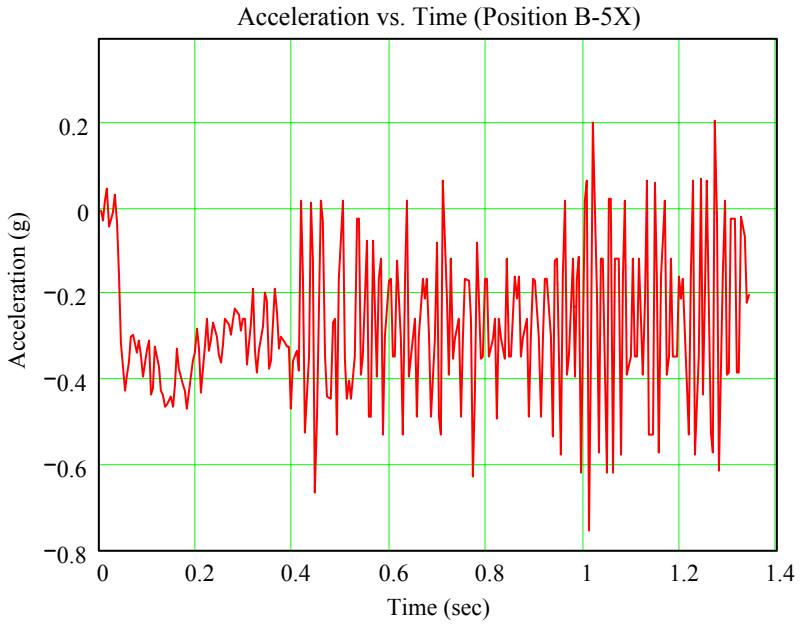

Figure 2.30 – Acceleration history at B-5 in the X direction

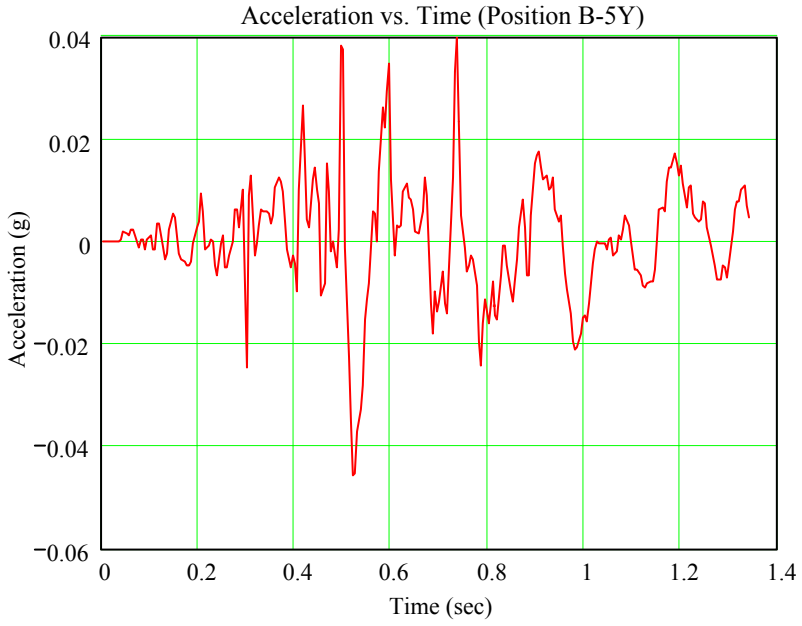

Figure 2.31 – Acceleration history at B-5 in the Y direction

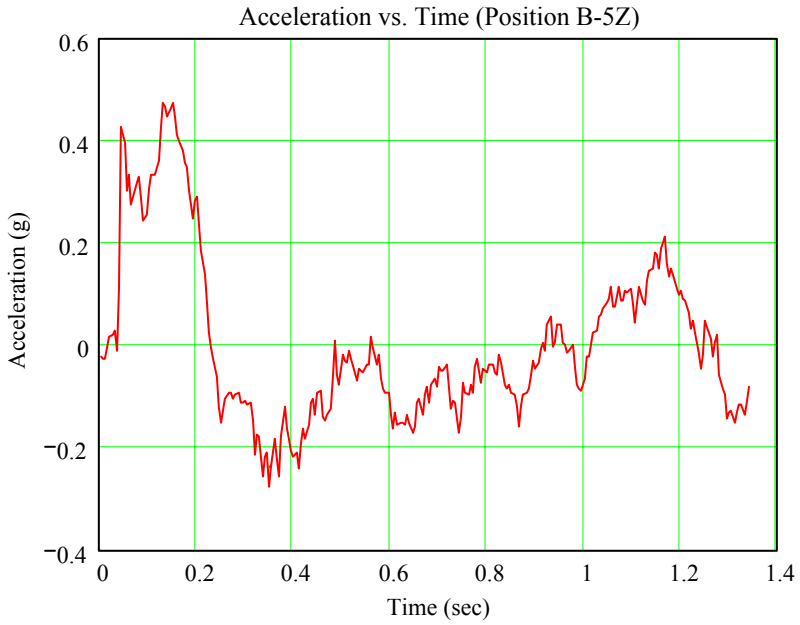

Figure 2.32 – Acceleration history at B-5 in the Z direction

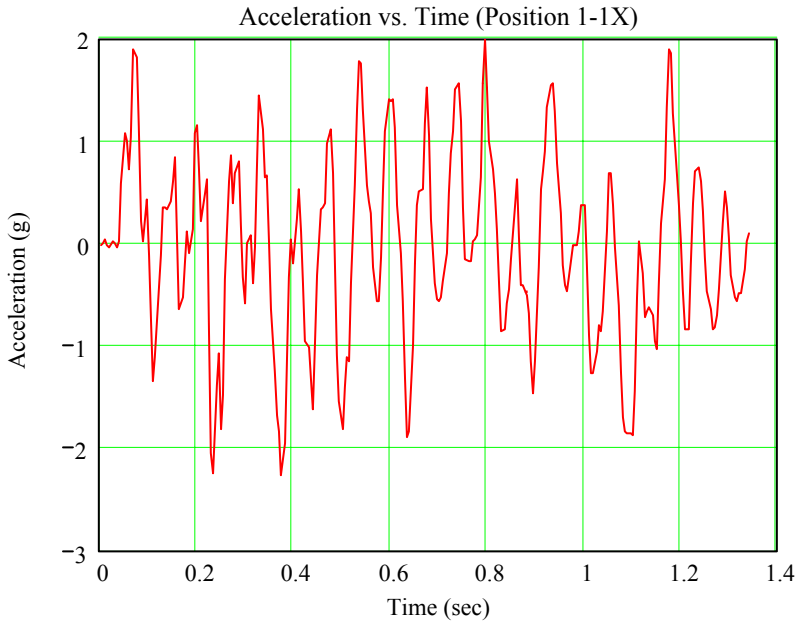

Figure 2.33 – Acceleration history at 1-1 in the X direction

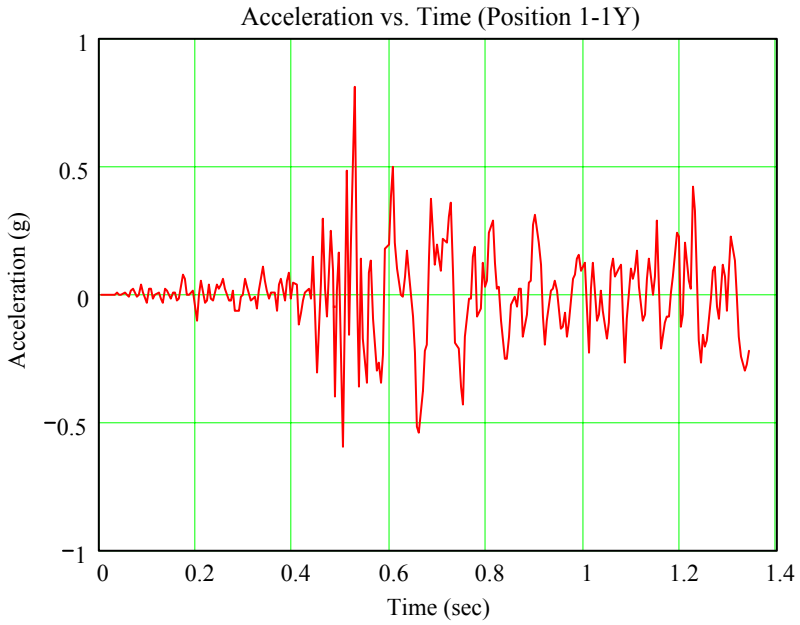

Figure 2.34 – Acceleration history at 1-1 in the Y direction

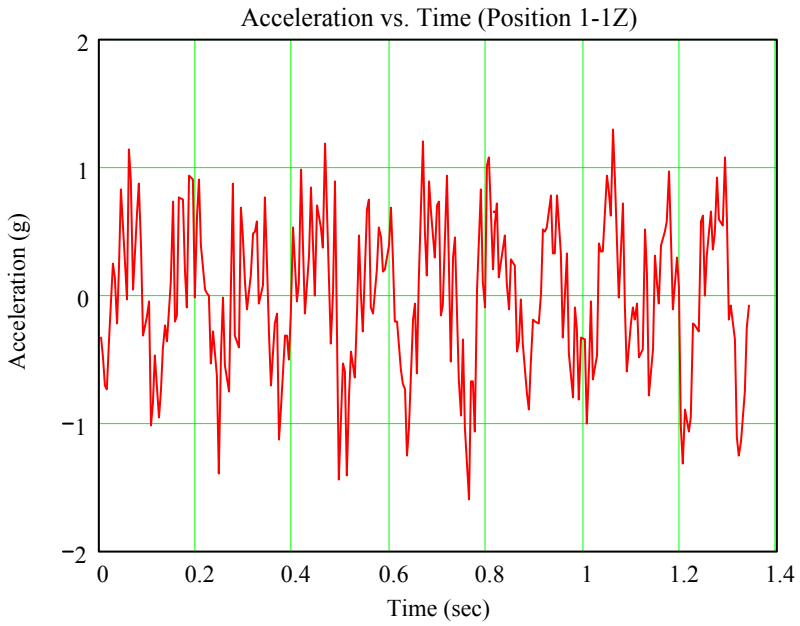

Figure 2.35 – Acceleration history at 1-1 in the Z direction

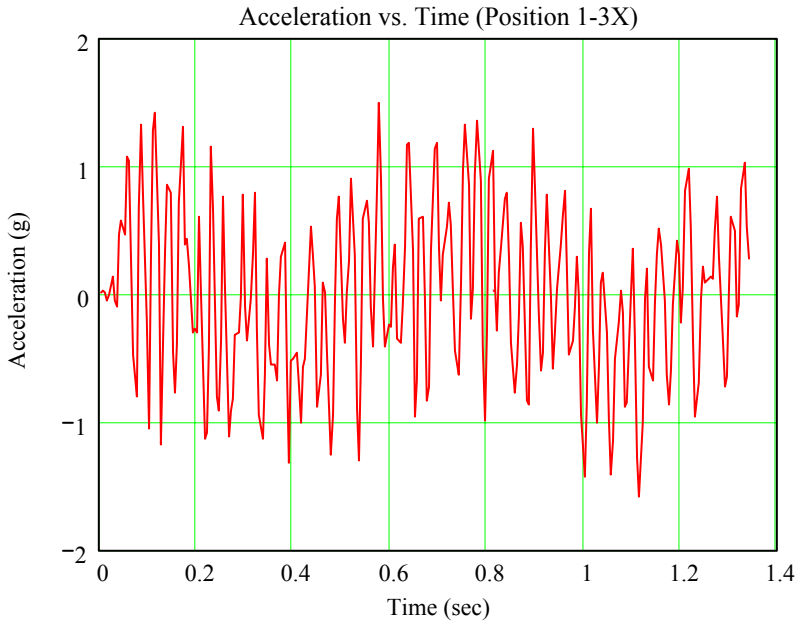

Figure 2.36 – Acceleration history at 1-3 in the X direction

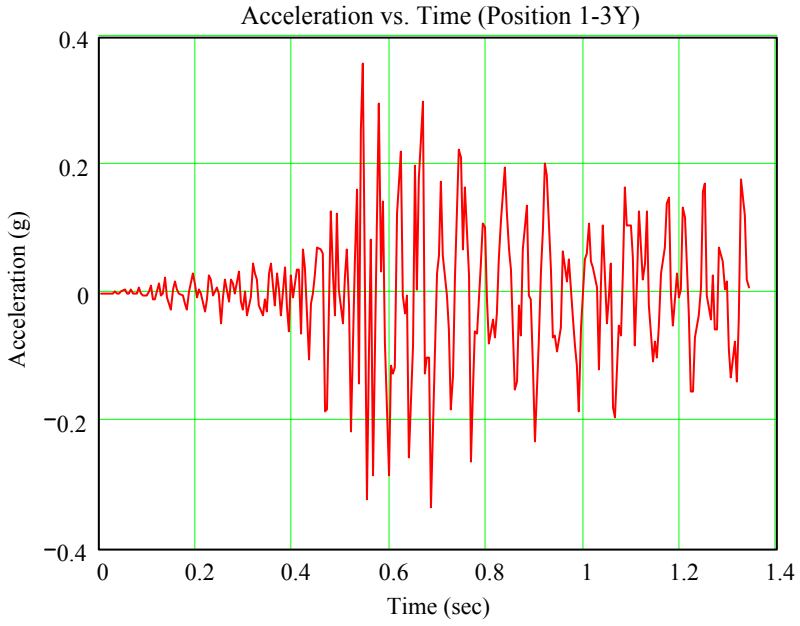

Figure 2.37 – Acceleration history at 1-3 in the Y direction

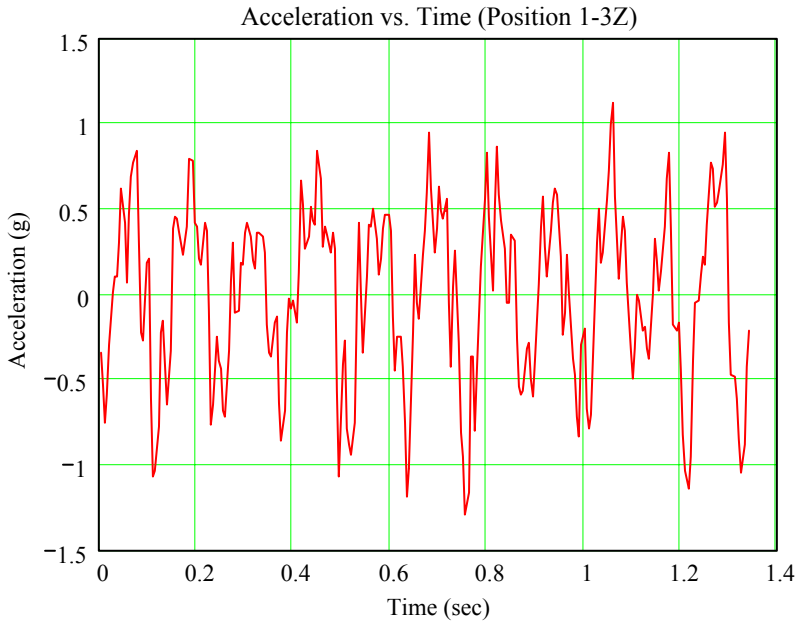

Figure 2.38 – Acceleration history at 1-3 in the Z direction

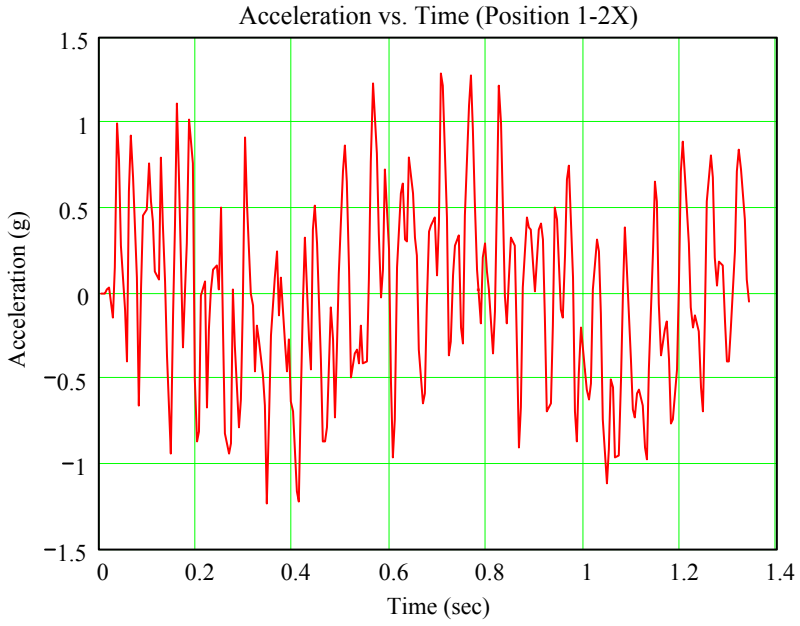

Figure 2.39 – Acceleration history at 1-2 in the X direction

Five knot, One-third Loaded Barge Impact on Pier-1

Acceleration histories were recovered from a simulation involving a one-third-loaded barge traveling at a speed of five-knots. In addition, the barge was traveling at an angle that was five degrees from the X-axis as shown in Figure 2.6. A comparison between Figure 2.40 and Figure 2.31 shows that significant accelerations in the Y-direction can be found on the barge during an angled impact.

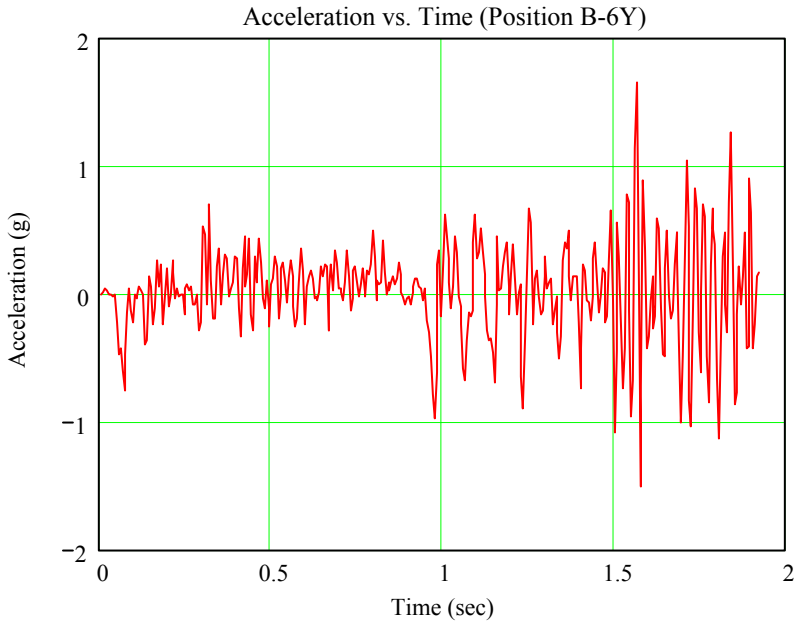

Figure 2.40 – Acceleration history at B-6 in the Y direction

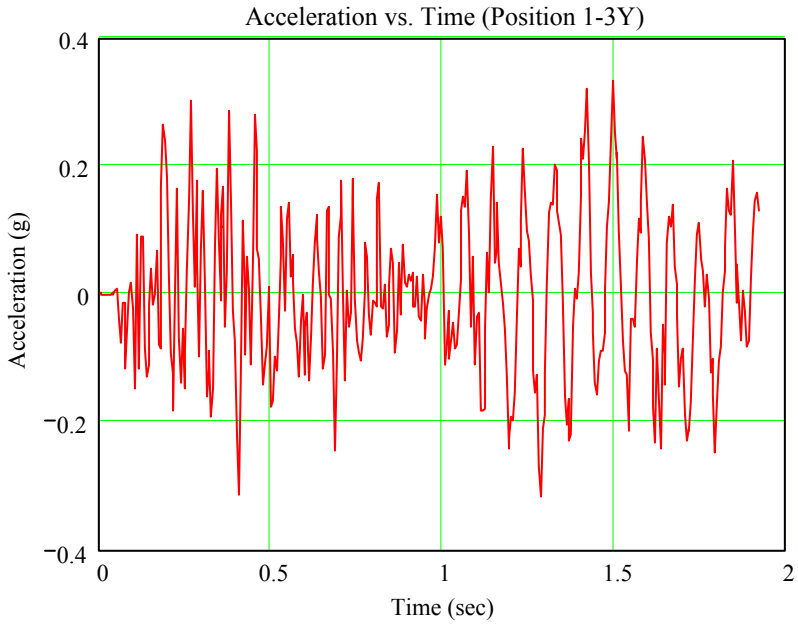

Figure 2.41 – Acceleration history at 1-3 in the Y direction

2.10.2 Strain gages

The strain gages required for this project need to measure the dynamic strain of the concrete piles below Pier-3, and must therefore be capable of operating effectively underwater. Furthermore, measuring the strain of concrete requires a gage length at least three times larger than the aggregate size of the concrete, so the strain measurement will never be taken across one piece of aggregate, but across an average mix of the components of the concrete. One of the difficult issues in measuring strain underwater is the attachment of the strain gages to the strained material. The strain gages can be pre-attached to a piece of metal and then bolted to the concrete pile, or permanently attached to the pier with an underwater curing epoxy. Both methods have been evaluated and difficulties associated with the underwater epoxy application have led to the tentative elimination of this option.

Chapter 3

Logistical Planning

3.1 Sequence of Tests

The actual event sequence schedule can be separated into three major categories. The first category involves impacts at various velocities on Pier-1 (see Figure 3.1). The second and third categories comprise impacts on Pier-3 with and without the superstructure respectively (see Figures 3.2 and 3.3). All of the impacts in the three major sequences will be conducted using a barge with a payload of approximately one-third of the barge's capacity.

During the Pier-1 impact sequence, four impacts will be conducted using the following barge velocities: one-half knot, one knot, two knots, and four knots. The purpose of this sequence is to observe the variation in results obtained from various impact conditions. After each impact, the data will be downloaded from the instrumentation network and analyzed. Furthermore, the barge and pier will be inspected to ensure the integrity of each, and to determine if the next impact is feasible.

All of the Pier-3 impacts will be conducted using only one impact velocity (one-half knot). The two Pier-3 sequences will be used to examine the effects of load redistribution to the adjacent piers though the superstructure. As with Pier-1, the results will be analyzed and the barge and pier will be inspected to assess their respective integrities between impacts.

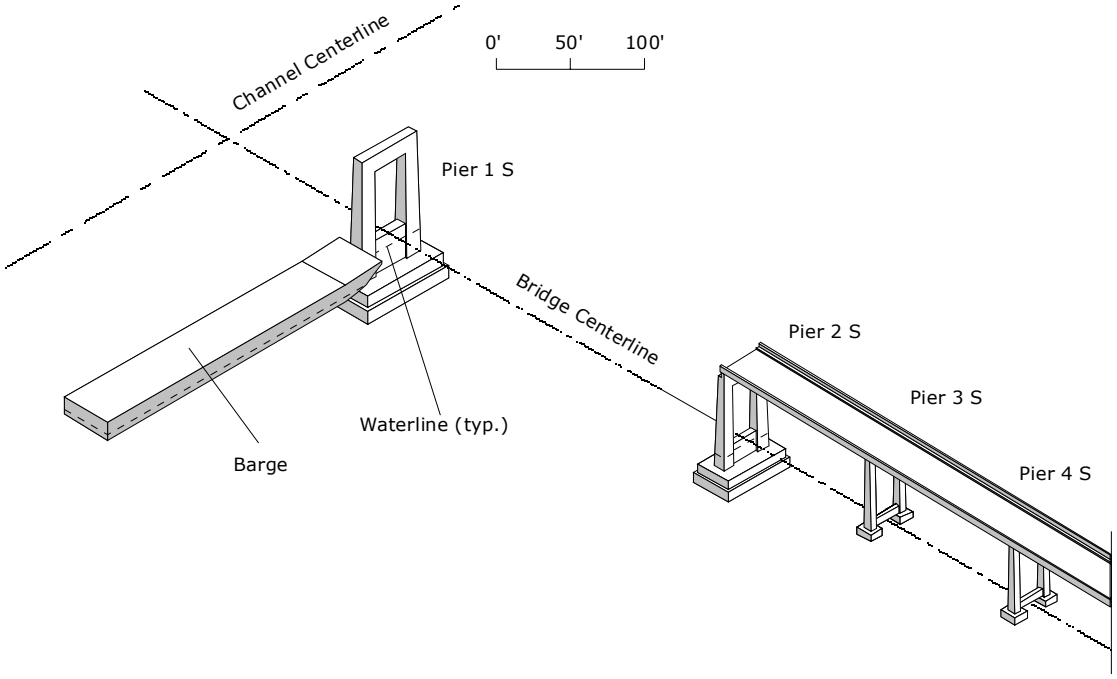

Figure 3.1. Pier-1 Impact Layout

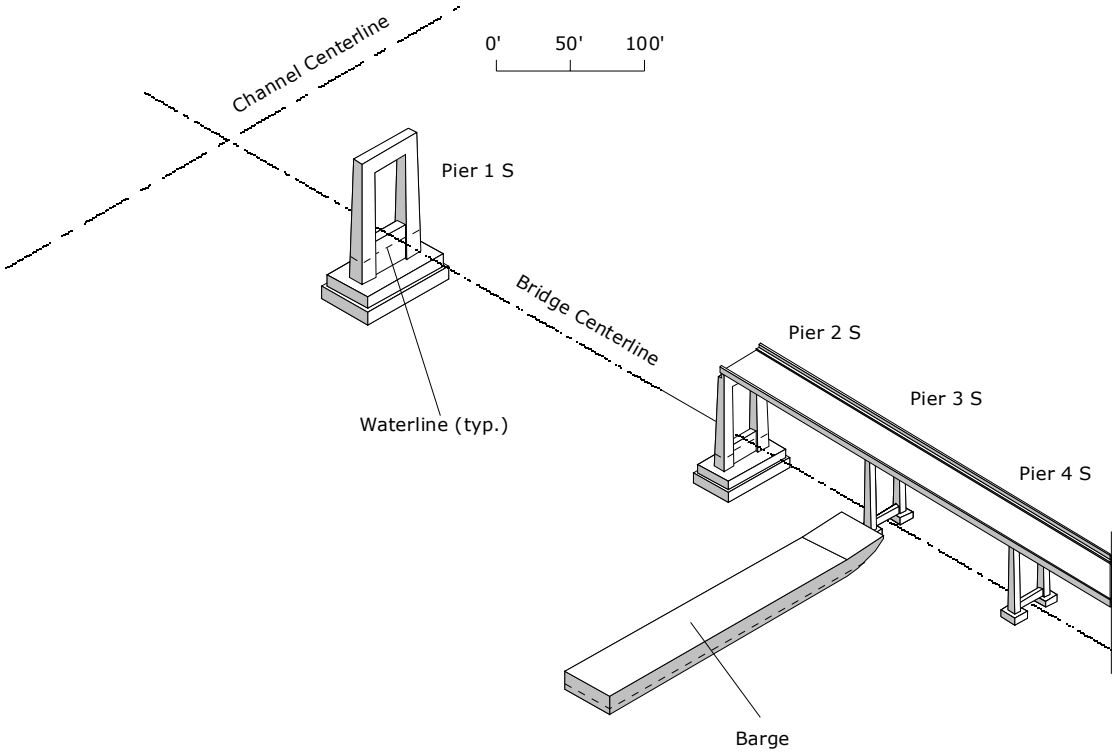

Figure 3.2. Pier-3 with Superstructure Impact Layout

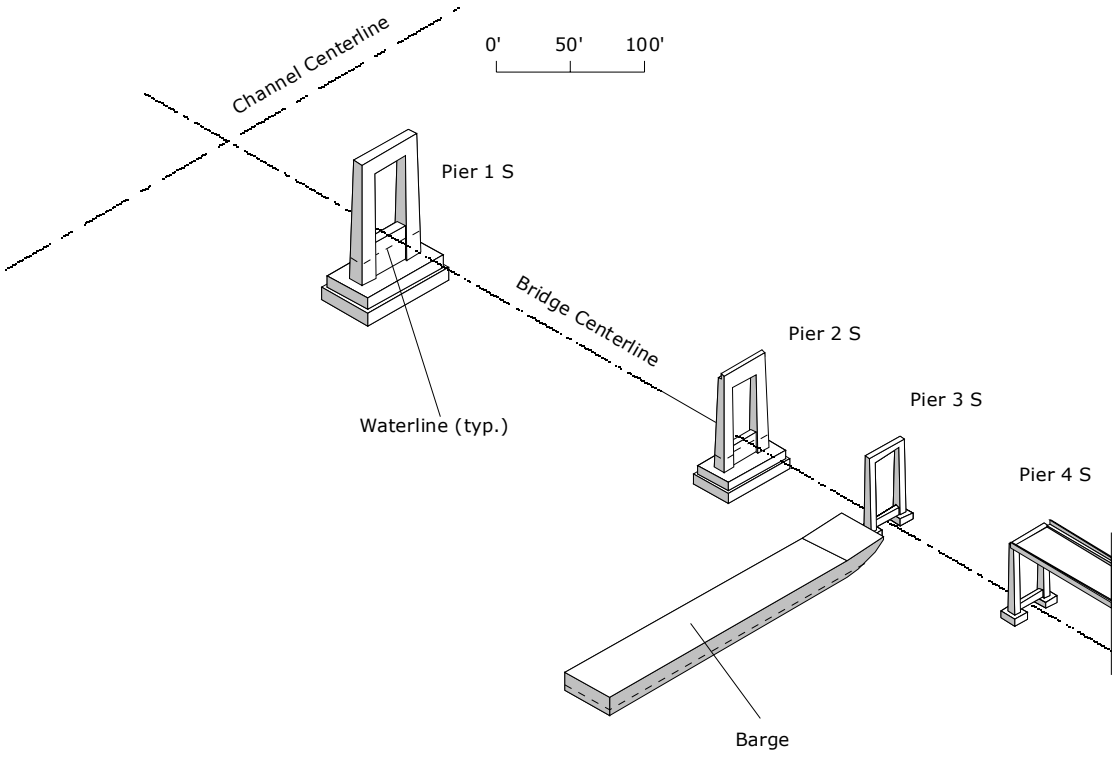

Figure 3.3. Pier-3 without Superstructure Impact Layout

3.2 Event Scheduling

The following event schedule was created to coordinate the project schedule with that of the contractor. Furthermore, the overall project schedule will be affected by the demolition schedule of the contractor due to the amount of time required to remove the superstructure of both the main span and the approach spans. In turn, the contractor's demolition schedule will be influenced by the time spent conducting the impact events, and attachment and removal of the instrumentation networks.

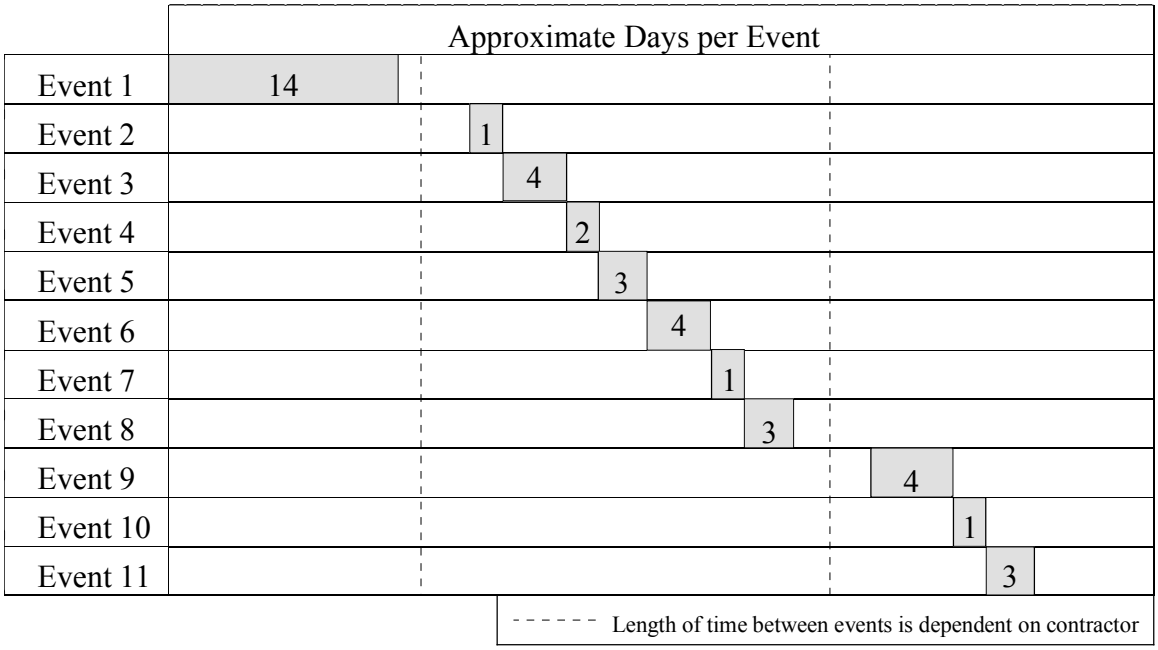

Event 1 – Initial attachment of strain gages, mounts and enclosures

Event 2 – Attachment of load cell apparatus

Event 3 – Attachment of instrumentation networks on pier-1 and barge

Event 4 – Impact events on pier-1

Event 5 – Removal of instrumentation from pier-1 including load cell apparatus

Event 6 – Attachment of instrumentation network on pier-3 and superstructure

Event 7 – Impact events on pier-3 with superstructure

Event 8 – Removal of instrumentation from pier-2, pier-3, pier-4 and superstructure

Event 9 – Attachment of instrumentation network on pier-3 without superstructure

Event 10 – Impact events on pier-3 without superstructure

Event 11 – Removal of instrumentation from pier-3 including load cell apparatus

Figure 3.4 – Approximate schedule of days per event

Event 1 - Initial attachment of strain gages, mounts and enclosures

1.1 Attach strain gages on pier-3 piles—Using scuba divers; attach eight underwater strain gages along with leads to the eight concrete piles below pier-3 (see Figure 3.5, positions 3-6 to 3-13). Leads should be at least 10 ft each and will be temporarily attached to the pier; so they can be attached to the network on pier-3 at a later date.

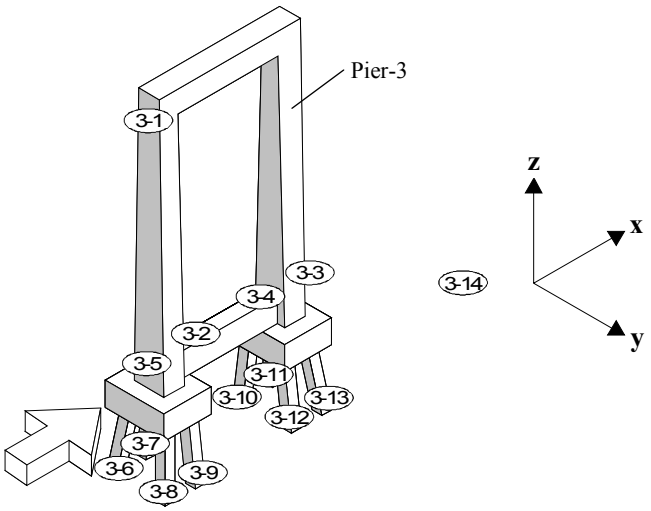

Figure 3.5 – Pier-3 positions

1.2 Attach accelerometer mounts to the top of pier-3—A 4”x4” accelerometer mount will be bolted to the concrete (Figure 3.5, position 3-1).

1.3 Attach accelerometer mounts to the impact height of pier-3 —Two 4”x4” accelerometer mounts will be bolted to the concrete (Figure 3.5, positions 3-2 and 3-3).

1.4 Attach signal conditioner, computer, and voltage supply enclosures to pier-3 (Figure 3.5, position 3-4).

1.5 Attach accelerometer mounts to the top of pier-1—A 4”x4” accelerometer mount will be bolted to the concrete (Figure 3.6, position 1-1).

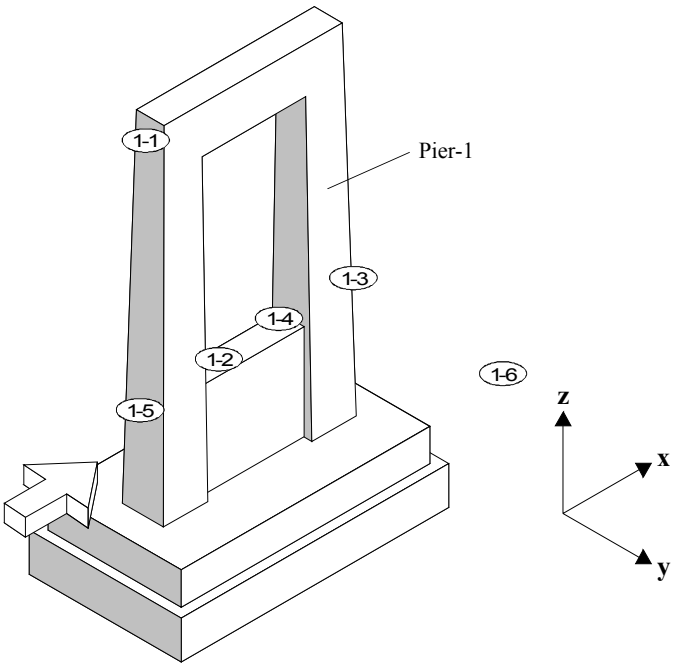

Figure 3.6 – Pier-1 positions

1.6 Attach accelerometer mounts to the impact height of pier-1—Two 4”x4” accelerometer mounts will be bolted into the concrete (Figure 3.6, positions 1-2 and 1-3).

1.7 Attach signal conditioner, computer, and voltage supply enclosures to pier-1—Three enclosures will be bolted to the shear wall; one for the computer, one for the signal conditioning chassis, and one for the voltage supply (Figure 3.6, position 1-4).

1.8 Four timber piles will be driven into the soil on the non impact side of pier-1 and pier-3 to later be attached to the displacement transducers (Figure 3.5 position 3-14, and Figure 3.6, position 1-6).

1.9 Attach accelerometer mounts to pier-2— Two 4”x4” accelerometer mounts will be bolted to the concrete (Figure 3.7, positions 2-1 and 2-2).

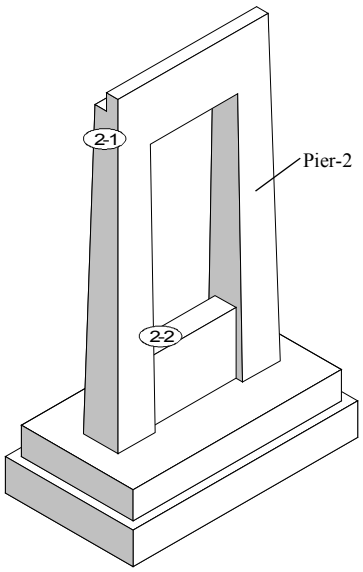

Figure 3.7 – Pier-2 positions

1.10 Attach a voltage supply enclosure to pier-2—A voltage supply enclosure will be bolted to the shear wall (Figure 3.7, position 2-2).

1.11 Attach accelerometer mounts to pier-4—Two 4”x4” accelerometer mounts will be bolted to the concrete (Figure 3.8, positions 4-1 and 4-2).

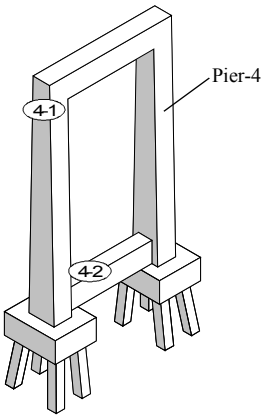

Figure 3.8 – Pier-4 positions

1.12 Attach a voltage supply enclosure to pier-4—A voltage supply enclosure will be bolted to the shear wall (Figure 3.8, position 4-2).

1.13 Attach accelerometer mounts to the pier-3 superstructure—Five 4”x4” accelerometer mounts will be bolted to the concrete (Figure 3.9, positions S-1 to S-5).

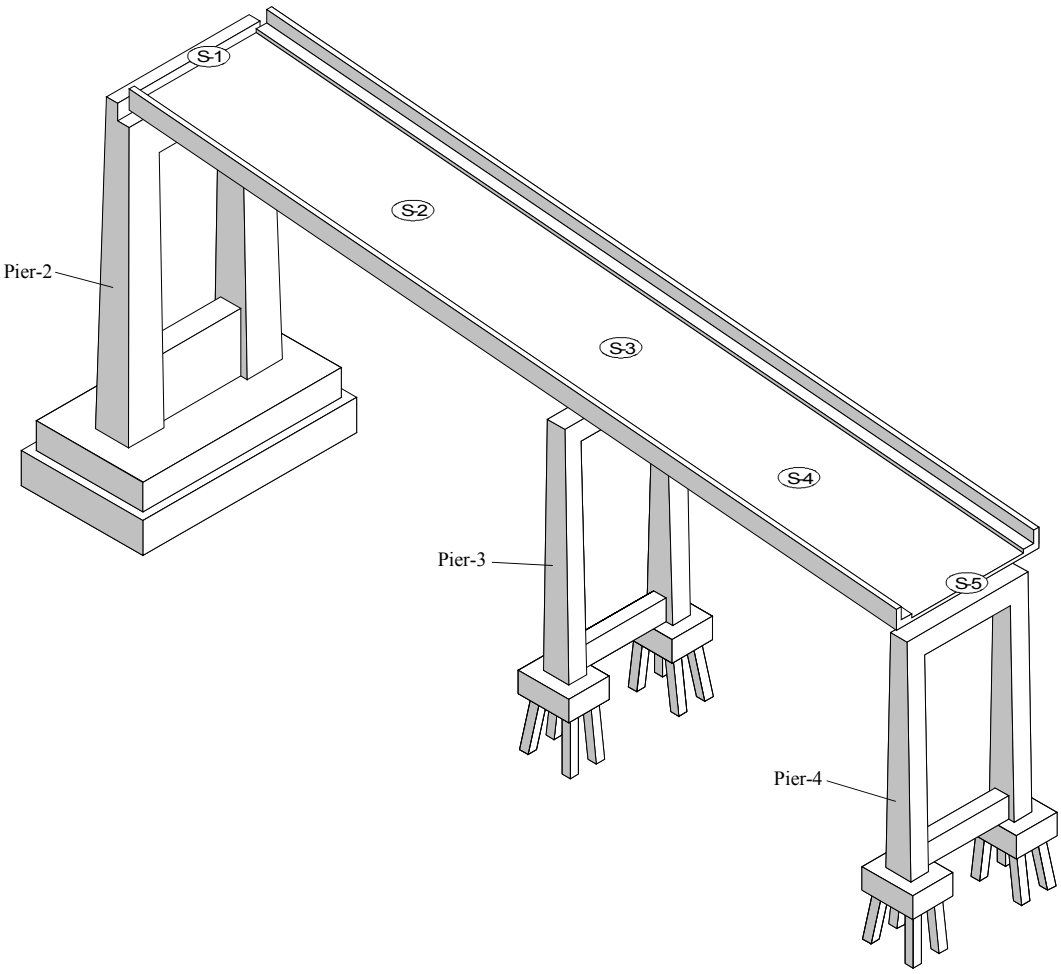

Figure 3.9 – Superstructure positions

1.14 Install anchor bolts to pier-1 and pier-3—Anchor bolts will be installed (by UF) to the pier column faces of pier-1 and pier-3, to later, mount the load cell apparatus to each pier.

Event 2 - Attachment of load cell apparatus

2.1 Attach the load cell apparatus to pier-1—Contractor to use crane to place approx. 8000 lb load cell apparatus (see Figure 3.10) on front of pier-1, and bolt it to the face of the pier column (Figure 3.6, position 1-5).

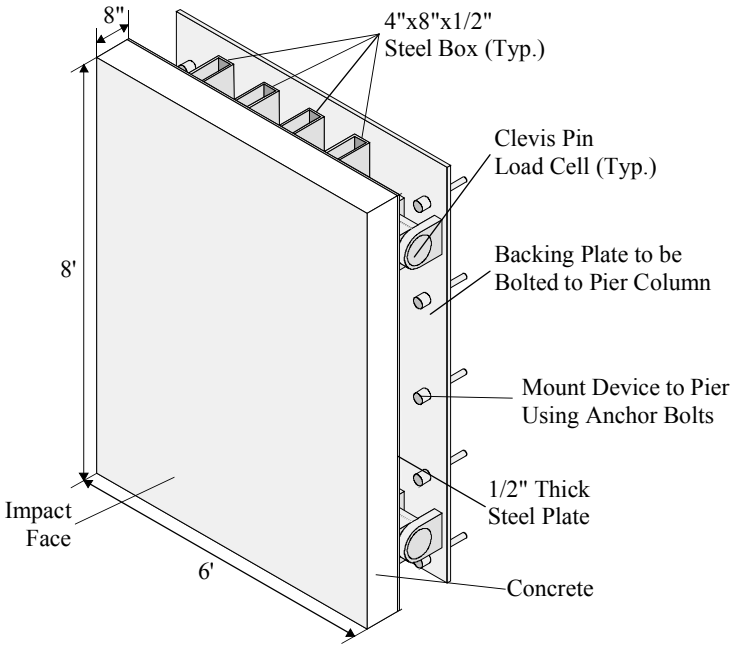

Figure 3.10 –Load Cell Apparatus for Pier-1

2.2 Attach the load cell apparatus to pier-3 —Contractor to use crane to place approx. 8000 lb load cell apparatus (see Figure 3.11) on front of pier-3, and bolt it to the face of the pier column (Figure 3.5, position 3-5).

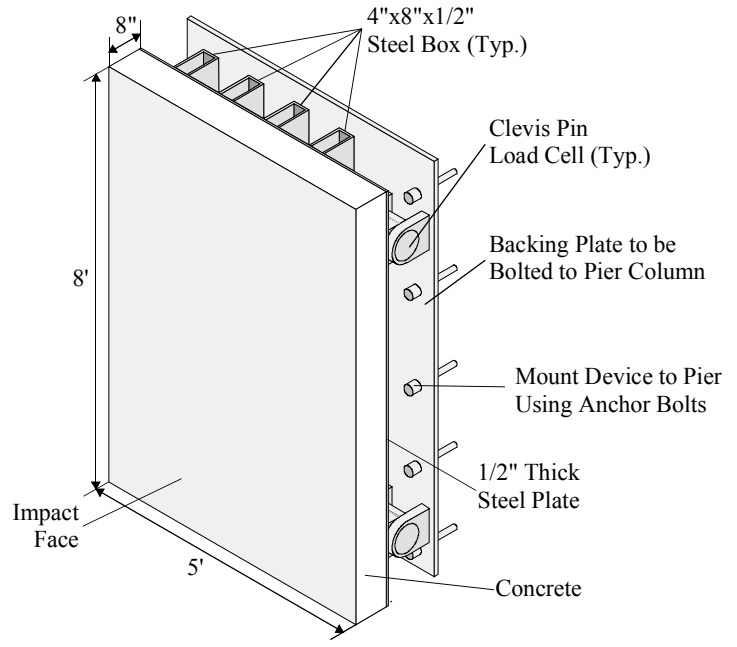

Figure 3.11 –Load Cell Apparatus for Pier-3

Event 3 - Attachment of instrumentation networks on pier-1 and barge

3.1 Attach accelerometers to the top of pier-1—Attach two accelerometers to the mounts already in place at the top of the pier-1 (Figure 3.6, position 1-1).

3.2 Attach accelerometers to the impact height of pier-1—Attach five accelerometers to the mounts already in place at the impact height of the pier-1 (Figure 3.6, positions 1-2 and 1-3).

3.3 Connect the displacement transducer on pier-1 to the timber piles next to the pier (Figure 3.6, position 1-6).

3.4 Attach signal conditioner, computer, and voltage supply to pier-1—Place the computer, signal conditioning chassis, and voltage supply into their respective enclosures on pier-1 (Figure 3.6, position 1-4).

3.5 Connect leads from the accelerometers, displacement transducer, signal conditioner and computer on pier-1 —Connect all the leads: voltage supply to the accelerometers, voltage supply to the load cells, voltage supply to the signal conditioner, voltage supply to the displacement transducer, accelerometers to the signal conditioner, load cells to the signal conditioner, displacement transducer to the signal conditioner, and the signal conditioner to the computer.

3.6 Test the network on pier-1—Using computer, confirm that all sensors are receiving voltage supply and are sending a voltage output.

3.7 Attach accelerometer mounts to barge—Five 4”x4” accelerometer mounts will be bolted to barge (Figure 3.12, positions B-1 to B-5).

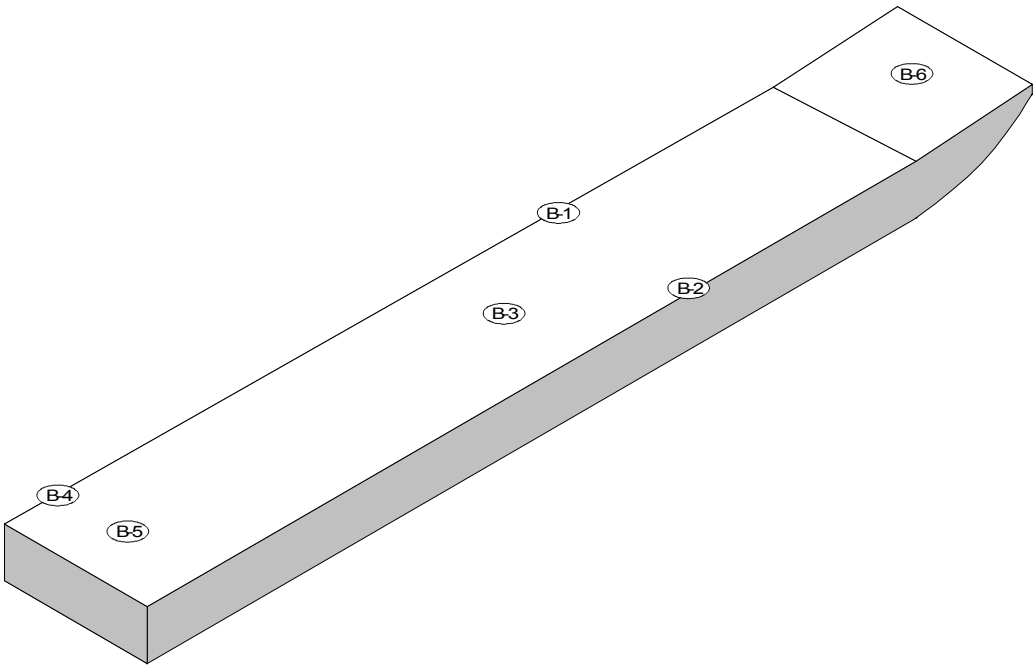

Figure 3.12 – Barge positions

3.8 Attach accelerometers to barge—Attach seven accelerometers to the mounts already in place on the barge (Figure 3.12, positions B-1 to B-5).

3.9 Attach instrumentation for measuring barge crush depth— (Figure 3.12, position B-6).

3.10 Attach signal conditioner, computer and voltage supply enclosures to barge—Enclosures for the signal conditioner, computer and voltage supply will be bolted to the barge (Figure 3.12, position B-3).

3.11 Attach signal conditioner, computer, and voltage supply to barge—The signal conditioner, computer, and voltage supply will be placed in their respective enclosures (Figure 3.12, position B-3).

3.12 Connect leads from accelerometers, signal conditioner, and computer on barge—Connect all the leads on the barge: voltage supply to accelerometers, and signal conditioner; accelerometers to signal conditioner; and then attach signal conditioner to computer.

3.13 Test the network on barge—Using computer, confirm that all sensors are receiving voltage supply and are sending a voltage output.

Event 4 – Impact events on pier-1

4.1 Conduct ½ knot impact on Pier-1

4.2 Conduct 1 knot impact on Pier-1

4.3 Conduct 2 knot impact on Pier-1

4.4 Conduct 4 knot impact on Pier-1

For each of the following Event 4 items listed above, the following tasks will be performed:

Move barge to starting position; accelerate barge to target impact speed; impact pier in head-on orientation; download and review sensor data from pier data collection network; download and review data from barge data collection network; download and review data from soil data collection network; measure permanent barge deformations; photograph and visually inspect both the barge and the pier.

Event 5 - Removal of instrumentation from pier-1 including load cell apparatus

5.1 Remove all the leads to sensors, signal conditioner, computer, and voltage supply on pier-1.

5.2 Remove the load cell apparatus from pier-1 —Contractor to remove load cell apparatus from pier-1 face (Figure 3.6, position 1-5).

5.3 Remove accelerometers and mounts from pier-1—All accelerometers and mounts on pier-1 to be removed (Figure 3.6, positions 1-1 to 1-3).

5.4 Remove signal conditioner, computer, voltage supply and their respective enclosures from pier-1 (Figure 3.6, 1-4).

5.5 Remove all leads to sensors, signal conditioner, computer, and voltage supply from barge.

5.6 Remove the accelerometers and mounts from barge—(Figure 3.12, positions B-1 to B-5).

5.7 Remove the barge crush depth instrumentation—(Figure 3.12, position B-6).

5.8 Remove the signal conditioner, computer, voltage supply, and enclosures from barge —(Figure 3.12, position B-3)

5.9 (Pier-1 ready for blasting)

Event 6 - Attachment of instrumentation network on pier-3 and superstructure

6.1 Attach accelerometers to the superstructure of pier-3—Five accelerometers will be attached to mounts already in place on the superstructure (Figure 3.9, positions S-1 to S-5).

6.2 Attach accelerometers to pier-2—Two accelerometers will be attached to mounts already in place on pier-2 (Figure 3.7, positions 2-1 and 2-2).

6.3 Attach voltage supply to pier-2—Voltage supply will be placed into enclosure already attached to pier-2 (Figure 3.7, position 2-2).

6.4 Attach accelerometers to pier-4—Two accelerometers will be attached to mounts already in place on pier-4 (Figure 3.8, positions 4-1 and 4-2).

6.5 Attach voltage supply to pier-4—Voltage supply will be placed into enclosure already attached to pier-4 (Figure 3.8, position 4-2).

6.6 Attach accelerometers to the top of pier-3 —Two accelerometers will be attached to the mount already in place on top of pier-3 (Figure 3.5, position 3-1).

6.7 Attach accelerometers to the impact height of pier-3 —Five accelerometers will be attached to mounts already in place at impact height of pier-3 (Figure 3.5, positions 3-2 and 3-3).

6.8 Connect the displacement transducer on pier-3 to the timber piles next to the pier (Figure 3.5 position 3-14).

6.9 Attach signal conditioner, computer, and voltage supply to pier-3—Signal conditioner, computer, and voltage supply will be placed into their respective enclosures already in place on pier-3 (Figure 3.5, position 3-4).

6.10 Connect leads from the accelerometers on pier-2, pier-4, and superstructure—Connect all the leads from the accelerometers on the pier-2, pier-4 and superstructure to the signal conditioner and their respective voltage supplies.

6.11 Connect leads from the accelerometers, strain gages, load cell, displacement transducer, signal conditioner, and computer on pier-3—Connect all the leads: voltage supply to the accelerometers, voltage supply to the signal conditioning chassis, accelerometers to the signal conditioning chassis, and signal conditioning chassis to the computer.

6.12 Attach accelerometers to barge—Attach seven accelerometers to the mounts already in place on the barge (Figure 3.12, positions B-1 to B-5).

6.13 Attach instrumentation for measuring barge crush depth— (Figure 3.12, position B-6).

6.14 Attach signal conditioner, computer, and voltage supply to barge—The signal conditioner, computer, and voltage supply will be placed in their respective enclosures (Figure 3.12, position B-3).

6.15 Connect leads from accelerometers, signal conditioner, and computer on barge—Connect all the leads on the barge: voltage supply to accelerometers, and signal

conditioner; accelerometers to signal conditioner; and then attach signal conditioner to computer.

6.16 Test the network on barge—Using computer, confirm that all sensors are receiving voltage supply and are sending a voltage output.

6.17 Test the network on pier-3—Using computer, confirm that all sensors are receiving voltage supply and are sending a voltage output.

6.18 Test the network on the barge—Using computer, confirm that all sensors are receiving voltage supply and are sending a voltage output.

Event 7 – Impact events on pier-3 with superstructure

7.1 Conduct ½ knot impact on Pier-3

7.2 Repeat ½ knot impact on Pier-3

7.3 Repeat ½ knot impact on Pier-3

For each of the following Event 7 items listed above, the following tasks will be performed:

Move barge to starting position; accelerate barge to target impact speed; impact pier in head-on orientation; download and review sensor data from pier data collection network; download and review data from barge data collection network; download and review data from soil data collection network; measure permanent barge deformations; photograph and visually inspect both the barge and the pier.

Event 8 - Removal of instrumentation from pier-2, pier-3, pier-4 and superstructure

8.1 Remove all the leads from pier-2, pier-3, pier-4, and superstructure.

8.2 Remove all the accelerometers from pier-2, pier-3, pier-4 and superstructure—(Figure 3.5, positions 3-1 to 3-3; Figure 3.9, positions S-1 to S-5; Figure 3.7, positions 2-1 and 2-2; and Figure 3.8, positions 4-1 and 4-2).

8.3 Remove all the voltage supply and enclosures from pier-2, pier-3, and pier-4—(Figure 3.5, position 3-4; Figure 3.7, position 2-2; and Figure 3.8, position 4-2).

8.4 Remove the signal conditioner, computer, and enclosures from pier-3—(Figure 3.5, position 3-4).

8.5 Remove all leads to sensors, signal conditioner, computer, and voltage supply from barge.

8.6 Remove the accelerometers and mounts from barge—(Figure 3.12, positions B-1 to B-5).

8.7 Remove the barge crush depth instrumentation—(Figure 3.12, position B-6).

8.8 Remove the signal conditioner, computer, voltage supply, and enclosures from barge —(Figure 3.12, position B-3)

8.9 (Pier-3 superstructure ready for removal)

Event 9 - Attachment of instrumentation network on pier-3 without superstructure

9.1 Attach accelerometers to the top of pier-3—Two accelerometers will be attached to mount already in place on top of pier-3 (Figure 3.5, position 3-1).

9.2 Attach accelerometers to the impact height of pier-3—Five accelerometers will be attached to mounts already in place at impact height of pier-3 (Figure 3.5, positions 3-2 and 3-3).

9.3 Connect the displacement transducer on pier-3 to the timber piles next to the pier (Figure 3.5 position 3-14).

9.4 Attach the signal conditioner, computer, and voltage supply to pier-3—Signal conditioner, computer, and voltage supply will be placed into their respective enclosures already in place on pier-3 (Figure 3.5, position 3-4).

9.5 Connect leads from the accelerometers, strain gages, load cell, displacement transducer, signal conditioner, and computer on pier-3—Connect all the leads: voltage supply to the accelerometers, voltage supply to the signal conditioning chassis, accelerometers to the signal conditioning chassis, and signal conditioning chassis to the computer.

9.6 Attach accelerometers to barge—Attach seven accelerometers to the mounts already in place on the barge (Figure 3.12, positions B-1 to B-5).

9.7 Attach instrumentation for measuring barge crush depth— (Figure 3.12, position B-6).

9.8 Attach signal conditioner, computer, and voltage supply to barge—The signal conditioner, computer, and voltage supply will be placed in their respective enclosures (Figure 3.12, position B-3).

9.9 Connect leads from accelerometers, signal conditioner, and computer on barge—Connect all the leads on the barge: voltage supply to accelerometers, and signal conditioner; accelerometers to signal conditioner; and then attach signal conditioner to computer.

9.10 Test the network on barge—Using computer, confirm that all sensors are receiving voltage supply and are sending a voltage output.

9.11 Test the network on pier-3—Using computer, confirm that all sensors are receiving voltage supply and are sending a voltage output.

9.12 Test the network on the barge—Using computer, confirm that all sensors are receiving voltage supply and are sending a voltage output.

Event 10 – Impact events on pier-3 without superstructure

10.1 Conduct ½ knot impact on Pier-3

10.2 Repeat ½ knot impact on Pier-3

10.3 Repeat ½ knot impact on Pier-3

For each of the following Event 10 items listed above, the following tasks will be performed:

Move barge to starting position; accelerate barge to target impact speed; impact pier in head-on orientation; download and review sensor data from pier data collection network; download and review data from barge data collection network; download and review data from soil data collection network; measure permanent barge deformations; photograph and visually inspect both the barge and the pier.

Event 11 - Removal of instrumentation from pier-3 including load cell apparatus

11.1 Remove all leads to sensors, signal conditioner, computer, and voltage supply on pier-3.

11.2 Remove the load cell apparatus from pier-3—Contractor to remove load cell apparatus from pier-1 face (Figure 3.5, position 3-5).

11.3 Remove the accelerometers and mounts from pier-3—(Figure 3.5, positions 3-1 to 3-3)

11.4 Remove the signal conditioner, computer, voltage supply, and enclosures from pier-3—(Figure 3.5, position 3-4)

11.5 Remove all leads to sensors, signal conditioner, computer, and voltage supply from barge.

11.6 Remove the accelerometers and mounts from barge—(Figure 3.12, positions B-1 to B-5).

11.7 Remove the barge crush depth instrumentation—(Figure 3.12, position B-6).

11.8 Remove the signal conditioner, computer, voltage supply, and enclosures from barge —(Figure 3.12, position B-3)

11.9 (Pier-2, pier-3, and pier-4 ready for removal and barge ready for repair)

3.3 St. George Bridge Pier Inspection

An underwater inspection was conducted by UF researchers at piers 1S, 2S, 3S, and 4S of the old St. George Island Bridge during July of 2002. The inspection included local bathymetry, examination of the condition of the piers and piles, underwater video, and underwater photographs.

The time at which the inspection was scheduled to occur depended upon the tidal currents on the day of the inspection. The tidal curve at Cat Point, FL for the day of the dive indicated that the tide was flat in the morning. Consequently, the dive inspection was scheduled to take place at this time, because high tidal currents decrease visibility—making underwater inspections more difficult. In spite of this small tidal change, the visibility was still rather poor—1 to 2 ft depending upon the depth. The tidal currents associated with the flood tide in the morning were approximately 1.5 ft/s to the West. Then, in the afternoon, ebb tide currents exceeded 2 ft/s. The local bottom had few bathymetric features and was covered with a veneer of oyster shells.

3.3.1 Piers 1S and 2S

The pile caps for piers 1S and 2S were in good condition. There were several small areas of concrete spalling and a light covering of marine growth, but neither the pile caps nor the tremie seals of these two piers were undermined, and none of the supporting piles were exposed. Table 3.1 summarizes depth measurements taken using a fathometer, and estimated distances from the pier for ranges. In the table, 20' N refers to a survey profile line in the East-West direction taken 20 feet north of the pier. Likewise, CL refers to an East-West line taken along the centerline of the pier, and 20' S refers to a survey profile line 20 feet south of the pier. In the East-West direction, soundings were

made 50 feet from the pier, 20 feet from the pier, at the East end of the pier, at the center of the pier, etc. The depths are in feet, and are corrected to the mean tide level.

The depth survey data shows little variation in the East-West direction of the predominant tidal flow. Pier 1S, however, shows some variation in the North-South direction. The dredged navigation channel to the north of pier 1S is responsible for the deeper depth to the north. Also, between the navigation channel and pier 1S is a large fender structure, which tends to modify local flows. Furthermore, riprap—approximately 500 lb stones—was observed along the base of this fender structure. The 20' N survey line for pier 1S was north of this structure.

Bathymetric measurements did not reveal a large scour hole around either pier, which was confirmed by visual observations. The intersection of the cap and the mud-line was examined around the entire perimeter of the pile cap for each pier to assess the degree of local scour. Pier 1S showed little local scour; however, there was a small scour hole approximately 2 ft deep on the SE corner of pier 2S. Fortunately, this scour hole did not extend below the concrete seal below the pile cap. Measurements from the top of the pile cap to the mud-line for pier 2S are given in Table 3.2. Since the distance from the top of the pile cap to the bottom of the concrete seal of pier 2S shown on the original bridge design plans is 9.5 ft, the piles are still approximately 1.5 feet beneath this scour hole (based upon the depths recorded in Table 3.2).

The current velocity at the time of the inspection of pier 1S was approximately 1.5 ft/s. As a result, visibility was rather poor, and underwater photographs did not provide useful observations. Furthermore, an underwater video was taken at the centerline of pier 1S on the south face of the pier, parts of which show the character of

the pier surface. The video goes from the water surface, down the pile cap, and to the bottom. Again, little is notable in terms of damage or exposure of the piles.

Table 3.1 Depth soundings at piers 1S and 2S (mean tide level ft)

Pier 1S			
	N to S		
E to W	20' N	CL	20' S
50' E	15	14	11
20' E	15	14	12
E end	14	11	12
CL	13		13
W end	12	9	13
20' W	10	8	13
50' W	11	9	13

Pier 2S			
	N to S		
E to W	20' N	CL	20' S
50' E	9	9	9
20' E	9	9	9
E end	9	11	10
CL	9		10
W end	9	11	10
20' W	10	11	10
50' W	10	11	9

Table 3.2 Top of pile cap to mud line measurements at pier 2S (ft)

NW	5.3
N	4.0
NE	4.6
SE	7.8
S	4.3
SW	3.8

3.3.2 Piers 3S and 4S

Local bathymetric surveys were made for piers 3S and 4S similar to those for 1S and 2S. The results of the surveys are summarized in Table 3.3. As the depth survey shows, the bottom is nearly featureless around these two piers. It is noted that the depth tends to decrease with distance from the navigation channel.

The distance along the pile from the bottom of the pile cap to the mud-line was measured for each pile in these two piers (see Table 3.4). Each pier has 8 piles, 4 on the east end pile cap and 4 on the west end pile cap (see Figure 3.13). The notation to define the location of each pile under its respective pile cap is given in Figure 3.13.

Table 3.3 Depth soundings at piers 3S and 4S (mean tide level ft)

Pier 3S			
	N to S		
E to W	20' N	CL	20' S
50' E	8	8	7
20' E	8	8	8
E end	9	9	8
CL	9		8
W end	9	10	8
20' W	10	9	9
50' W	10	9	9

Pier 4S			
	N to S		
E to W	20' N	CL	20' S
50' E	6	6	6
20' E	7	7	7
E end	8	7	7
CL	8		7
W end	8	8	7
20' W	8	8	8
50' W	9	9	8

Each of these piles was also visually inspected. This inspection showed no structural damage, and a very light cover of marine growth.

Table 3.4 Bottom of cap to mud-line measurements at piers 3S and 4S (ft)

Pier 3S		
West End	NW	11.0
	NE	11.3
	SW	10.6
	SW	11.5
East End	NW	11.2
	NE	11.3
	SW	11.3
	SW	11.4

Pier 4S		
West End	NW	9.8
	NE	10.0
	SW	9.3
	SW	9.8
East End	NW	9.8
	NE	9.7
	SW	9.8
	SW	9.6

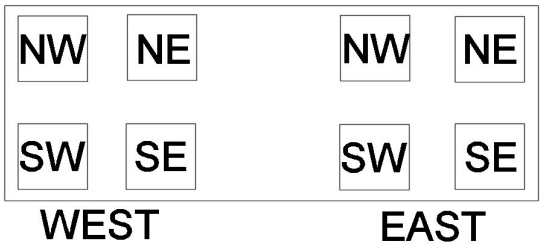

Figure 3.13. Pile locations for pier-3 and pier-4

Chapter 4

Finite Element Model Updates

4.1 Barge Material Model

In the barge model developed during Phase-I of this study [1], the shell elements of Zone-1 (Figure 4.1 for zone definitions) were modeled using a nonlinear material with the properties of grade A36 structural steel. This material model was developed using stress-strain data measured from tests conducted on standard test coupons at the University of Florida. Although the steel from the test was A36, indicating a minimum yield stress of 36 ksi, the actual yield point was considerably higher (approximately 48 ksi) (Figure 4.2). Therefore, it was determined that a material model more representative of A36 steel was needed. Thus, data was obtained from another test conducted at the University of Florida that yielded results more characteristic of minimum strength A36 steel. This new material model has an initial yield stress of approximately 36 ksi (Figure 4.2), and makes use of the `*MAT_PIECEWISE_LINEAR_PLASTICITY` material model in LS-DYNA. Simulations were run for both cases with a barge velocity of 4-knots and a full payload to examine the effect of changing the steel yield point.

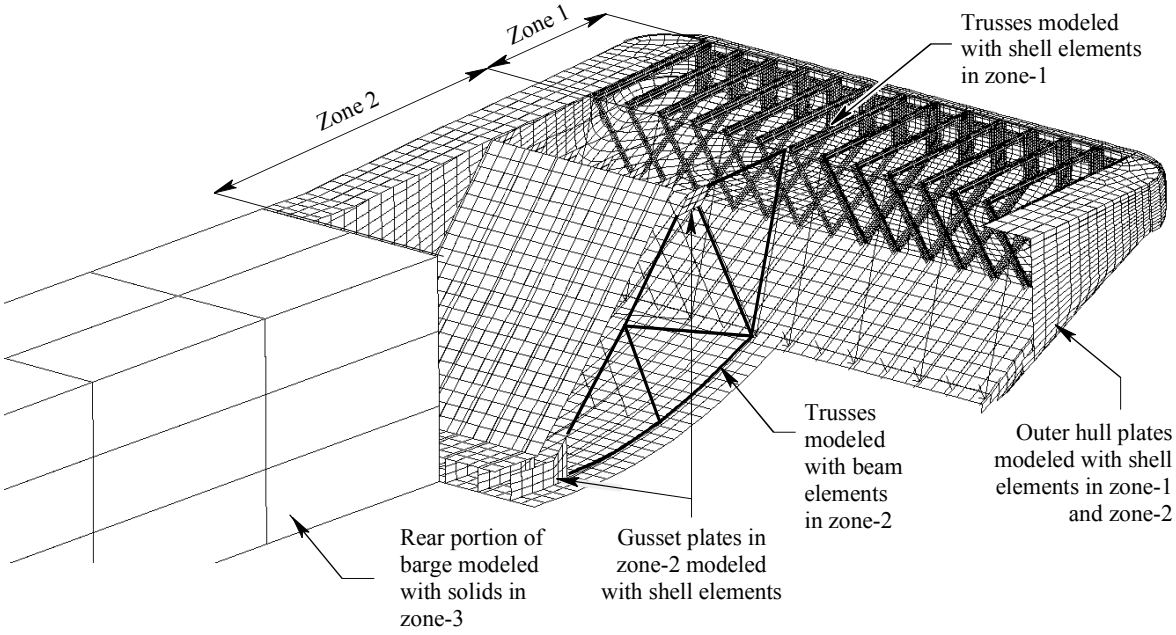

Figure 4.1 Barge Zone Definitions

For the purposes of conducting a sensitivity study, a higher strength steel (HSLA-80)—which has a yield stress of approximately 80 ksi (Figure 4.2)—was also considered. A simulation was conducted using this higher strength material in Zone-1. Once again, the barge impact speed was 4-knot, and the barge was fully loaded. The results of this simulation were compared to results extracted from a 4-knot, fully loaded barge impact using the previous A36 steel as the material model.

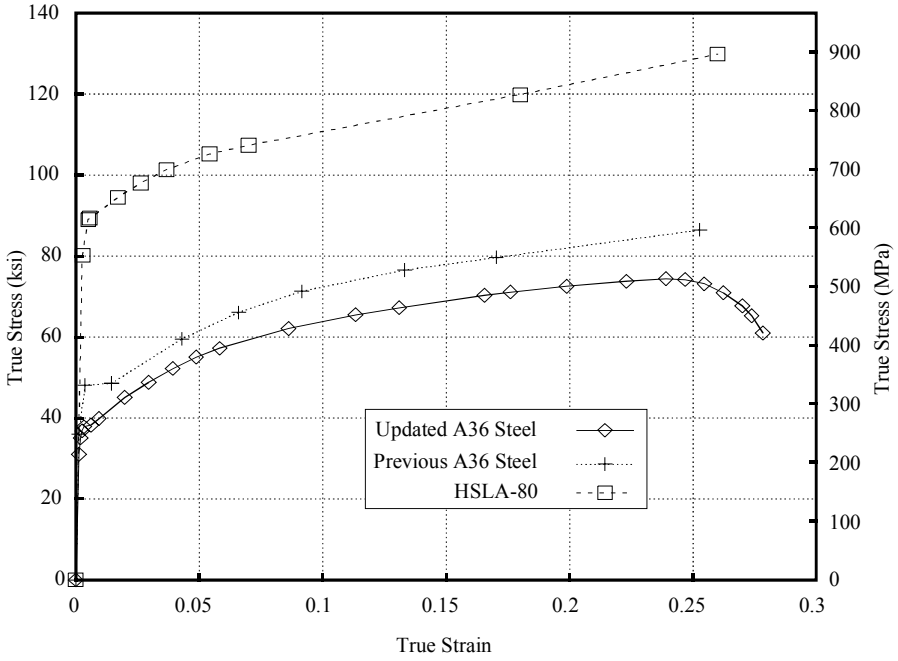

Figure 4.2 Steel Stress Strain Comparison

In Figure 4.3, each type of steel is given a 2-digit code to identify the steel material model used. The identification number represents the actual yield stress of the steel:

- Case 48—Previous "A36 model" (~ 48 ksi)
- Case 36—New A36 model (~ 36 ksi)
- Case 80—HSLA-80 (~ 80 ksi)

Peak impact forces predicted by the 36 ksi and 48 ksi steel models are seen to be nearly identical, whereas moderately increased barge deformations are noted in the 36 ksi case. The peak force predicted by the 80 ksi model was noticeably higher than the 36 ksi and 48 ksi cases. However, it also stands to reason that barges constructed from higher strength materials such as HSLA-80 would make use of smaller structural elements (given the increased material strength). Use of lighter structural elements would tend to once again reduce the peak forces from those shown for the 80 ksi case in Figure 4.3.

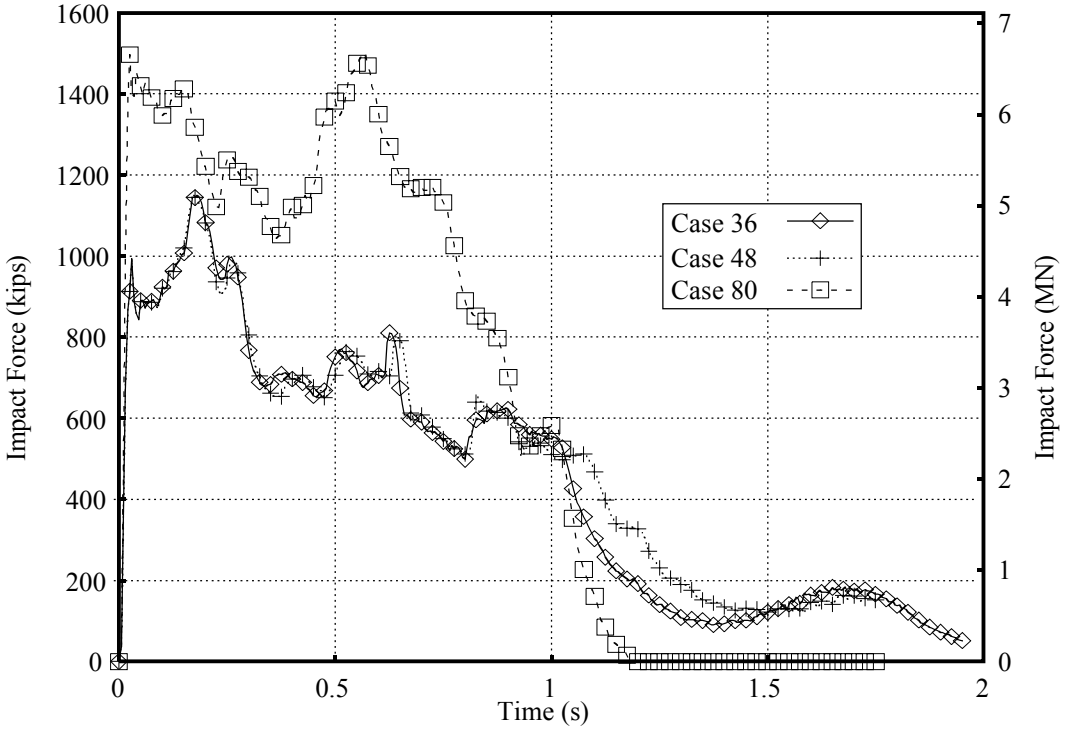

a) Force history comparison

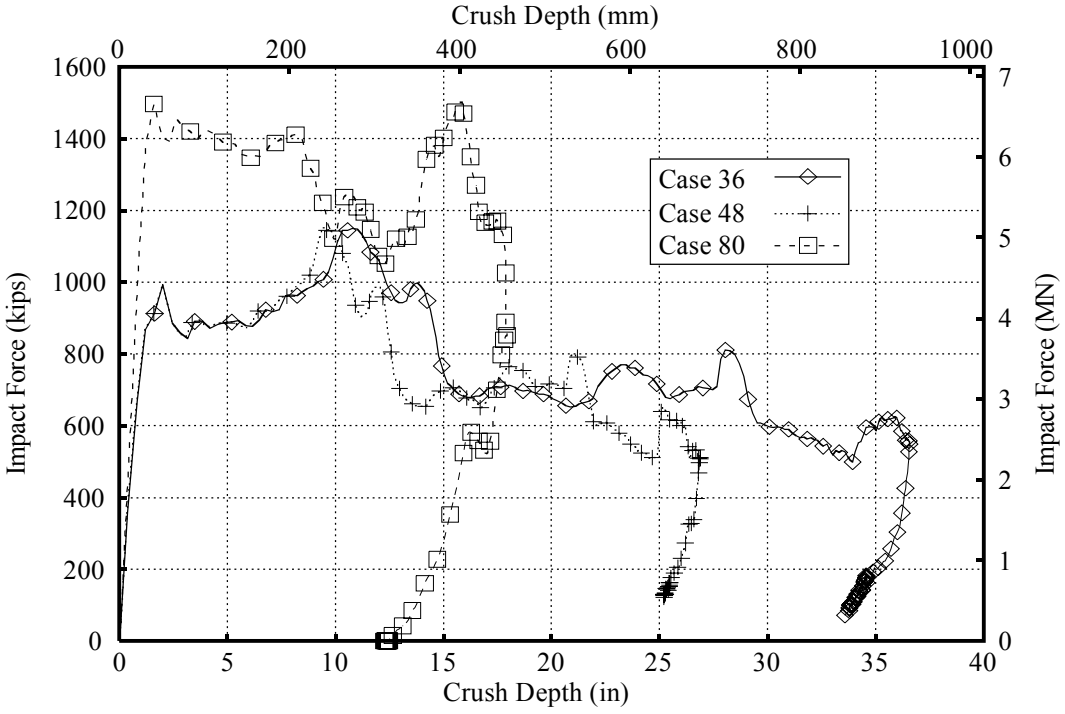

b) Crush depth comparison

Figure 4.3. Data from Steel Comparison Simulations

4.2 Integration Comparison

In the Phase-I report [1], it was stated that the solid elements in the impact region of the piers were modeled such that these elements would exhibit the least amount of distortion possible. This was accomplished by fully integrating the elements in this region. Elements outside of the impact zone were modeled using single-point integration for reasons of computational efficiency. However, elements using a single-point integration scheme can potentially exhibit zero-energy modes—otherwise known as hourglass-energy modes.

To determine if hourglass-energy modes were present in the pier models, a simulation was run in which pier-1 was excited with a pulse load, and allowed to vibrate freely after the load dropped off. Since no global viscous damping was prescribed in the system, the amplitude of the pier displacement should not decrease during free vibration. However, a plot of the displacement history for this pier shows a noticeable decay in the amplitude (Figure 4.4.a). Furthermore, a plot of the total energy and hourglass energy with respect to time shows that the hourglass energy is large compared to the total energy of the system (Figure 4.4.b). In general, it is desirable that the hourglass energy remain small relative to the total system energy. The same model was also run with all of the solid elements in the pier fully integrated. The displacement response exhibited no amplitude decay during free vibration, and the hourglass energy was negligible compared to the total energy of the system (Figure 4.4). In addition, it was also determined that solid elements in the barge should also be fully integrated as well. Thus, beginning with Phase II, all pier and barge solid elements use a full integration element scheme.

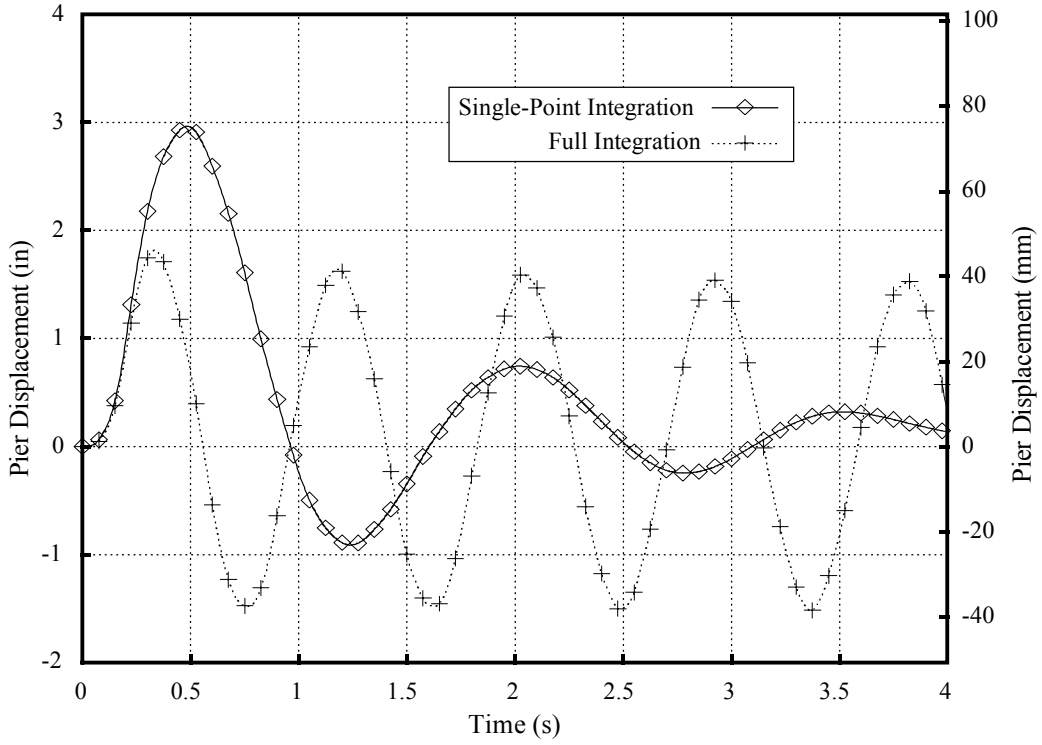

a) Pier displacement history

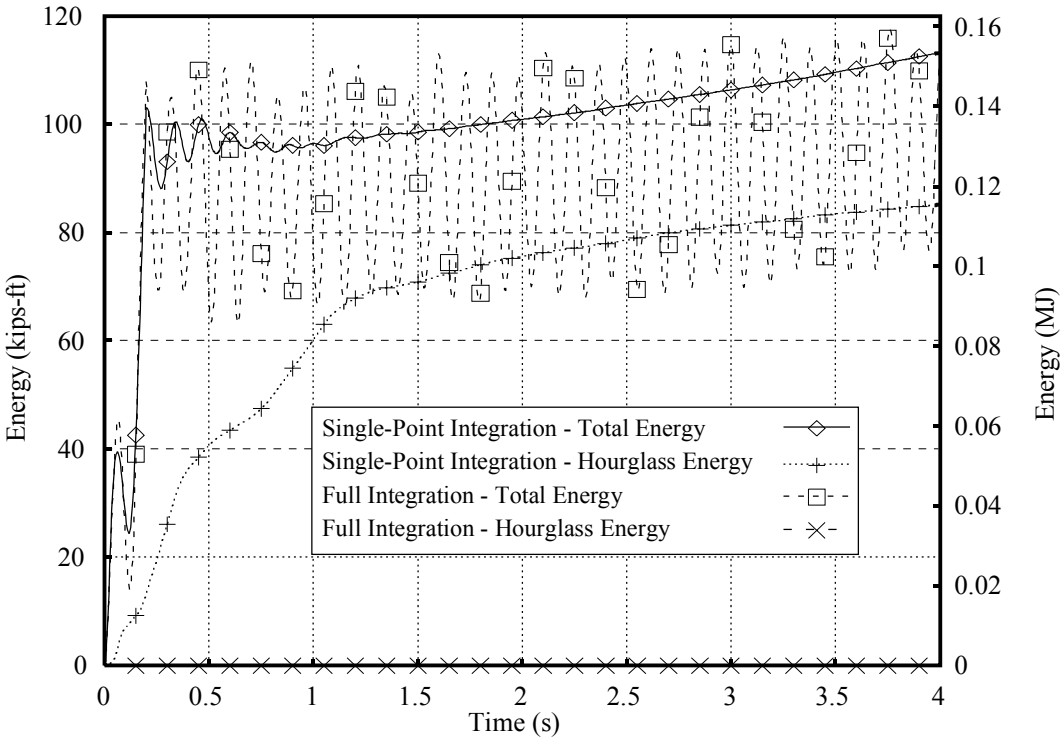

b) Energy comparison

Figure 4.4 Hourglassing Example for Pier-1

4.3 Pile Lengths

When the original pier-1 model was created, lengths of the piles were approximated as 40 feet in length. During Phase II of this study, the piles were updated to the lengths indicated on the construction plans (50.5 feet). Therefore, approximately 10.5 feet of pile length was added to each pile. Subsequently, both of the models—the previous pier-1 model with the shorter piles, and the updated model with the extended piles—were simulated with a constantly increasing force of 1200 kips per second. As anticipated, given the location of the point of effective fixity within the piles, the results showed that there was little difference between the load-displacement responses for each model (Figure 4.5). Nevertheless, beginning with Phase II of this study, the pile lengths are now 50.5 feet in length for pier-1.

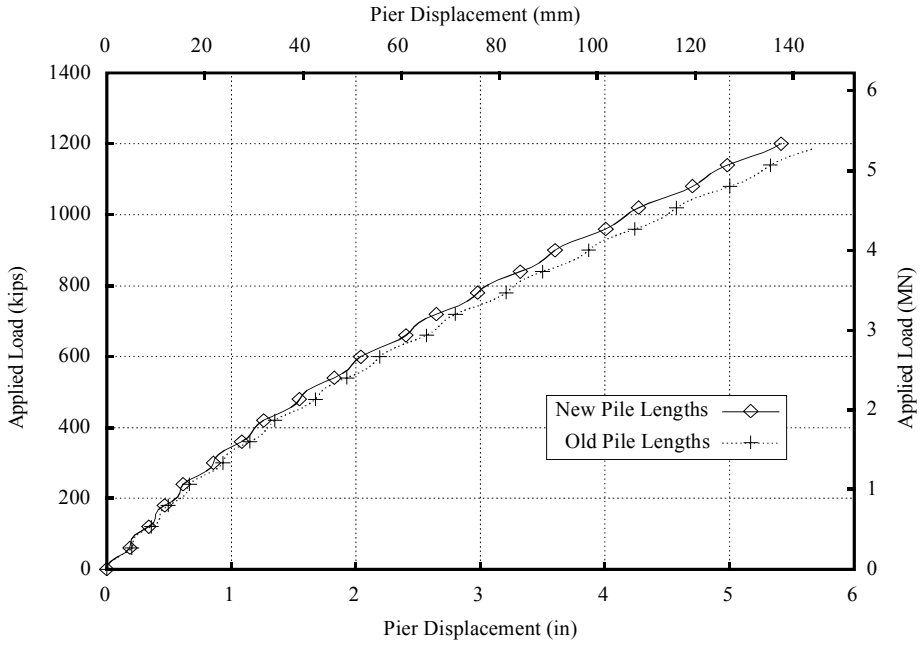

Figure 4.5. Pier Displacement Comparison for Different Pile Lengths

Chapter 5

Soil-Pile Interaction Modeling

5.1 Introduction

To characterize the dynamic response of a bridge pier, it is important that the resistance of the surrounding soil to the movement of the pier be adequately modeled. For this study, soil-pile interaction is modeled using nonlinear springs positioned at nodes along the length of the piles. At each pile node, a group of five soil springs is attached to the pile to model the soil's resistance to the movement of the structure. Each group of five soil springs consists of two perpendicular sets of lateral soil springs and one vertical axial spring. Furthermore, each set of lateral soil springs consists of two individual soil springs: one resists pile movement in the positive direction, while the other resists movement in the negative direction. The axial soil spring is used to model either skin friction along the length of the pile, or end bearing at the tip of the pile. Each of these soil spring groups must accurately model the load-deformation characteristics of the soil. Furthermore, each of the three sets of soil springs (two lateral and one vertical) within a group, must remain orthogonal each other. The effect each pile has on the surrounding piles, i.e. pile "group" effects, must also be considered.

5.2 Refinement of the Soil Spring Curves

In the Phase I report [1], it was stated that the soil spring curves were generated from the bridge substructure analysis software, FB-Pier [2,3]. Using soil data from the original St. George Island bridge design drawings as input, FB-Pier was used to generate two soil curves for each layer—one at the top and one at the bottom of the layer. Linear

interpolation was then performed on the soil curve data to obtain soil curves for intermediate depths.

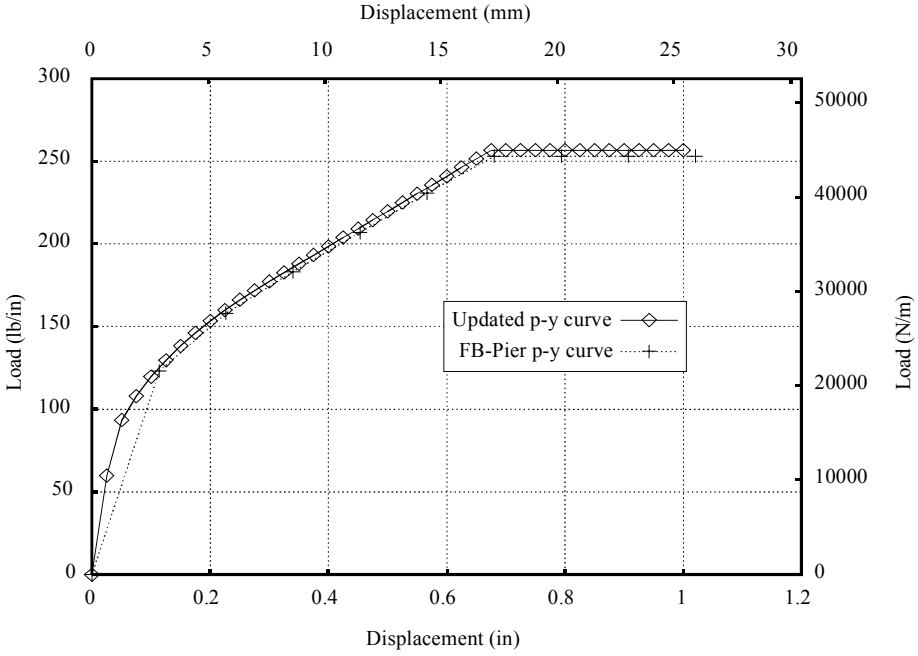

Figure 5.1. PY-Curve Comparison

It was determined that the process for generating the soil spring curves needed to be refined for several reasons. First, FB-Pier only reports data for ten points along each soil spring curve. This limited number of data points can yield initial spring stiffnesses that are too small (Figure 5.1), which may lead to erroneous results demonstrated later in this chapter. Furthermore, linearly interpolating the lateral soil resistance between different points along the depth of the piles is only an approximation. The actual variation of soil resistance with depth is nonlinear, and therefore an improved method for generating soil spring data was desirable.

5.2.1 Lateral Soil Spring Curves

FB-Pier calculates lateral soil spring curves—referred to as p-y curves from now on—using the method of Reese, Cox, and Koop [3,4] for sandy soils, and Matlock's

method for "soft clay in the presence of water" was used for clayey soils (see [1] for an explanation of soil model selection). Since it was deemed desirable to refine the py-curves, a Mathcad worksheet was created that calculated the p-y curves—based upon the exact methods used in FB-Pier—given the appropriate soil data.

The Reese, Cox, and Koop method and Matlock's method assume the presence of only a single layer of soil. If more than one layer of soil is present, then the layers must be adjusted to appear as a single layer. The method of Georgiadis [3,4] was used to incrementally transform each layer—based upon the relative capacities of the layers—until an equivalent soil profile with only a single layer is acheived.

The first step in the method of Georgiadis is to integrate the capacity of the top layer (p_{u1}) through its depth (z_{bot1}) to obtain a force (F_1). Then, the capacity of the second layer (p_{u2}) is integrated through a corrected depth (z'_{bot1}), such that these two integrals are equal, as given in Equation 5.1.

$$F_1 = \int_0^{zbot1} p_{u1} dz = \int_0^{z'bot1} p_{u2} dz \tag{5.1}$$

Once the corrected depth (z'_{bot1}) is found, a depth correction factor (z_{cor1}) is calculated by taking the difference between the initial depth (z_{bot1}) and the corrected depth (z'_{bot1}). This depth correction is then applied to the subsequent layers. All of the soil from the top of the profile to the bottom of the second layer—which is at a corrected depth ($z'_{bot2} = z_{bot2} + z_{cor1}$)—then has the properties of the second layer from the initial soil profile (see Figure 5.2b).

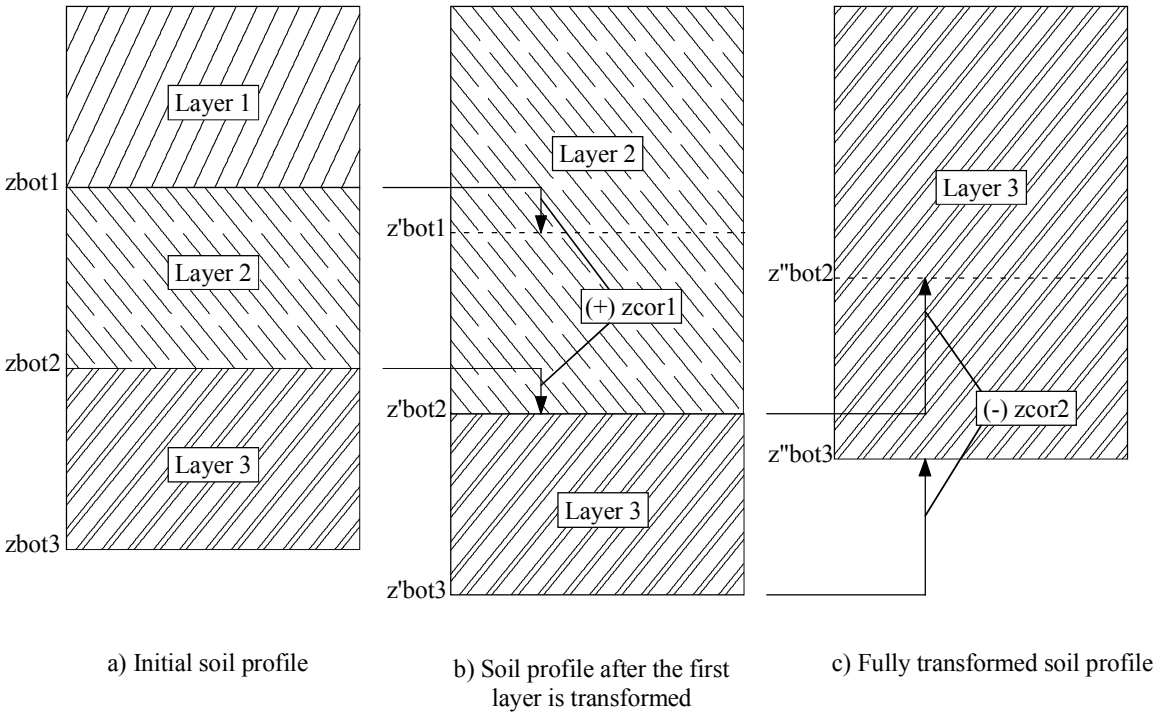

Figure 5.2. Depth Correction by the Method of Georgiadis

This process is repeated until all of the soil is transformed into an equivalent single layer as in Figure 5.2c. After all of the depths have been corrected, the p-y curve values are calculated using the corrected depth values and the original soil properties.

5.2.2 Axial Soil Spring Curves

FB-Pier calculates values for the axial soil spring curves—referred to as t-z curves from now on—using the method developed by McVay et al. [5]. In this method, the vertical deflection of a node on a pile is calculated as a function of the shear stress at that depth on the surface of the pile. The vertical deflection is also a function of the radial distance outward to a point in the soil where the shear stress is negligible (r_m)—referred to as the zone of influence. The zone of influence is in turn dependent upon the ratio of the soil's shear modulus at the mid-depth of the pile to the soil's shear modulus at the tip

of the pile. Furthermore, these shear moduli vary with the shear stress in the soil. Thus, the t-z curves vary with the vertical deflection of the pile.

The t-z curves that FB-Pier displays graphically correspond to an initial zone of influence ($r_m = 1.1r_o$) where r_o is the radius of the pile [3]. Internally, FB-Pier updates the t-z curves based on current deformation levels (at each stage of loading), however, only data corresponding to the initial condition is reported in the graphical user interface (GUI). After the initial condition, the zone of influence is calculated from the following equation:

$$r_m = 2.5\rho\, L(1-\nu) \tag{5.2}$$

where L is the length of the pile, ν is Poisson's ratio for the soil, and

$$\rho = \frac{G_{L/2}}{G_L} \tag{5.3}$$

where, $G_{L/2}$ and G_L are the shear moduli of the soil at the mid-length and at the tip of the pile, respectively. Since the equation for the zone of influence is a function of the pile length—which is typically large compared to the pile radius—the zone of influence will greatly increase beyond $1.1r_o$ after the pile has moved from its initial position. Furthermore, as the zone of influence increases, the deflection will be greater for a given shear stress value on the pile. Therefore, using only the initial condition t-z curve displayed in the FB-Pier GUI will overestimate the stiffness of the soil if it is used throughout the analysis (Figure 5.3). Consequently, an r_m-value is needed that will estimate the overall load displacement history fairly accurately. It was determined that calculating the zone of influence from Equation 5.2 using the small-strain moduli at the

mid-depth and tip of the pile would be adequate for this purpose. This assumption wad then used to generate new t-z curves (Figure 5.3) for use in the LS-DYNA simulations.

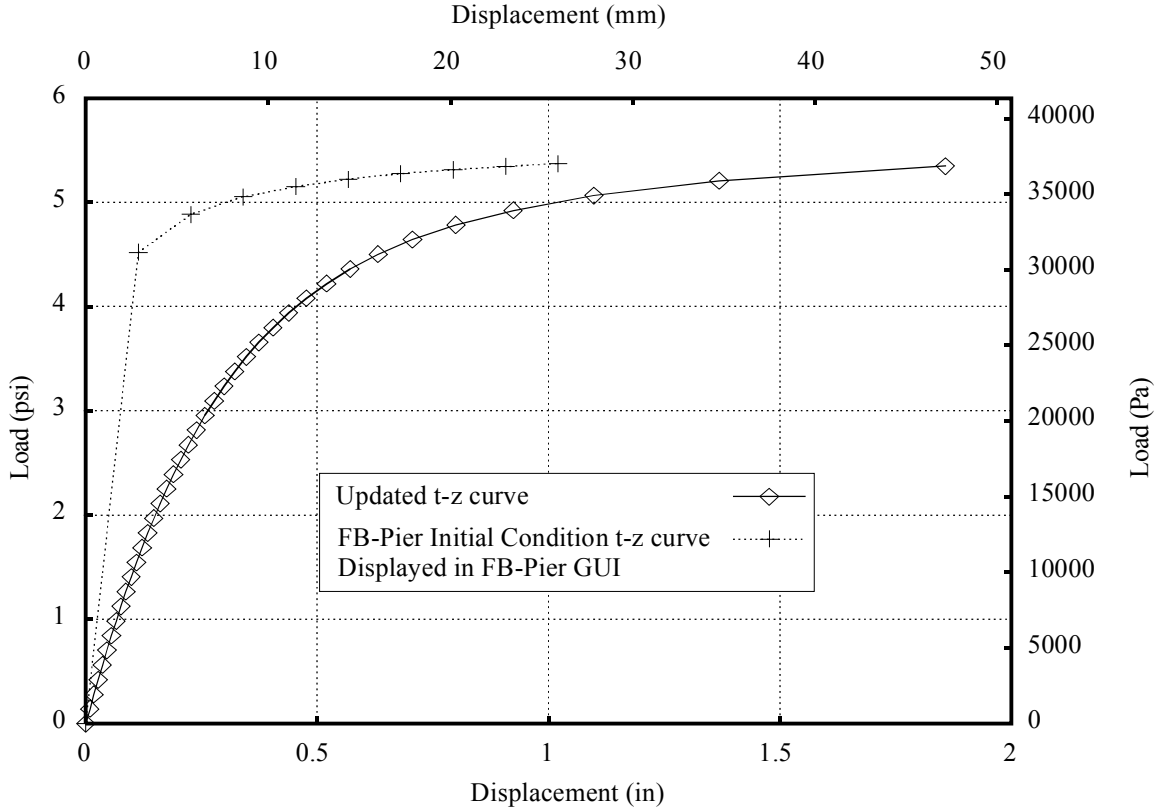

Figure 5.3. TZ-Curve Comparison

5.3 Soil Spring Alignment

When modeling soil-pile interaction using nonlinear springs, the p-y curves are intended to model the load-deflection behavior in a direction transverse to the pile, while the t-z curves model load-deflection behavior in an axial direction along the pile. Therefore, it is preferable that these springs—lateral and axial—remain orthogonal throughout each impact simulation. To ensure that the soil springs remain orthogonal, each of the soil spring anchor nodes can be constrained to move with the pile node in the directions perpendicular to the axis of the spring (see Figure 5.4a). If a load is applied in

the positive x-direction, then the pile node will move in the positive x-direction. Simultaneously, the anchor node of the axial spring should also move in the x-direction, preventing the axial spring from changing orientation. Thus, force is not developed in the axial spring as a result of the horizontal motion, and the pile node undergoes no vertical displacement, which is desirable.

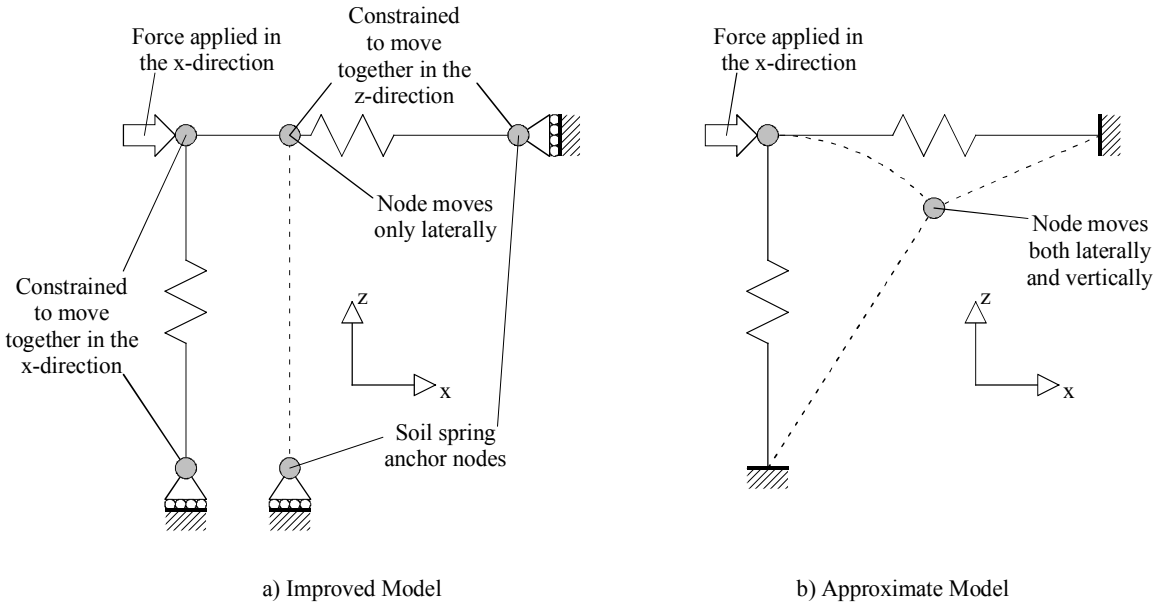

Figure 5.4. Soil spring constraint comparison

If the anchor nodes of the springs are constrained from movement in any direction, and the same load is applied to the pile node in the x-direction, the pile node will move laterally. However, the lateral movement of this node will draw the axial spring out of its intended alignment, which causes the axial spring to develop a tension force. This tension force will displace the pile node vertically. Consequently, the lateral spring will also be drawn out of its intended alignment as in Figure 5.4b. The lateral spring may then erroneously contribute to the axial soil behavior. Similarly, the axial spring could contribute to the lateral behavior of the soil. In Phase I of this study [1],

proper alignment of soil springs was approximated by choosing appropriate soil spring lengths (as the length of the soil spring increases, the springs become less sensitive to the phenomenon illustrated in Figure 5.4b).

Preliminary superstructure modeling efforts (described in Chapter 7) undertaken during Phase II of this study revealed that the additional weight of the superstructure can be sufficient to cause significant misalignment of the lateral p-y springs in selected cases. As a result, an improved method of maintaining soil spring orientations making use of nodal constraints was developed and implemented.

Expanding the two-dimensional example given above into three dimensions, nodal constraints can be applied to the nodes in each soil-pile spring group in LS-DYNA to ensure that the soil springs remain orthogonal. In Figure 5.5 the pile node—denoted as 1—is allowed move in any direction. The x-direction lateral spring anchor nodes—denoted as 2 in the figure—are constrained to move with the pile node in both the y and z directions. Likewise, the y-direction lateral spring anchor nodes—denoted as 3 in the figure—are constrained to move with the pile node in both the x and z directions. Finally, the axial spring anchor node—denoted as 4 in the figure—is constrained to move with the pile node in both the x and y directions.

There would be a total of six constraints—two for each of the node combinations described above—if the nodal constraints were defined in the LS-DYNA keyword file using the above organization. Taking this approach, however, would result in LS-DYNA issuing an error statement stating that the pile node has conflicting nodal constraints. This error arises because the pile node would be in multiple separate constraint definitions for each of three directions.

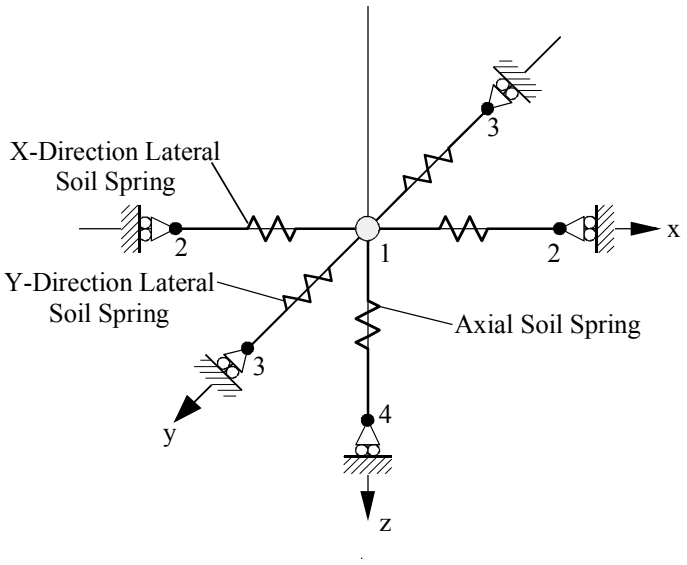

Figure 5.5. Three dimensional soil spring constraints

The solution is to define three constraint sets—one for each global direction. Then, all of the nodes that must be constrained to move with each other in the x-direction—nodes 1, 3, and 4 in Figure 5.5—are placed in the x direction constraint. Likewise, nodes 1, 2, and 4 are constrained to move with each other in the y-direction, and nodes 1, 2, and 3 are constrained to move with each other in the z-direction.

5.4 Reversible Group Effect p-y Curve Multipliers

Piles deforming as a group tend to act differently than when they are isolated. The soil resistance acting on a pile in a group is typically lower than the resistance on a single pile in isolation. To model this phenomenon, soil resistance is scaled down by a factor, referred to as a py-multiplier when multiple piles act as a group. The py-multipliers vary based on position within the group, and based on the direction of movement of the pile group (Figure 5.6). Since a pile group may cycle between forward and backward motion during a barge impact, the py-multipliers should be specified so as to reflect this fact. The model developed during Phase I of this study only applied the py-

multipliers in one direction. Even within the foundation engineering community, there remains some level of debate as to the most accurate means of selecting p-y row multipliers for cyclic loading. Despite this fact, beginning with this Phase II study, reversible p-y multipliers of the form shown in Figure 5.6 are now used in all LS-DYNA models.

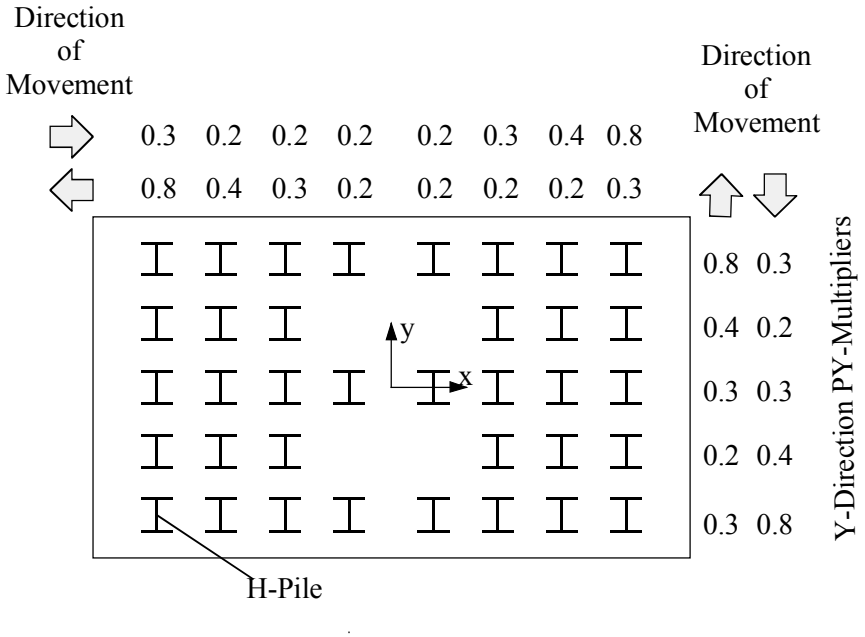

Figure 5.6. PY-Multipliers for Pier-1 Pile Group

5.5 Static Pushover Validation Modeling

After the previous updates were made, several test cases were run comparing the LS-DYNA soil model to the FB-Pier soil model. These comparisons involved running static pushover analyses on both single piles and pile groups. Several single pile simulations were run using different numbers of soil layers and different pile types.

The first analysis was run using a 50-foot long 14X73 steel H-pile embedded in one layer of sand. As with all of these analyses, the pile was given a linear elastic material property, and the soil was modeled using nonlinear springs. Furthermore, in modeling these piles, the number of nodes along the length of the pile was kept constant between the two programs (LS-DYNA and FB-Pier) to ensure displacements along the pile were calculated at the same depths. It can be concluded from Figure 5.7 that the load-displacement response of the single pile in one layer of soil calculated using LS-DYNA matched well with that of FB-Pier.

The second pushover simulation was run using a 40-foot long 18-inch pre-cast concrete pile embedded in four soil layers. A different pile type was chosen to ensure the formulation used for the soil spring curves was implemented correctly. In addition to the simulations run in LS-DYNA using the calculated soil spring curves and those run in FB-Pier, a simulation was run in LS-DYNA using the curves displayed in the FB-Pier GUI (consisting of only a limited number of points) for the soil springs to demonstrate differences in the results. Results for these three cases are compared in Figure 5.8 where the new Mathcad based generation of soil data for LS-DYNA produces improved results.

The third single pile simulation was run using a 50-foot long 14X73 steel H-pile embedded in the soil profile used for pier-1 of the St. George Island Bridge (documented in detail in [1]). Soil data for the LS-DYNA simulation was once again computed using

the Mathcad worksheets described earlier in this chapter. Similar to the single pile in one layer of soil, the LS-DYNA results from this analysis matched well with the results from FB-Pier (see Figure 5.9).

With the LS-DYNA results from the single pile runs in agreement with those from FB-Pier, the next step was to test pile group behavior. A 2 X 2 pile group model was set up using 50-foot long 18-inch pre-cast concrete piles embedded in four soil layers. Furthermore, the piles were fixed to the pile cap—though no py-multipliers were applied, as loading is in one direction only. Like the single pile models, the results from the LS-DYNA analyses agreed well with the results of the FB-Pier analyses (see Figure 5.10).

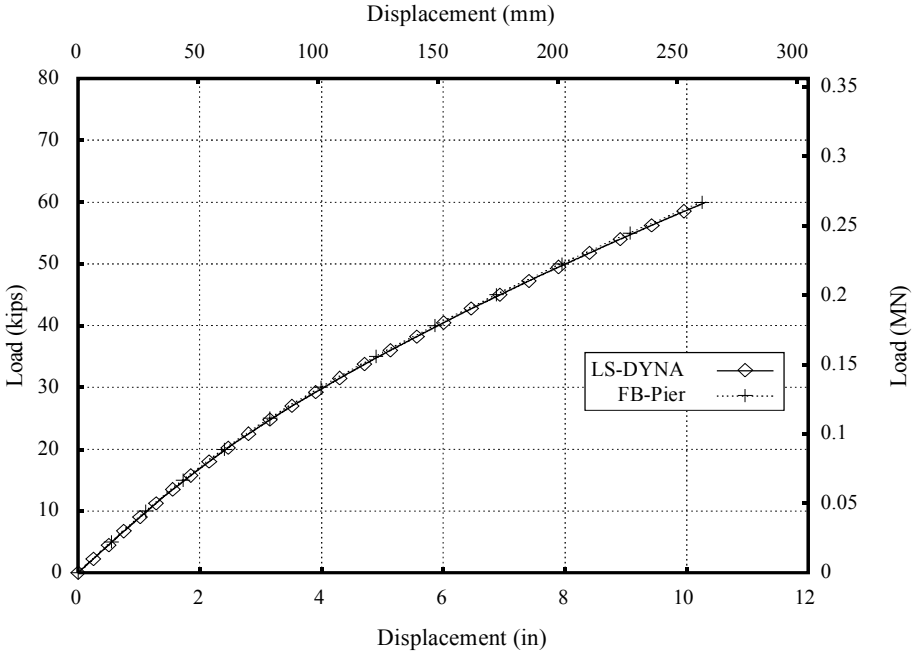

Figure 5.7. Single Pile Comparison with One Soil Layer

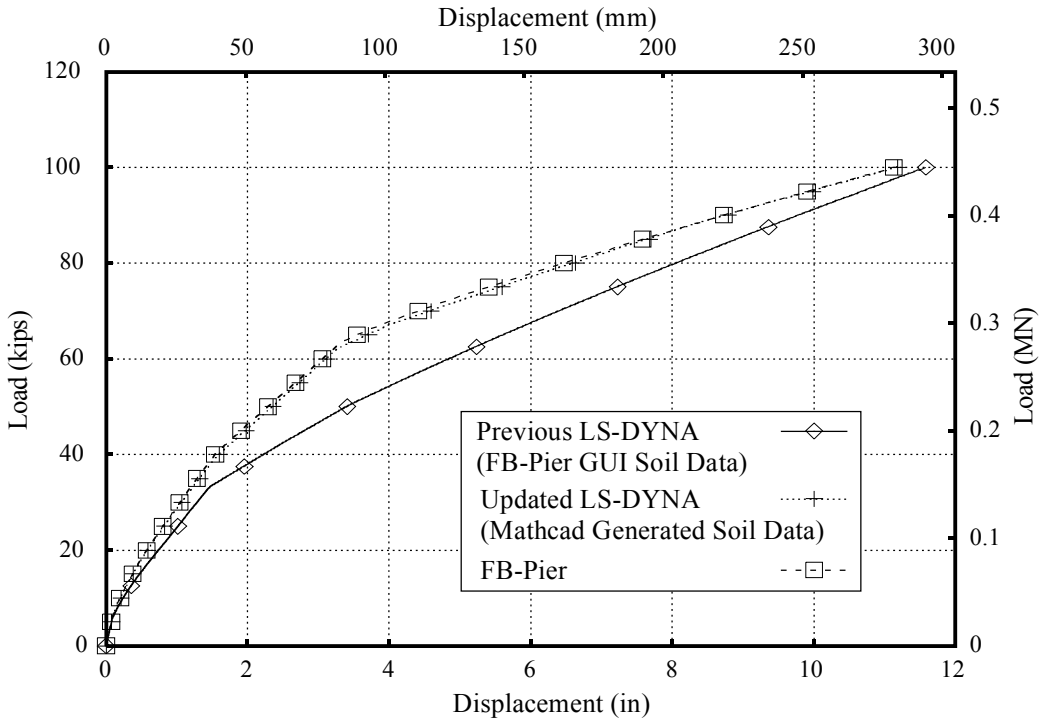

Figure 5.8. Single Pile Comparison with Four Soil Layers

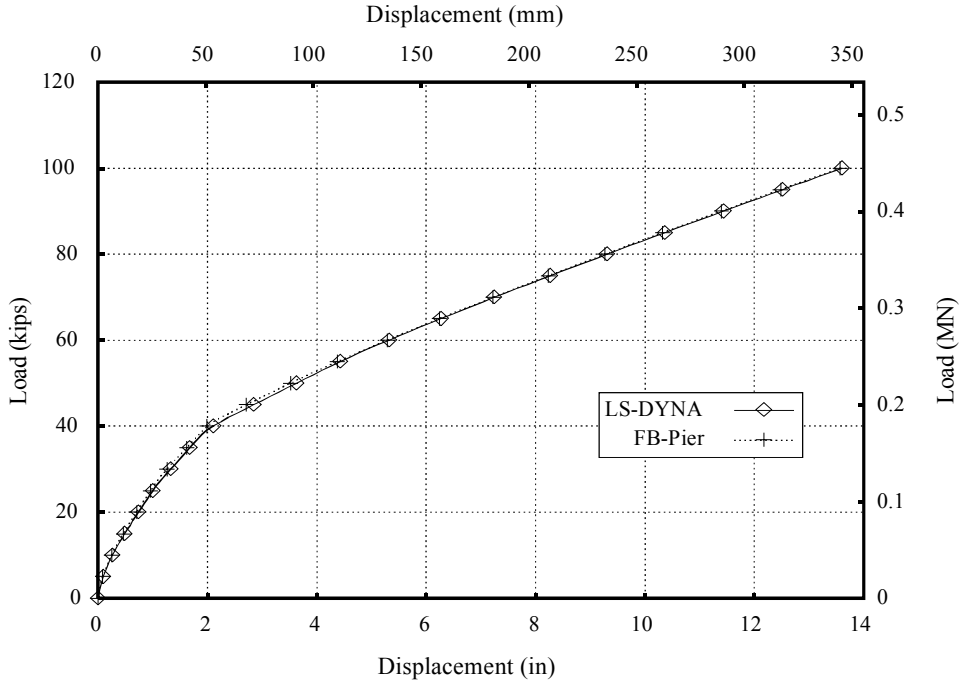

Figure 5.9. Single Pile Comparison with St. George Island Soil Profile

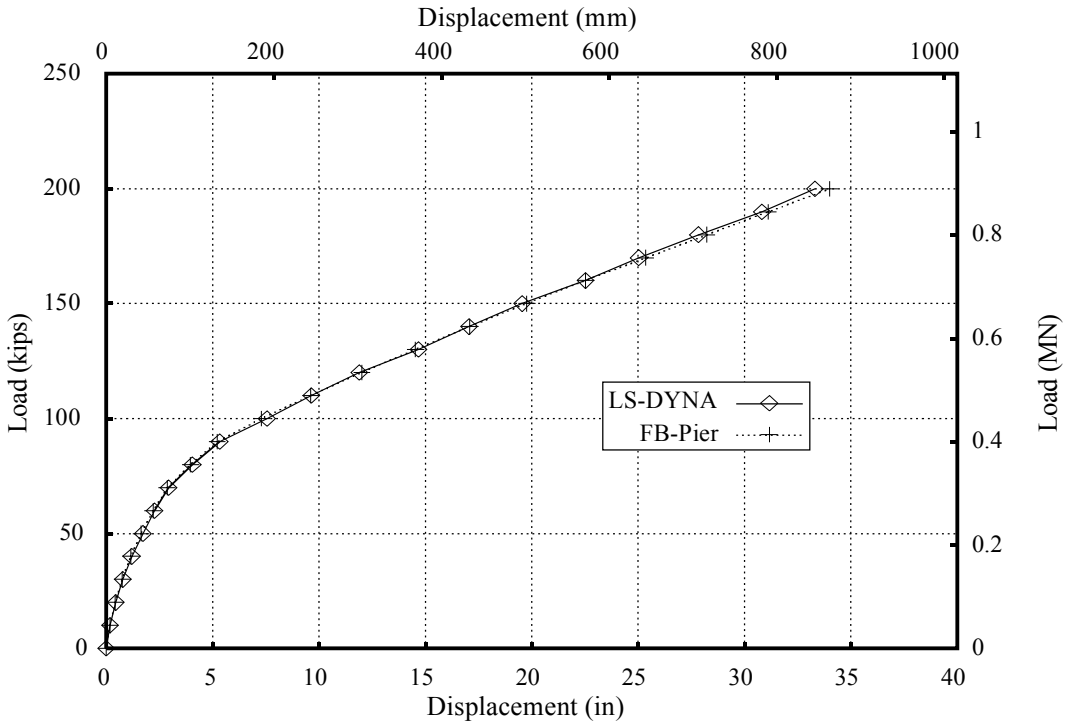

Figure 5.10 Pile Group Comparison

Chapter 6

Nonlinear Barge Crush Behavior

6.1 Introduction

Given that barge impact loads are generated by moving vessels having substantial mass, loads of this type are fundamentally dynamic in nature. As such, the magnitude of the load imparted to the bridge pier will vary with respect to time. The peak load generated and the rate of load oscillation during the impact are functions of the type, structural configuration, mass, and initial velocity of the impacting vessel; the structural configuration and mass of the pier; and the soil conditions. Given the complex nature of such dynamic events and the degree of scatter found in the loads generated [6], bridge design specifications generally provide simplified procedures for computing equivalent static loads as an alternative to conducting fully dynamic impact analyses. These loads are applied to the bridge in a static manner and are intended to produce approximately the same structural response as that due to the application of the corresponding time-varying dynamic impact load.

In the U.S., the AASHTO (American Association of State and Highway Transportation Officials) bridge design specifications [7, 8] contain procedures for computing equivalent static loads for both ship collision and barge collision events. Included in the AASHTO provisions are equations relating vessel kinetic energy, vessel deformation level (crush depth), and the equivalent static impact force to be applied to the bridge [6-9]. Separate relationships are given by AASHTO for ship impact loads and barge impact loads because the experimental and analytical bases for each type of vessel differ [6-10]. The ship impact provisions derive primarily from experimental studies conducted by Woisin [11] that focused on protecting reactors in nuclear powered ships

against accidental impact by other ships. The basis for the barge impact provisions, however, comes from experimental tests conducted by Meir-Dornberg [12] on European hopper barges (discussed in further detail later in this chapter).

Comparing ship and barge impact incidents, the latter type occurs at a higher frequency because a greater number of waterways (having bridge crossings) are navigable by relatively shallow draft vessels (barges) than by deeper draft vessels (ships). However, despite this fact, vessel impact studies published in the literature focus more frequently on ship collision mechanics than on barge impact behavior. Even fewer studies focus specifically on barge crush behavior during collisions with bridge piers.

Given that new bridge designs are often controlled by code-stipulated barge impact loading conditions, developing an improved understanding of barge collision mechanics is highly desirable. In this chapter, nonlinear finite element crush simulations are used to gain a better understanding of barge crush behavior during collisions with bridge piers. All crush analyses presented herein were conducted using the high-resolution finite element barge model that was developed during the Phase I research effort [1] and enhanced during Phase II (as discussed in previous chapters of this report). Importantly, the model has been developed strictly based on *structural vessel plans* obtained from a U.S. barge manufacturer. The finite element model is in no way dependent on the empirical relationships used in the AASHTO provisions. As such, the finite element crush results presented can be considered to be an independent source of barge crush data for purposes of making comparisons to the current AASHTO code provisions.

6.2 AASHTO methodology for prediction of barge impact loads

Barge impact load calculations conducted according to the AASHTO provisions involve the use of both an empirical load prediction model and a risk assessment procedure. The AASHTO guide specification for vessel collision design [7] and the AASHTO LRFD bridge design specifications [8] differ in the risk assessment methods available in each document (Ref. [8] provides only a subset of the options available in Ref. [7]). However, the load prediction model implemented, which is the item of interest here, is the same in both of these documents.

AASHTO based load calculations for barge impact design begin with selection of the "design" impact condition (barge type and impact speed). Factors such as the characteristics of the waterway, expected types of barge traffic, and the importance of the bridge (critical or regular) enter in to this selection process. Once the impact conditions have been identified, the kinetic energy of the barge is computed as [7]:

$$KE = \frac{C_H W V^2}{29.2} \tag{6.1}$$

where is KE is the barge kinetic energy (kip-ft), C_H is the hydrodynamic mass coefficient (a factor that approximates the influence of water surrounding the moving vessel), W is the vessel weight (in tonnes where 1 tonne = 2205 lbs.), and V is the impact speed (ft/sec). It is noted that Eq. 6.1 is simply an empirical version (derived for a specific set of units) of the more common relationship:

$$KE = C_H \left(\tfrac{1}{2} M V^2 \right) \tag{6.2}$$

where KE, M (the vessel mass), and V are all dimensionally consistent.

Once the kinetic energy of the barge has been determined, a two-part empirical load prediction model is then used to determine the static-equivalent impact load. The first component of the model consists of an empirical relationship that predicts crush deformation as a function of kinetic energy:

$$a_B = \left(\sqrt{1 + \frac{KE}{5672}} - 1 \right) \cdot \left(\frac{10.2}{R_B} \right) \tag{6.3}$$

In this expression, a_B is the depth (ft.) of barge crush deformation (depth of penetration of the bridge pier into the bow of the barge), KE is the barge kinetic energy (kip-ft) and $R_B = \left(B_B / 35 \right)$ where B_B is the width of the barge (ft).

The second component of the load prediction model consists of an empirical barge-crush model that predicts impact loads as a function of crush depth :

$$P_B = \begin{cases} 4112\, a_B\, R_B & a_B < 0.34 \text{ ft.} \\ \left(1349 + 110\, a_B \right) R_B & a_B \geq 0.34 \text{ ft} \end{cases} \tag{6.4}$$

where P_B is the equivalent static barge impact load (kips) and a_B is the barge crush depth (ft). The crush model represented by Eq. 6.4 is illustrated graphically in Figure 6.1.

Unfortunately, as a consequence of the fact that very little barge collision data has ever been published in the literature, Eqs. 6.3 and 6.4 are based on a single experimental study. During the early 1980s, a study was conducted in Germany by Meir-Dornberg [12] that involved physical testing of *reduced-scale* standard European (type IIa) barges. Experimental barge crush data was collected by Meir-Dornberg and then used to develop empirical relationships relating kinetic energy, depth of barge crush deformation, and impact load. AASHTO's relationships, Eqs. 6.3 and 6.4, are virtually identical to those

developed by Meir-Dornberg except that a width-modification factor—the R_B term—has been added to approximately account for deviations in barge width from the baseline width of 35 ft. (the width of barges most often found operating in U.S. inland waterways).

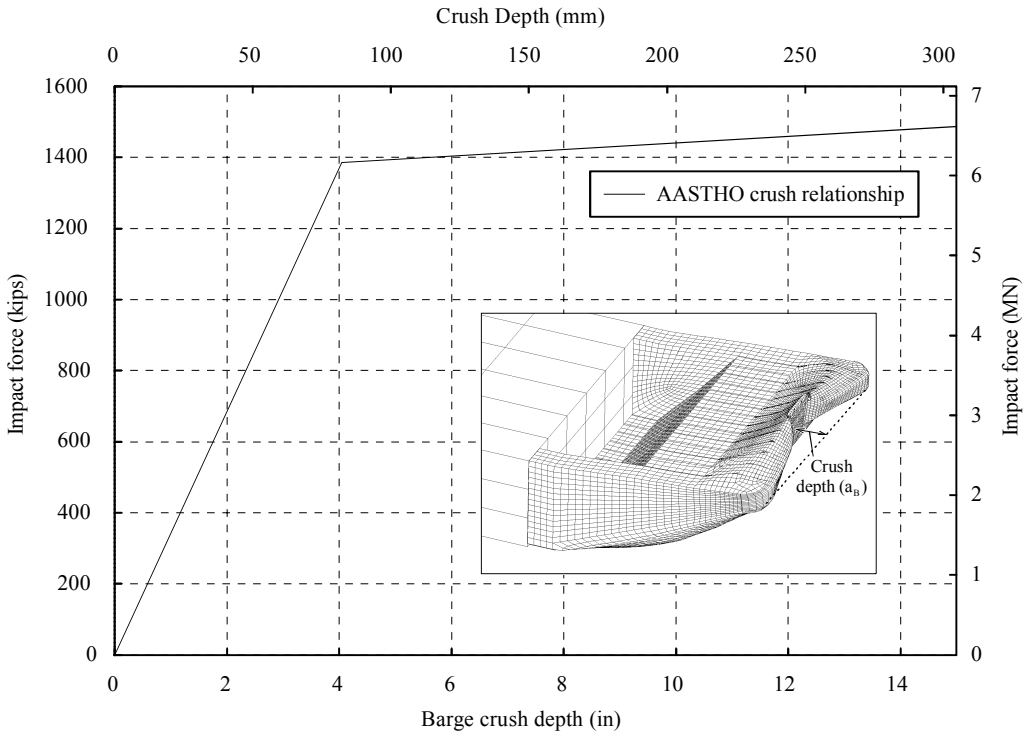

Figure 6.1 – Barge crush model used in AASHTO bridge design specifications

Interestingly, while Eq. 6.3 utilizes the R_B term to reflect the influence of barge width, no such factor has been included to account for variations in either the size (width) or geometric shape of the bridge pier being impacted. Furthermore, since Eq. 6.4 indicates that the impact load (P_B) increases monotonically with respect to crush depth (a_B), the AASHTO provisions implicitly assume that maximum impact force occurs at

maximum crush depth and, therefore, peak impact load can be uniquely correlated to peak crush depth.

A primary goal of this study was to generate—using finite element analysis—independent force-deformation data that would serve to supplement the experimentally derived crush-relationships reported by Meir-Dornberg. By comparing simulation results to the crush-model assumed by AASHTO (i.e. Eq. 6.4), areas of potential future improvement in the bridge design specifications can be identified. In addition, relationships generated in this manner may be used in future efforts focusing on the development of simplified, design-oriented nonlinear dynamic models of barge-pier interaction.

6.3 Finite element analysis procedures and models

Finite element code and solution algorithms

Analysis of structural crushing is very often handled using nonlinear contact finite element simulation. In the case of vessel crush simulation, the finite element code used must be capable of robustly representing nonlinear inelastic material behavior (with failure), part-to-part contact, self-contact, and large displacements (due to the significant geometric changes that often occur). The LS-DYNA finite element code [13] meets all of these requirements and has been shown in previous studies to be capable of accurately simulating complex structural crushing. LS-DYNA was thus employed throughout the present investigation to study crushing of barges.

Pier impactor models and crush conditions

Clearly, of particular interest in this study is the crush behavior that occurs when barges collide with concrete bridge piers. As such, the geometric shapes of the impactors

developed herein matched the two most common bridge pier shapes—circular and square. Each impactor was modeled using eight-node solid elements, was assigned a nearly-rigid linear elastic material model, and was positioned along the longitudinal axis of the barge (Figure 6.2) at a location that initially produced a small gap between the surfaces of the barge and the pier impactor. A contact definition was then defined between these surfaces with a friction value of $\mu = 0.3$ (approximate frictional coefficient for steel sliding on concrete). Nodes on the back face of the impactor (opposite the contact surface) were assigned a displacement time history that translated the pier toward the barge at a constant rate of 10 in/sec to generate crushing at the barge bow.

6.4 Discussion of crush simulation results

Static barge crush analyses were conducted for five circular impactors (diameters: 2 ft., 4 ft., 6 ft., 8 ft., 10 ft.) and for three square impactors (widths: 2 ft., 4 ft., 6 ft., 8 ft., 10 ft.). For each level of imposed impactor penetration, i.e. barge crush depth, the total force acting at the contact interface between the pier and the barge was extracted from the finite element simulation data. Results obtained from the circular crush simulations are presented in Figure 6.3. Forces acting on the pier (i.e. the impactor) are shown to gradually and monotonically increase with corresponding increases in crush depth. In general, the crush characteristics are also shown to be slightly sensitive to variations in pier width, but the effect is not strongly pronounced.

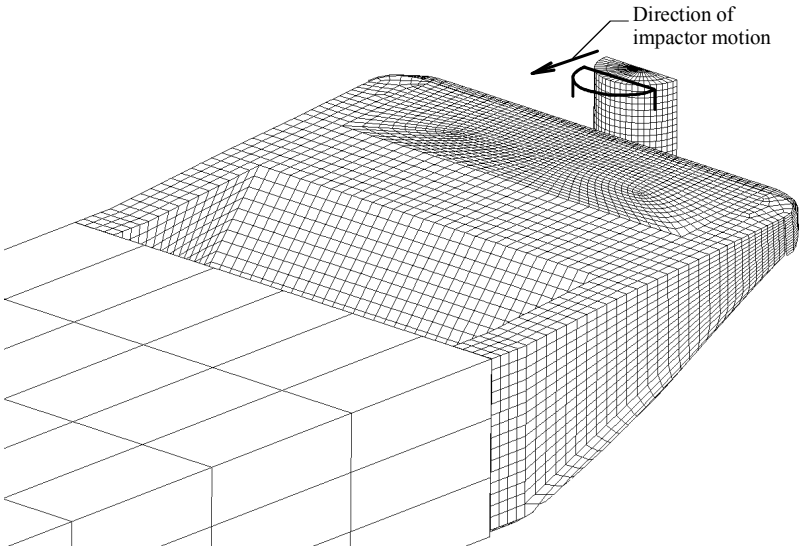

a) Crush model consisting of barge and circular pier impactor

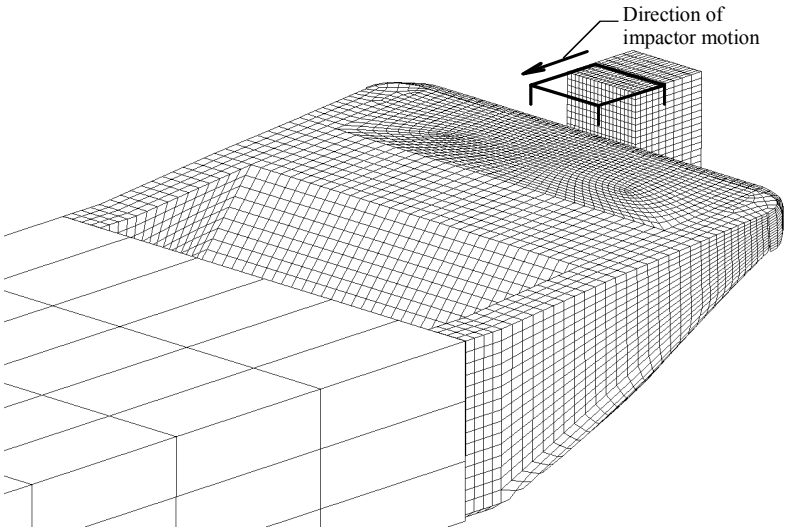

a) Crush model consisting of barge and square pier impactor

Figure 6.2 – Crush simulation models

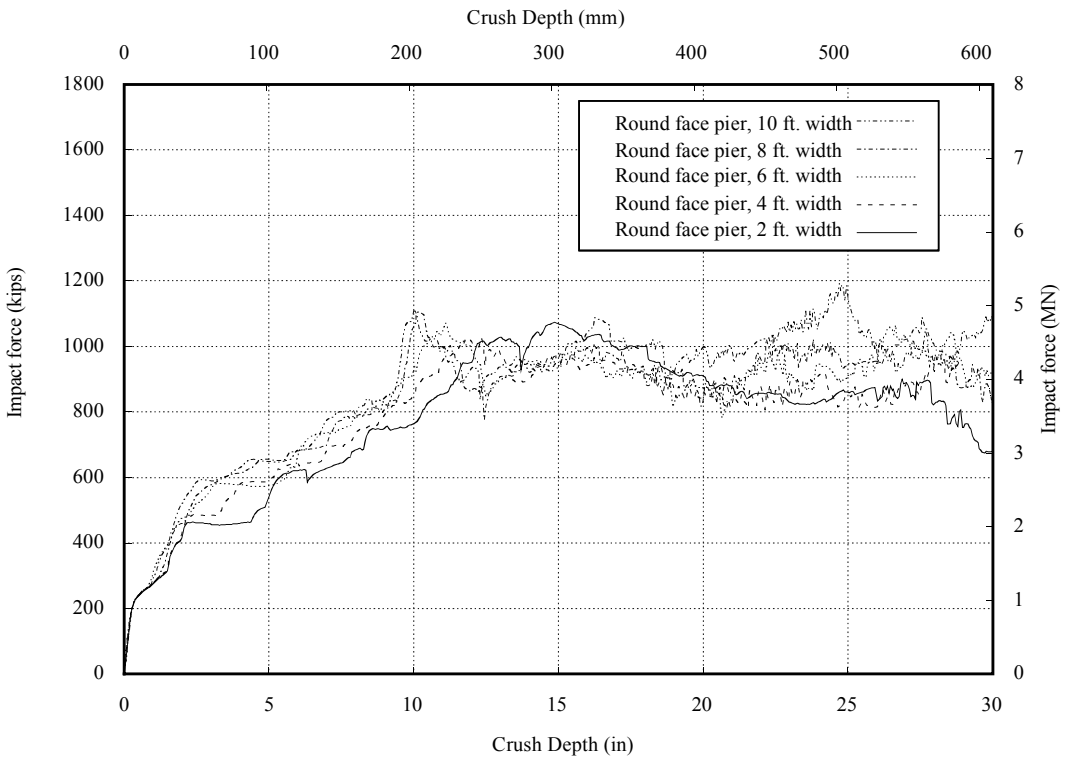

Figure 6.3 – Predicted barge crush behavior for circular impactors

In Figure 6.4, crush results are presented for the square impactor simulations. Several key differences between the circular and square crush cases are immediately evident. In the square crush cases, the contact forces are observed to rise very rapidly and—for small deformation levels—the overall crush behavior is seen to be much stiffer than in the circular cases. However, after the contact force has maximized, the stiffness of the barge diminishes rapidly in the square cases. In fact, whereas all of the *circular* crush analyses predicted a monotonically increasing relationship between force and crush depth, *none* of the square analyses exhibited this characteristic. In addition, whereas diameter had very little effect on the crush behavior observed for circular piers, Figure 6.4 indicates that in square crush conditions, there is a definite relationship between pier width and force generated.

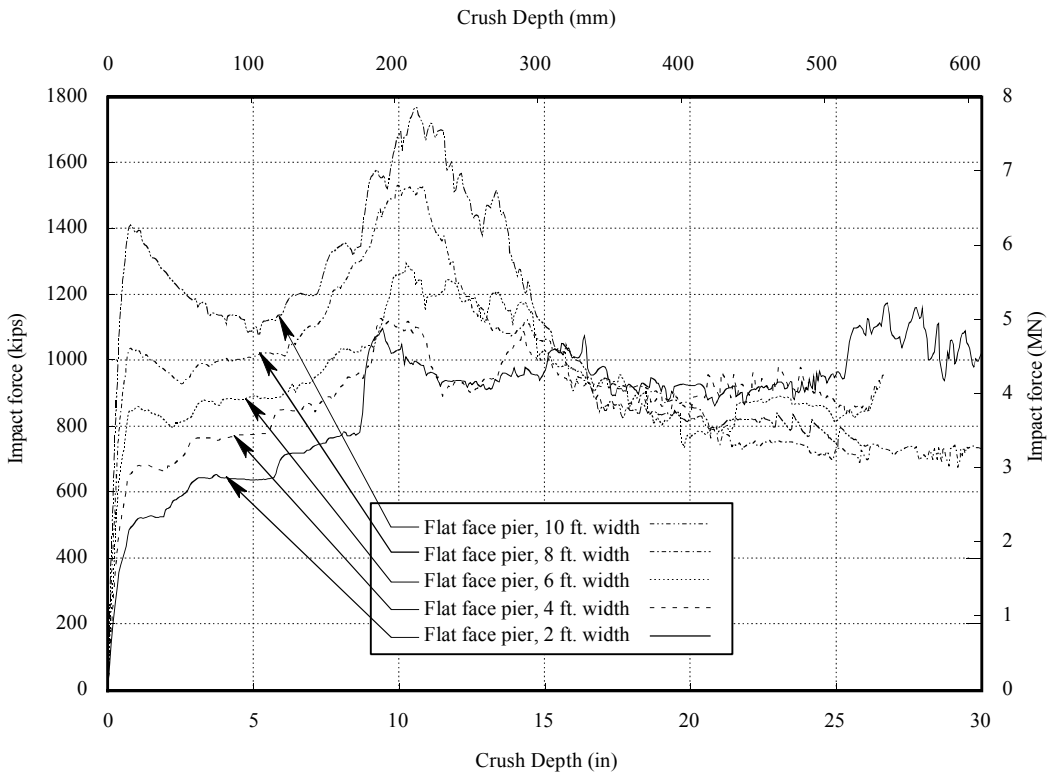

Figure 6.4 – Predicted barge crush behavior for square impactors

That pier geometry can influence the crush behavior of a barge is not surprising when consideration is given to the internal structure of such vessels. In the bow of a barge, numerous internal trusses run parallel to one another resulting in significant stiffness in the longitudinal direction. During impact with a pier, both the shape and size of the pier determine the number of internal trusses that actively participate in resisting bow crushing. Figure 6.5 illustrates the internal deformation produced by 12 in. of crush depth imposed by a 6 ft. diameter circular impactor. Figure 6.6 illustrates the same scenario, but for a 6 ft. wide square impactor. In the circular case, bow deformation is concentrated in a narrow zone near the impact point and only the trusses immediately adjacent to this location generate significant resistance. As increasing crush deformation

occurs, additional trusses participate and the force increases in an approximately monotonic manner.

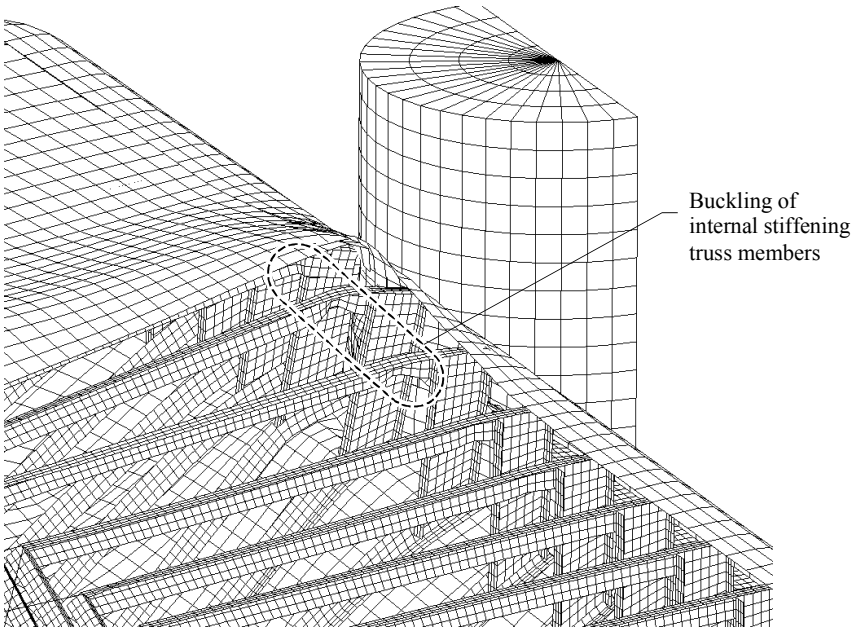

Figure 6.5 – Barge deformation generated by circular pier impactor

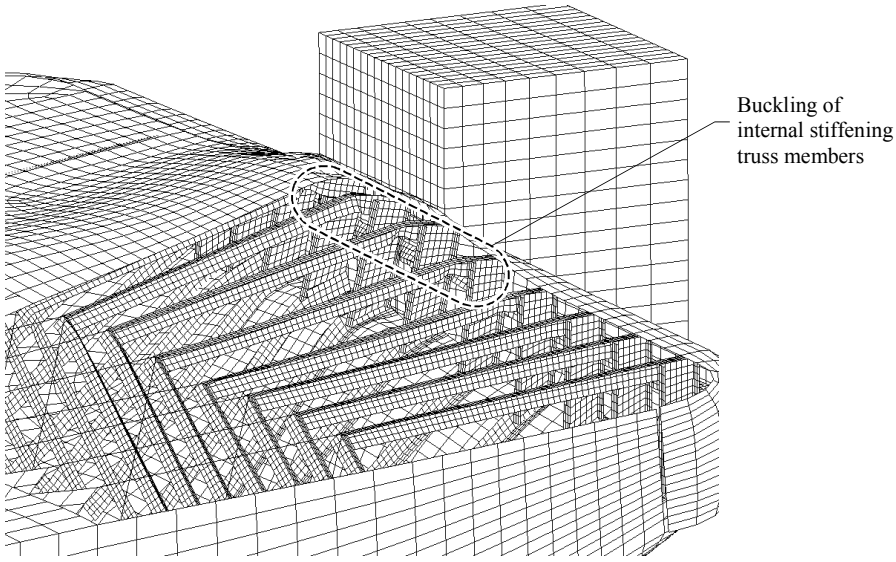

Figure 6.6 – Barge deformation generated by square pier impactor

In contrast, when a *flat-surface* square impactor bears against the barge, several trusses immediately and simultaneously resist crushing, thus producing a very stiff response. However, when the trusses buckle, and therefore soften (Figure 6.6), they all do so at approximately the same deformation level. As a result, there is an abrupt decrease in the overall stiffness of the barge (as was illustrated in Figure 6.4 where the crush forces plateau or even decrease after maximizing). In addition, increasing the width of a square pier increases the number of trusses that simultaneously participate in crushing, thus explaining the sensitivity of force magnitude to impactor width that was evident in the square crush simulations. As was noted earlier, the AASHTO crush model given in Eq. 6.4 includes a correction factor (R_B) for barges that deviate from the 35 ft. width of the standard hopper barge. However, the finite element results presented here suggest that it may also be appropriate to include parameters reflecting the effects of pier shape and pier size in the crush model as well.

A comparison of the empirical AASHTO crush model, Eq. 6.4, and finite element predicted crush behavior (for the 6 ft. circular and 6 ft. square crush cases) is presented in Figure 6.7. For cases involving significant barge crushing (e.g. more than 6 in.), the forces predicted by finite element simulation are significantly less than those predicted by the AASHTO crush model. Finally, the *square* impactor data shown in Figures 6.4 and 6.7 demonstrate that, for some pier configurations, the static crush force does not necessarily increase monotonically with respect to crush depth. In such cases the maximum force generated cannot necessarily be correlated to the maximum crush depth sustained (e.g. in an impact condition). This fact is important because the AASHTO load prediction procedure described earlier in this paper (Eqs. 6.1, 6.3, and 6.4) appears to

assume that the equivalent static impact force can be uniquely correlated to (or predicted from) peak crush deformation sustained by a barge during an impact event. The square impactor crush results presented here indicate that this procedure should be reexamined since impact force does not appear to be uniquely correlated to maximum deformation.

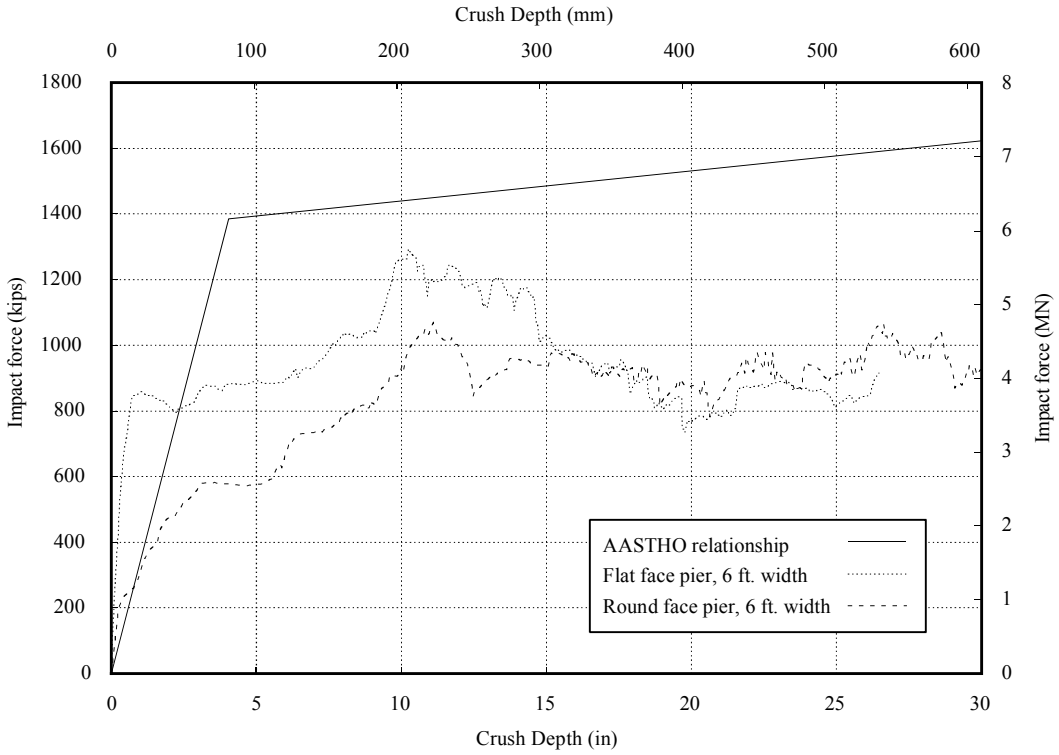

Figure 6.7 – Comparison of crush simulation data and AASHTO crush model

Chapter 7

Preliminary Study of Multiple Pier Systems

7.1. Overview of the Multiple Pier System

During the experimental impact testing, several impacts will be conducted on pier-3 with the bridge superstructure still intact. The purpose of these impacts is to determine how the force will be redistributed through the superstructure to the adjacent piers. Therefore, as a preliminary study, a finite element model of the superstructure connecting three of the bridge piers was created (Figure 7.1). This model is expected to help characterize the behavior of a multiple pier system connected through a superstructure. For simplicity, pier-2 is currently used to model the multiple pier system connected through the superstructure. However, at a later time, the actual experimental layout—which incorporates pier-3 as the impact pier, and pier-2 and pier-4 as the adjacent piers—will be used to model this system.

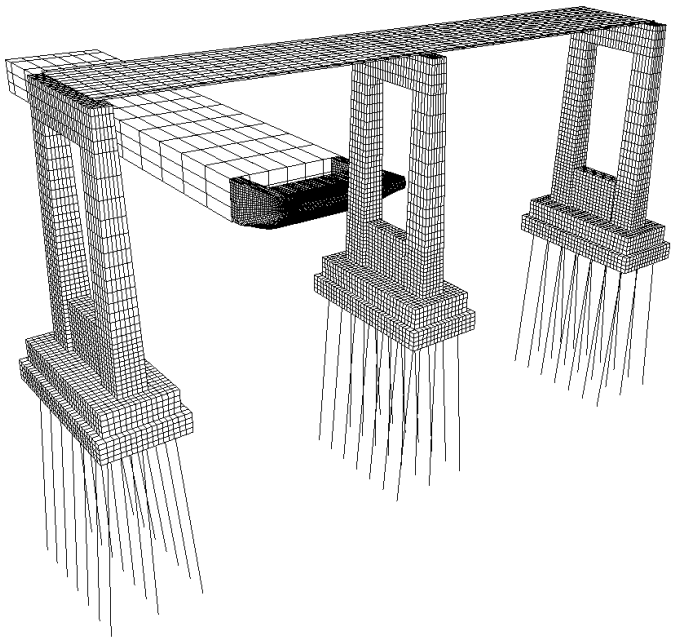

Figure 7.1 Two-span model

7.2. Superstructure Model

Since the superstructure is not expected to undergo large deformations, all of the bridge components in the preliminary superstructure model were given linear-elastic material properties. In LS-DYNA, the linear elastic material is defined as `*MAT_LINEAR-_ELASTIC`. Moreover, the material properties throughout the superstructure were kept consistent with each other for simplicity.

The bridge deck was modeled using shell elements placed at the mid-plane of the deck. These shell elements were given a thickness equal to the bridge deck thickness taken from the St. George Island bridge construction plans. The superstructure spans were modeled as discontinuous over the piers to account for deck joints between consecutive spans.

One anticipated problem in modeling the bridge deck in this manner is the closure of the deck joint. If the pier undergoes substantial displacements, then the deck joint could close as shown in Figure 7.2. Consequently, a significant force might develop across the interface between the adjoining decks due to the contact between the two deck spans. However, a simple analysis of the superstructure alone demonstrated that the displacements expected during the experiment will not cause the deck joint to close.

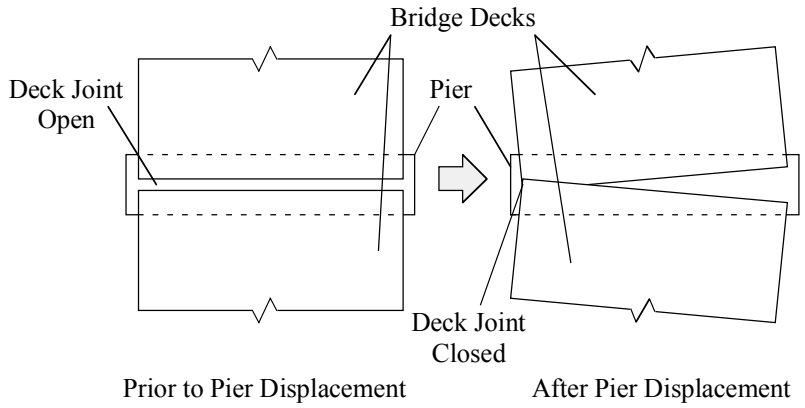

Figure 7.2 Deck Joint Closure

The bridge girders were modeled using resultant beam elements with section properties obtained from the original construction plans. The resultant beam elements used to model the girders were then attached to the shell elements that model the bridge deck using the `*CONTACT_TIED_NODES_TO_SURFACE_OFFSET` option in LS-DYNA. This option allows the nodes of the beam elements used to model the girders to be tied rigidly to the nodes of the bridge deck without specifying the individual connections—which are numerous. The beam elements used to represent the bridge girders are connected to the piers at discrete points using the `*CONSTRAINED_NODAL_RIGID_BODY` option in LS-DYNA. In addition, the parapets on the superstructure were also modeled using resultant beam elements, and also connected to the bridge deck using tied contact.

7.3. Preliminary Results

Initially, a simulation was run that used pre-compression to gravitationally equilibrate the buoyancy springs on the barge, as documented in the Phase I report [1]. However, when the analysis was conducted, the superstructure exhibited a large oscillatory motion due to the sudden application of gravity at the beginning of the

analysis. Consequently, the vertical motion of the superstructure affected the behavior of the overall system. It was determined that the method used to equilibrate the model needed to be refined to eliminate the undesirable superstructure motion.

To remove the dynamic effects due to the sudden application of gravity, a separate gravity analysis was run, during which the model was subjected to the same abrupt gravity change. However, in this instance, each component of the model was subjected to global viscous damping, which allowed the model to rapidly settle into its gravity equilibrium position. The damping was then removed, and the impact analysis was initiated. Thus, at the beginning of the impact simulation, the system was already in gravitational equilibrium, and the superstructure—as well as the rest of the model—did not display any unintended movement due to the abrupt application of gravity.

In Figure 7.3, results are shown for half-loaded barge impacts on Pier-2 at 4-knot impact speeds. The two simulations differ only in the manner in which gravity loads were applied. It must be noted that updated soil constraints discussed in Chapter 5 were not implemented in these conjoint superstructure and substructure models yet. Impact forces for the two cases are shown in Figure 7.3, while force-crush data are shown in Figure 7.4. The crush depth was much lower for the analysis that allowed the system to settle under gravity versus the analysis that used pre-compression to gravitationally equilibrate the barge. Future efforts will focus on using both experimental data and analytical modeling to quantify the degree of impact load transfer that occurs through the bridge deck.

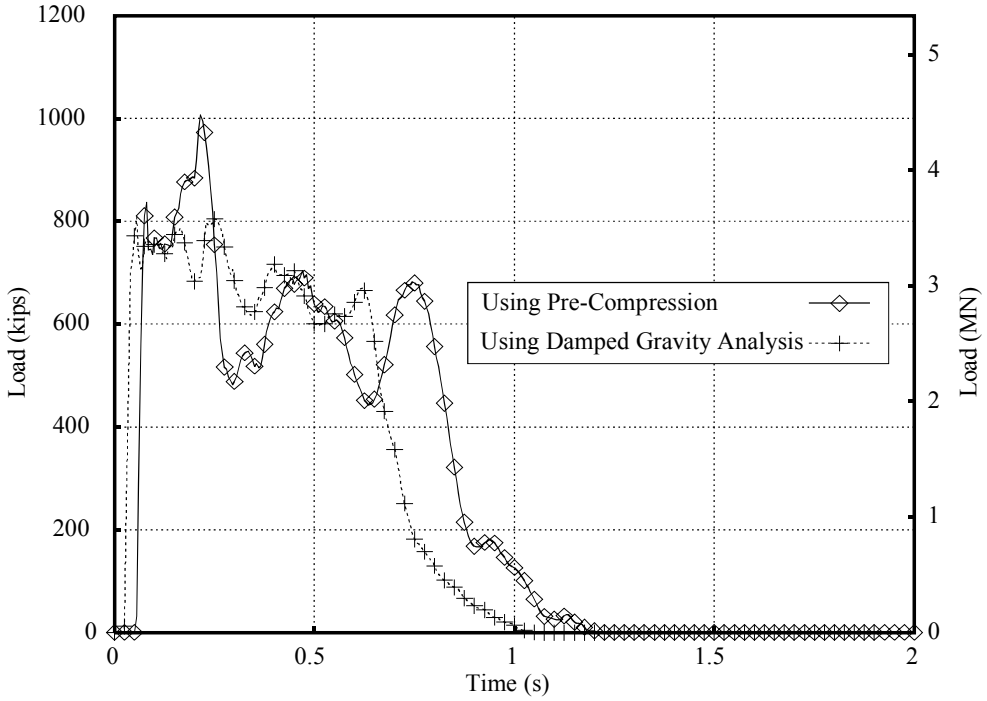

Figure 7.3 Force History Comparison

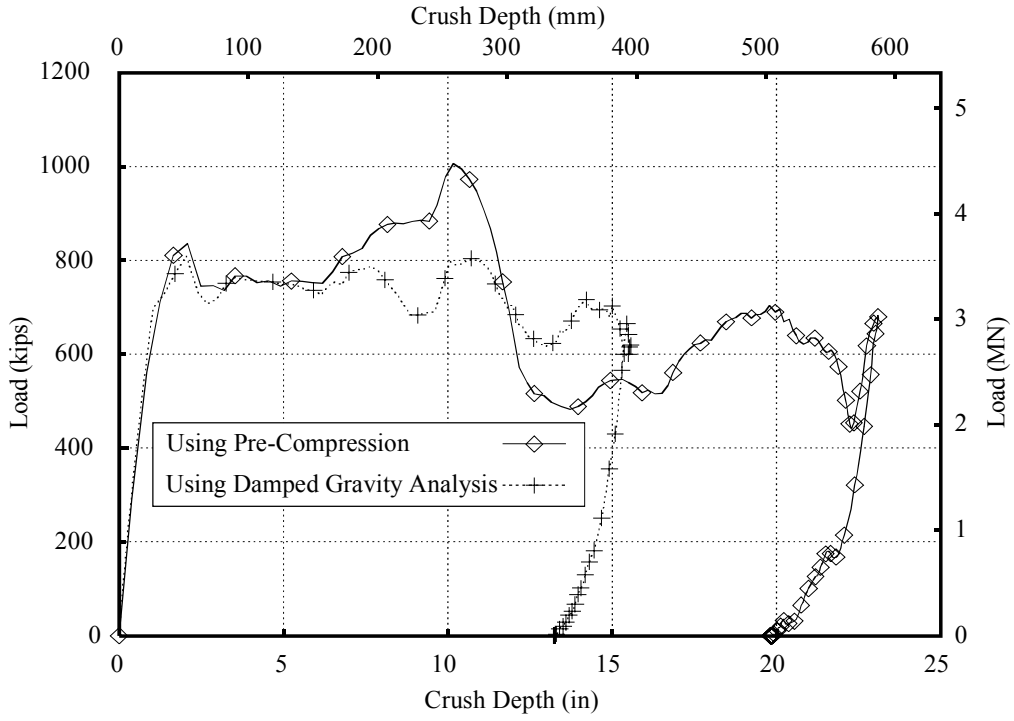

Figure 7.4 Crush Depth Comparison

Chapter 8

Conclusions

With the completion of Phase II of the barge impact study, significant progress has been made towards ensuring successful completion of the physical impact tests that will be conducted during Phase III. The instrumentation systems that have been designed as part of Phase II effort will be fabricated and tested during Phase III. In addition, scheduling and logistical planning will continue in coordination with the bridge contractor.

The finite element models developed initially during Phase I and enhanced during Phase II continue to be important components of the overall planning process, enabling selection of impact conditions; determination of design loads on instrumentation packages; selection of appropriate sensors; and evaluation of anticipated barge damage. In addition, impact simulation results obtained thus far have yielded significant insights into the mechanics of barge collisions with piers. Information of this form will be extremely valuable in the future Phase III effort, especially with regard to interpreting experimentally collected data.

Finally, validation of the LS-DYNA models under prescribed non-barge impact loading conditions—e.g. static pushover—has served to enhance not only confidence in the LS-DYNA structural and soil modeling techniques, but also in the robustness of the FB-Pier program. Future efforts will involve validation of the LS-DYNA and FB-Pier models (representing the St. George Island piers) against experimentally collected data, and against each other (cross-program validation) but in the dynamic analysis realm. Efforts of this type will continue to enhance the reliability of both the LS-DYNA and FB-Pier analysis tools.

References

1. Consolazio, G.R., Cook, R.A., Lehr, G.B., Bollmann, H.T., Barge Impact Testing of the St. George Island Causeway Bridge Phase I : Feasibility Study, Structures Research Report No. 783, Engineering and Industrial Experiment Station, University of Florida, Gainesville, Florida, January 2002.

2. Hoit, M.I., McVay, M., Hays, C., and Andrade, W., Nonlinear Pile Foundation Analysis Using Florida-Pier, ASCE Journal of Bridge Engineering, Volume 1 Number 4, pp 135-142, 1996.

3. Florida Bridge Software Institute, "FB-PIER Users Manual," University of Florida, Gainesville, FL, 2000.

4. ENSOFT, Inc., "GROUP 5.0 Technical Manual," Austin, Texas, 2000

5. McVay, M.C., O'Brien, M., Townsend, F.C., Bloomquist, D.G., and Caliendo, J.A. "Numerical Analysis of Vertically Loaded Pile Groups," ASCE, Foundation Engineering Congress, Northwestern University, Illinois, July, 1989, pp. 675-690.

6. Knott M, Prucz Z. Vessel collision design of bridges: Bridge Engineering Handbook. CRC Press LLC, 2000.

7. AASHTO. Guide Specification and Commentary for Vessel Collision Design of Highway Bridges. American Association of State Highway and Transportation Officials, 1991.

8. AASHTO. LRFD Bridge Design Specifications and Commentary. American Association of State Highway and Transportation Officials, 1994.

9. Whitney, M.W., Harik, I.E., Griffin, J.J., and Allen, D.L., Barge Collision Design of Highway Bridges, ASCE Journal of Bridge Engineering, Volume 1 Number 2, pp 47-58, 1996.

10. Knott M.A., Vessel collision design codes and experience in the United States. In: Gluver H, Olsen D, editors. Ship collision analysis. Rotterdam: A. A. Balkema, 1998.

11. Woisin, G. The Collision Tests of the GKSS. Jahrbuch der Schiffbautechnischen Gesellschaft, 1976; 70:465- 487.

12. Meir-Dornberg KE. Ship Collisions, Safety Zones, and Loading Assumptions for Structures in Inland Waterways. VDI-Berichte 1983;496:1-9.

13. Livermore Software Technology Corporation (LSTC), "LS-DYNA Keyword Manual : Version 950", Livermore, C.A., 1999.